A Theory-Based Approach to Industrial Cultivation of Cyanobacteria

By

Ryan L. Clark

A dissertation submitted in partial fulfillment of

the requirements for the degree of

Doctor of Philosophy

(Chemical and Biological Engineering)

at the

UNIVERSITY OF WISCONSIN-MADISON

2017

Date of final oral examination: 7/24/2017

The dissertation is approved by the following members of the Final Oral Committee:

Brian F. Pfleger, Associate Professor, Chemical and Biological Engineering
Thatcher W. Root, Professor, Chemical and Biological Engineering
Jennifer L. Reed, Associate Professor, Chemical and Biological Engineering
Christos T. Maravelias, Professor, Chemical and Biological Engineering
Victor M. Zavala, Assistant Professor, Chemical and Biological Engineering
Ophelia S. Venturelli, Assistant Professor, Biochemistry

A Theory-Based Approach to Industrial Cultivation of Cyanobacteria

Ryan L. Clark

Under the supervision of Professors Brian F. Pfleger and Thatcher W. Root

At the University of Wisconsin-Madison

Abstract

Cyanobacteria are photosynthetic microorganisms whose metabolism can manipulated to produce industrially relevant molecules. This work applied a theoretical understanding of cyanobacterial photon utilization and carbon dioxide fixation to guide the design of efficient and safe scaled-up cyanobacterial bioprocesses. First, a theoretical framework and experimental conditions were developed for understanding and comparing cyanobacterial growth and product secretion with light as the sole-limiting substrate. The resulting framework is useful for scaling growth and product secretion in culture vessels of differing geometry. Second, a theoretical model of the cyanobacterial CO_2 concentrating mechanism (CCM) was developed to understand situations in which CO_2 can become a limiting substrate in wild type cyanobacteria and mutants lacking the CCM. Finally, this understanding of CO_2-limitation was used to develop a CCM-disruption based genetic containment mechanism for cyanobacteria. The resulting CCM-lacking cyanobacteria were unable to propagate in ambient air but grew and produced secreted molecules at the same rate as CCM-containing cyanobacteria when grown in 5% CO_2, an environment which could be created in an industrial process using CO_2 waste streams.

Acknowledgements

"The spirit of research and conquest is the permanent soul of evolution."
Pierre Teilhard de Chardin, *The Phenomenon of Man*

"Limits of survival are set by climate, those long drifts of change which a generation may fail to notice. And it is the extremes of climate which set the pattern. Lonely, finite humans may observe climatic provinces, fluctuations of annual weather and, occasionally may observe such things as 'This is a colder year than I've ever known.' Such things are sensible. But humans are seldom alerted to the shifting average through a great span of years. And it is precisely in this alerting that humans learn how to survive on any planet. They must learn climate."
Frank Herbert, *Children of Dune*

"A scientist is always fine."
Cecil Palmer, *Welcome to Night Vale*

There are many whose support and friendship made this work (and my sanity) possible. Thanks to my wonderful girlfriend Molly for her love and support and for helping me to get through frustrating times in graduate school. I would like to thank my parents and my siblings, Kristen, Nick and my soon to be sister-in-law Amanda, for the constant encouragement over the entire course of my academic career and for understanding the times when I forgot to let them know that I still exist, sometimes for weeks. It's great that we can always pick up right where we left off. I would like to also thank my extended family, cousins, aunts and uncles and grandparents for always showing interest in my life even when I fall out of contact for months on end. It means a lot.

The Pfleger Lab has been an incredible place to work and I have truly enjoyed working with and getting to know every single person who has come through over the years. The guidance and advice of our great Post-Docs over the years was crucial (special thanks to Jeff Cameron, Matt Copeland, Andrew Markley, and Chris Jones for research advice and friendship). Travis Korosh, Mark Politz, and Jackie Rand were a constant reassuring presence over the years, and were a talented group of people to learn with and from. Too many memories to choose from (or that shouldn't be put in writing). Although my overlap with Dan Agnew was very short, he has become a great friend since, and I will always remember when he taught me how to clone. Thanks to Tyler Youngquist, Daniel Mendez, and Matt Begemann for playing the roles of wise older graduate students when I was getting started. Your advice was invaluable. Thanks to Gina Gordon for her insight from outside of my wheelhouse and for not making me feel stupid whenever I forgot (or never learned) basic concepts in microbiology. Thanks to Nestor Hernandez, Chris Mehrer, and Taylor Cook for always being willing to grab a cup of coffee or lunch and talk science (or politics, economics, memes, etc.). Thanks to Austin Comer for fun conversations about our shared hobby of board games. Thanks to Dylan

Courtney for some refreshing new perspective on cyanobacteria. I am looking forward to seeing your work over the next few years. I was fortunate to work with many talented undergraduate students over the years, many of whom carried out experiments used in this work. Thank you to Daniel Quevedo, Frances Ruiz-Deliz, Tania Class-Martinez, Bea Ongwong, Patrick Radish, Richard Mikel, Nate Bennett, Haoxiang Lyu, and Laura McGinley. I couldn't have done this work without them.

All the faculty and staff in the CBE Department have helped to make our workplace a fun and comfortable place to be. Thanks to my advisors, Brian Pfleger and Thatcher Root, for the advice and support over the years. Thanks to Andrew Greenberg for providing opportunities to learn more about research mentoring. Thanks to Eric Codner, Joel Lord, and Steve Schumacher for helping me figure out how to build research equipment without losing limbs in the process. Thanks to Tony Wu, Kirti Yenkie, and Christos Maravelias for their process systems insight. I greatly enjoyed our discussions. Thanks to Mary Heimbecker for answering my almost constant questions over the years. Thanks to Jackie Cooper for keeping our lab well-stocked and for HPLC advice.

Thank you to Kelly Wetmore, Morgan Price, Adam Deutschbauer, and Adam Arkin for hosting me for training last summer and for the resulting collaboration. I really enjoyed the experience.

My friends, both in Madison and elsewhere, have truly helped me to stay sane over the years. Thanks to my former Madison roommates Scott Shaheen, Joe Pompeani, Eric Richards, Travis Korosh, Steve Peck, Ben Strobheen, and Luke Claflin for some great times. Thanks to Dan Agnew, Matt Stillwell, Mark Politz, and Tom Gostanian for awesome game nights. Thanks to my fellow graduate students, particularly Zach Brentzel, Matt Long, Joe Chada, Tyler Perlenfein, and Tim Smith, for the comradery. Thanks to Claudia and Jason Guy for hosting more than their fair share of dinner parties. Thanks to everyone who played with me on the CBE Department Ultimate teams over the years for giving me motivation to exercise. Thanks to Vanessa Grosskopf, Dan Noreika, Daniel Mendez, and Brian Richards for giving me places to stay in Berkeley during my trip there for training last summer. Thanks to my friends from college and high school Peter Nguyen, Brad Herbig, John Gideon, Luke Widolff, Michael Puthoff, Chelsea Pflum, and Michelle Amiott for keeping in touch. It means a lot.

Table of Contents

List of Figures and Tables

Chapter 1: Motivation and Goals

1.1. Mitigating Climate Change Under Land Use Constraints

The Intergovernmental Panel on Climate Change has stated that warming of the climate system is clearly the result of human activities and recommends limiting warming to less than 2°C relative to pre-industrial conditions by reducing greenhouse gas emissions to prevent severe, pervasive, and irreversible impacts for people and ecosystems (IPCC 2014). Towards this goal, first-generation biofuels like corn ethanol have been proposed as "carbon neutral" alternatives to petroleum fuel sources. However, large scale production of biofuels from crops would actually increase greenhouse gas emissions relative to petroleum sources due to land use changes as forest and grassland are converted to new cropland (Searchinger et al. 2008). Political limits on atmospheric CO_2 concentration while including emissions from land use change is predicted to increase afforestation and decrease the available cropland resulting in increased food prices (Wise et al. 2009). Consequently, methods for increasing photosynthetic production that fall outside these constraints of land use are essential to mitigating climate change while feeding a growing population.

Like plants, cyanobacteria can be cultivated photoautotrophically such that they produce organic carbon directly from CO_2 and sunlight. Like many crops, cyanobacteria store organic carbon by accumulating starch (in the form of glycogen) which can easily be processed into soluble sugars for heterotrophic bioprocesses like yeast ethanol fermentation (Aikawa et al. 2014; Möllers et al. 2014; Song et al. 2016). In addition, their metabolism can be manipulated to produce fuel molecules (Liao et al. 2016) and commodity chemicals (Angermayr, Gorchs Rovira, and Hellingwerf 2015) directly. While plants utilize nutrients from the rich soil surrounding their roots, cyanobacteria consume nutrients from the surrounding aqueous medium. This allows potential cultivation of cyanobacteria on traditionally non-arable land using seawater supplemented with nutrients from waste sources (Korosh et al. 2017), thus

increasing photosynthetic productivity without the land use problems inherent in first-generation biofuel processes.

This work investigates process factors affecting the implementation and scale-up of photoautotrophic cyanobacterial cultivation processes. The two major costs affecting bioprocess economics are (1) the product stream composition entering downstream processing and (2) capital costs associated with microbial cultivation (Yenkie et al. 2016; Yenkie, Wu, and Maravelias 2017). To reduce these costs, a cyanobacterial cultivation process should seek to maximize productivity and final concentration of products of interest while minimizing the costs of cultivation equipment. Outdoor open ponds are the least capital intensive cyanobacterial cultivation vessel and were therefore the target implementation considered in this work.

The work described in this work addresses two important issues associated with outdoor open pond cultivation of cyanobacteria. First, towards maximizing areal productivity and final concentration of products of interest we developed and evaluated a theoretical framework for the analysis of cyanobacterial growth and product secretion when light is the sole limiting substrate (**Figure 1.1A**). Second, as open ponds risk introduction of industrial cyanobacterial strains to nearby natural ecosystems we developed a containment mechanism for cyanobacteria by exploiting the CO_2-concentrating mechanism (CCM) to introduce a requirement for high CO_2 concentration (**Figure 1.1B**).

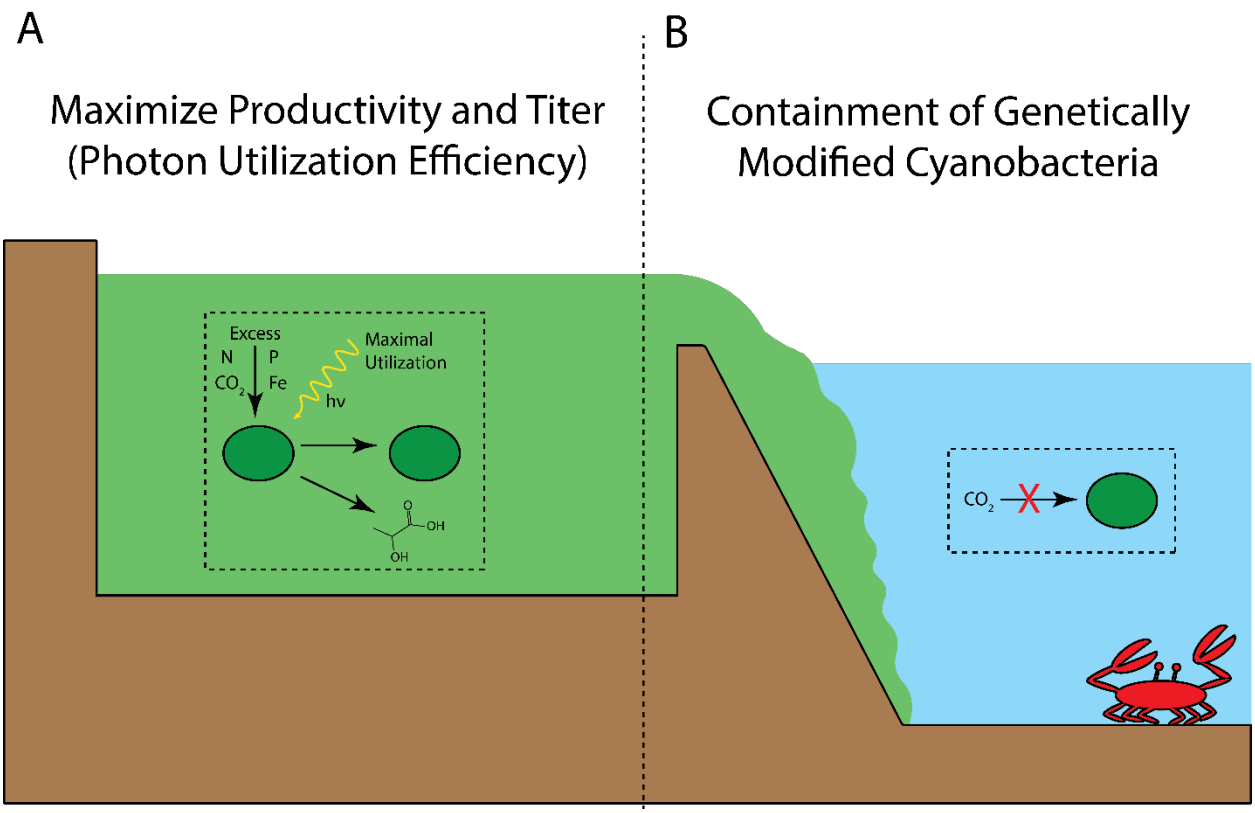

Figure 1-1. Project Overview. This work focused on two areas of study related to open pond cultivation of cyanobacteria. (A) Cyanobacterial growth and chemical production were studied in the presence of excess soluble nutrients to maximize photon utilization efficiency. (B) A containment mechanism was developed for cyanobacteria in which a high CO_2 concentration requirement was introduced to prevent propagation outside of a high CO_2 industrial environment.

1.2. Project Overview

Chapter 2 provides a critical review of the literature beginning with a comparison of heterotrophic and photoautotrophic cultivation processes to highlight key differences that motivate the focus of this research. The theory of bacterial growth and bioenergetics is reviewed to give context for investigation of light-limited or CO_2-limited growth. Background is provided into experiments performed on light-limited growth of photoautotrophic organisms in continuous culture. An overview of CO_2 utilization in cyanobacteria is provided including the CO_2-concentrating mechanism.

Chapter 3 investigates light-limited growth and chemical production of cyanobacteria in batch culture. We first identify experimental conditions in which light is the sole limiting substrate. We then discuss a theoretical framework capturing the phenomena that drive the phases of light-limited growth in batch

culture. We then present demonstrative experiments to understand the key factors affecting photon utilization efficiency.

Chapter 4 provides a model for CO_2-limited growth in cyanobacteria with an emphasis on the function of the CCM. We investigate the dependence of CO_2-fixation potential on the concentration of inorganic carbon in the media for wild type cyanobacteria as well as a mutant lacking the CCM to understand the required CO_2 concentrations for industrial cyanobacteria cultivation.

Chapter 5 investigates a containment mechanism based on the results of the modeling work described in **Chapter 4.** The proposed mechanism creates a requirement for high CO_2 concentration by eliminating essential CCM genes. The resulting mutants thrive in a high CO_2 environment, but are unable to propagate in ambient CO_2 conditions.

Chapter 6 provides a summary of the results, reflecting on the work described in the previous chapters and providing ideas of future directions.

Appendix A describes the development of photobioreactor systems used in some experiments described in this work.

Appendix B describes my work involved with random barcode transposon insertion sequencing (RB-TnSeq) in *Pseudomonas putida*. This work is unrelated to the main goal of this work, but this chapter proposes ways in which this method could be applied to problems relevant to cyanobacterial chemical production processes.

1.3. References

Aikawa, Shimpei et al. 2014. "Glycogen Production for Biofuels by the Euryhaline Cyanobacteria *Synechococcus* Sp. Strain PCC 7002 from an Oceanic Environment." *Biotechnology for Biofuels* 7(88).

Angermayr, S. Andreas, Aleix Gorchs Rovira, and Klaas J. Hellingwerf. 2015. "Metabolic Engineering of Cyanobacteria for the Synthesis of Commodity Products." *Trends in Biotechnology* 33(6):352–61.

IPCC. 2014. Climate Change 2014: Synthesis Report. Contribution of Working Groups I, II and III to the Fifth Assessment Report of the Intergovernmental Panel on Climate Change.

Korosh, Travis C., Andrew Dutcher, Trina McMahon, and Brian F. Pfleger. 2017. In Preparation.

Liao, James C., Luo Mi, Sammy Pontrelli, and Shanshan Luo. 2016. “Fuelling the Future: Microbial Engineering for the Production of Sustainable Biofuels.” *Nature Reviews Microbiology* 14:288–304.

Möllers, K.Benedikt, David Cannella, Henning Jørgensen, and Niels-Ulrik Frigaard. 2014. “Cyanobacterial Biomass as Carbohydrate and Nutrient Feedstock for Bioethanol Production by Yeast Fermentation.” *Biotechnology for Biofuels* 7:64.

Searchinger, Timothy et al. 2008. “Use of U.S. Croplands for Biofuels Increases Greenhouse Gases Through Emissions from Land-Use Change.” *Science* 319:1238–41.

Song, Kuo, Xiaoming Tan, Yajing Liang, and Xuefeng Lu. 2016. “The Potential of *Synechococcus Elongatus* UTEX 2973 for Sugar Feedstock Production.” *Applied Microbiology and Biotechnology* 100:7865.

Wise, Marshall et al. 2009. “Implications of Limiting CO_2 Concentrations for Land Use and Energy.” *Science* 324(5931):1183–86.

Yenkie, Kirti M. et al. 2016. “A Roadmap for the Synthesis of Separation Networks for the Recovery of Bio-Based Chemicals: Matching Biological and Process Feasibility.” *Biotechnology Advances* 34(8):1362–83.

Yenkie, Kirti M., Wenzhao Wu, and Christos T. Maravelias. 2017. “Synthesis and Analysis of Separation Networks for the Recovery of Intracellular Chemicals Generated from Microbial-Based Conversions.” *Biotechnology for Biofuels* 10:119.

Chapter 2: Critical Review of the Literature

Part of this chapter is adapted from *Biotechnology Advances*, Vol. 34, No. 8, Yenkie, Kirti M; Wu, WenZhao; Clark, Ryan L; Pfleger, Brian F; Root, Thatcher W; Maravelias, Christos T; A roadmap for the synthesis of separation networks for the recovery of bio-based chemicals: Matching biological and process feasibility, p. 1362-1383, Copyright 2016, with permission from Elsevier.

2.1. Overview

From a sustainability point of view, the goal of any bioprocess is to reduce the net increase in atmospheric CO_2 by converting it to useful products using energy from the sun. Traditional heterotrophic bioprocesses utilize plants to capture solar energy and store it in the organic carbon molecules that make up plant biomass. This plant biomass is then processed into soluble sugars that can be metabolized by heterotrophic microorganisms engineered for production of a molecule of interest, be it a pharmaceutical product (*i. e.* artemisinin) or a commodity product (*i. e.* ethanol) (**Figure 2-1, Red Arrows**). Cyanobacterial or other photoautotrophic bioprocesses follow an alternative route in which CO_2 from industrial processes or from the atmosphere is fed to acres of cyanobacterial culture that has been engineered to synthesize products of interest using energy from sunlight (**Figure 2-1, Blue Arrows**). Integration of these two processes is a further possibility wherein cyanobacterial biomass can be utilized by heterotrophic microorganisms for product synthesis at higher titer (**Figure 2-1, Purple Arrow**). While there are other alternative strategies for converting atmospheric CO_2 to desired chemicals (Liao et al. 2016), this chapter will focus on the aforementioned strategies, namely:

(i) Indirect CO_2 utilization by heterotrophs – atmospheric carbon dioxide is captured in terrestrial plant biomass, which is subsequently harvested, deconstructed into sugar-rich feedstocks, and converted to central metabolites by heterotrophic microorganisms

(ii) Direct CO_2 utilization by photoautotrophs - carbon dioxide from industrial process waste is captured and fixed to central metabolites by photoautotrophic microorganisms.

The first part of this analysis will focus on feedstock processing and microbial cultivation, in which CO_2 is captured and converted into central metabolites inside of the microbes. The second part of this analysis

will discuss the current state of metabolic engineering to upgrade these central metabolites into desired products with a focus on the differences between heterotrophic and photoautotrophic microorganisms. This section will include case studies for the development of (1) heterotrophs engineered to produce artemisinic acid and (2) cyanobacteria engineered to produce ethanol to compare the different challenges for heterotrophic and photoautotrophic metabolic engineering.

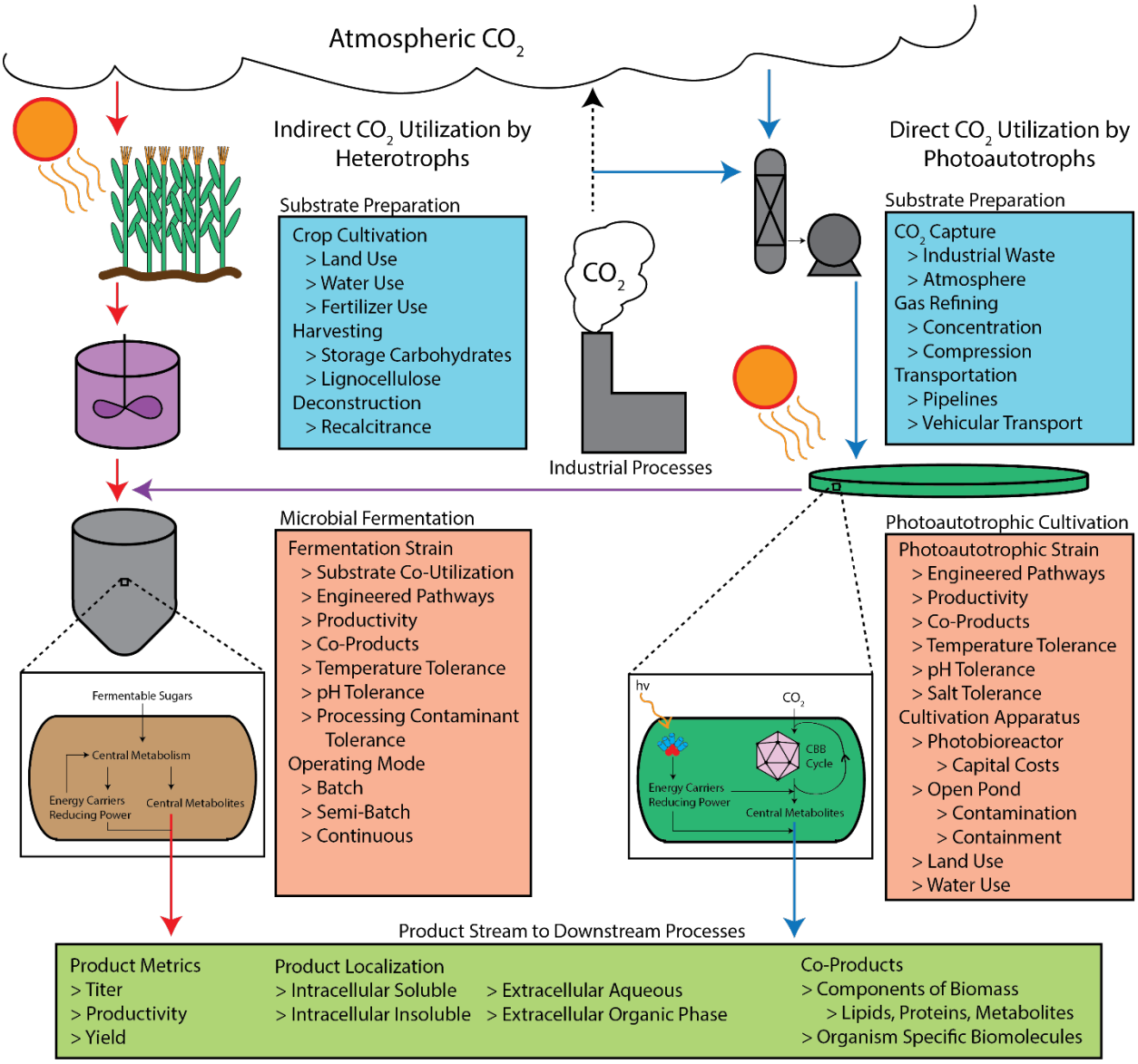

Figure 2-1. Bioprocessing Overview. Atmospheric CO_2 can be converted into useful products through several processes including direct utilization by photoautotrophs (Blue Arrows) or indirect utilization by heterotrophic conversion of crops (Red Arrows) or cyanobacterial biomass (Purple Arrow). The boxes list key factors affecting process economics.

2.2. Atmospheric CO_2 to Central Metabolites

Indirect CO_2 Utilization by Heterotrophs

Accessible storage carbohydrates, such as corn starch or sugar cane juice, are historically the most commonly used sources of sugar for microbial fermentation due to their ease of saccharification (Bothast and Schlicher 2005; Canilha et al. 2012). Lignin and structural carbohydrates including cellulose and hemicellulose are more recalcitrant, but are abundant in woody biomass waste products from forest

management and agricultural byproducts, such as corn stover or sugarcane bagasse. These substrates are converted into soluble sugars using a number of strategies both biological (Liao et al. 2016; Lynd et al. 2002) and physicochemical (Huber, Iborra, and Corma 2006).

Technoeconomic and life-cycle analyses have been performed for the conversion of plant-based carbohydrates into fermentable sugars, primarily for the production of ethanol (Gnansounou and Dauriat 2010; Hamelinck, Hooijdonk, and Faaij 2005; Humbird et al. 2011). Depending on the composition of the initial biomass as well as the processing conditions, the stream entering the microbial cultivation will contain some combination of soluble sugars (primarily hexoses and pentoses) and potential fermentation inhibitors (phenolic compounds, terpenoids, organic acids, and reduced sugar products) whose concentration will affect the yield and productivity in the following microbial cultivation (Hahn-Hagerdal et al. 2001).

Microbial fermentation of glucose derived from corn starch, primarily for the production of ethanol, is a mature technology (Bothast and Schlicher 2005; Jullesson et al. 2015). Through heterologous expression of transporters and enzymes, industrial microorganisms can be engineered to consume other sugars, including the hemicellulose derived xylose, with similar yields of central metabolites (Hahn-Hagerdal et al. 2001). By overcoming catabolite repression mechanisms that lead to preferential utilization of glucose, co-utilization of mixed sugar substrates could provide higher productivity (Kim et al. 2012). Once the soluble sugars are converted to central metabolites, reducing power, and energy carriers, molecules of interest can be produced through metabolically engineered pathways as discussed later.

Direct CO_2 Utilization by Photoautotrophs

Photoautotrophic microorganisms, including cyanobacteria and microalgae, use photosynthetic pigments to capture photons from sunlight. The captured light energy is used to split water, reduce electron carriers, and produce a proton gradient (Lea-Smith et al. 2015). The process ultimately leads to the generation of NADPH and ATP that is used to assimilate CO_2 in the form of 3-phosphoglycerate and

subsequently G3P through the Calvin-Benson-Bassham Cycle (Nelson and Cox 2008). These metabolites can then be upgraded to products of interest through metabolic pathways analogous to those found in heterotrophic organisms.

As the two major substrates for phototrophic process are CO_2 and light, the considerations are very different from heterotrophic conversion of sugar. While phototrophic microorganisms can grow in ambient air, high-concentration CO_2 streams can help deliver CO_2 to the bioreactors at a rate necessary for large scale cultivations (Clark et al. 2014). These high-concentration streams can be generated by capturing CO_2 from industrial emissions through emerging technologies (reviewed by (Herron et al. 2015)) and transported to the photoautotrophic cultivation.

Efficient light delivery is equally essential for enhanced productivity and CO_2-fixation by phototrophs and will ultimately limit the final biomass titers of photoautotrophic cultures to values much lower than heterotrophic cultures. Many photobioreactor designs have been considered for their ability to deliver light to photoautotrophic cultures, including open ponds, flat plate, tubular and column types (Brennan and Owende 2010). The most important characteristic of a photobioreactor for determining productivity and titer is the ratio of the illuminated surface area to the volume (Lee et al. 2014). An open pond cultivation scheme could alleviate the cost-prohibitive capital investment associated with complex photobioreactors (Jones and Banholzer 2014). An expansion on recent work on the containment of genetically modified microorganisms could assuage fears of environmental contamination associated with open pond cultivation (Clark et al. 2014; Mandell et al. 2015).

2.3. Upgrading Central Metabolites to Desired Products

Once atmospheric carbon has been captured and converted to central metabolites within industrial organisms through the previously described processes, a vast number of metabolic pathways can be used to upgrade these molecules into chemicals of interest. A lot of work has been done on enhancement of yield and productivity of target molecules in microbial cultivations through metabolic engineering of these

pathways (Angermayr, Gorchs Rovira, and Hellingwerf 2015; Knoop and Steuer 2015) and these can vary greatly based on the host organism (Angermayr et al. 2015; Jullesson et al. 2015; Knoop and Steuer 2015; Liao et al. 2016; Xue and He 2015).

When a molecule of interest is produced by the cell, it is then localized to one of four phases through a combination of active and passive processes: (1) intracellular soluble (*i. e.* soluble metabolites), (2) intracellular insoluble (*i. e.* aggregates in an inclusion body or insoluble storage granules), (3) extracellular soluble in the aqueous medium (*i. e.* secreted metabolites), or (4) extracellular and partitioned into an organic phase. Most products of interest are initially produced intracellularly in the cytoplasm of the cell and elevated concentrations of these molecules can provide negative feedback on producing pathways and/or negatively impact cell physiology (Jones, Hernandez Lozada, and Pfleger 2015). Some high molecular weight products, such as polyhydroxyalkanoates (PHAs) or glycogen, aggregate inside the cell (Agnew et al. 2012; Aikawa et al. 2014). Some products are localized extracellularly to the aqueous medium through passive diffusion or through active transport by protein transporters (Jones et al. 2015). Depending on the chemical equilibrium, products with low water-solubility will partition into an organic phase; this process can be facilitated through co-culturing with a metabolically inert organic phase (Kato et al. 2017; Newman et al. 2006; Youngquist et al. 2013).

The characteristics of the process stream entering separations, including product location and titer, will largely determine the necessary separation process (**Figure 2-1**) (Yenkie et al. 2016; Yenkie, Wu, and Maravelias 2017). The composition of impurities will also have significant impact on downstream processing. Product streams will contain co-product molecules (**Tables 2-1 and 2-2**) as well as components of biomass, including lipids, proteins, and other organism specific biomolecules (Wang et al. 2013). The concentrations of these impurities can be minimized by metabolic engineering and bioreactor engineering to maximize the yield of desired product on the substrate of choice (Youngquist et al. 2012).

Table 2-1 gives examples of products produced in heterotrophic organisms that are typically localized into each of the four phases. **Table 2-2** gives examples of similar products produced in photoautotrophic processes for comparison. The first major difference to note is that biomass titers and productivities for photoautotrophic processes are an order of magnitude lower than for heterotrophic bioprocesses. As will be discussed in **Chapter 3**, biomass titer in photoautotrophic bioprocesses is limited by the volumetric photon delivery rate, because at sufficient density, all photons are used for cellular maintenance and no energy remains for the synthesis of new biomass. This is intuitively important for products in either of the intra-cellular phases as the product is a component of the biomass, so biomass metrics directly affect the product composition of the process stream going into separations. Thus, for intra-cellular products in photoautotrophs, the key to minimizing separation costs is to maximize biomass titer as well as product content of the biomass. Capital costs will largely be determined by the biomass productivity, which is limited by the volumetric photon delivery rate.

Photoautotrophic biomass productivity is also informative for extra-cellular products as the maximum achievable rate of product synthesis from CO_2 is limited by the rate of CO_2-fixation just as with biomass. Due to this limitation, engineered photoautotrophs secrete extra-cellular products at productivities several orders of magnitude lower than in heterotrophic systems (**Table 2-2**). However, if production of a desired product can be decoupled from biomass production as has been shown in a few cases (Kopka et al. 2017), then the potential product titer could be much higher than the biomass titer. Thus, for extra-cellular products in photoautotrophs, the key to minimizing separation costs is to choose a product that can be easily separated from the culture medium and maximize product titer. Capital costs will largely be determined by productivity of the product of interest, which can be maximized by decoupling the pathway of interest from biomass production.

Table 2-1. Sample metrics for heterotrophic microbial processing with details about product localization, microbial species, typical biomass titers, productivity, yields, and potential co-products.

Energy source		Carbon source		Biomass titer		Biomass productivity	
Organic carbon		Organic carbon		High (100 – 268 g/L)		High (0.01 – 6.6 g/L h)	
Localization & solubility	Product	Species	Titer (g/L)	Productivity (g/L h)	Yield	Co-products	Reference
Intra-cellular (insoluble)	Lipids, PHAs (25 – 80% CDW)	Bacteria (A. latus), yeast (C. laurentii)	10–200	0.01 –2.5	0.1 –0.3 g/g on different substrates	Organic acids	Castanha et al. (2013), Choi and Lee (1997)
Intra-cellular (soluble)	Proteins (2 –70% CDW)	Bacteria (E. coli), yeast, Archaea	5–268	0.01 –6.6	Various	Similar proteins	Hatti-Kaul and Mattiasson (2003), Riesenberg and Guthke (1999)
Extra-cellular (organic/insoluble)	Fatty alcohols	Bacteria (E. coli)	1.6	0.01	0.13 g/g glucose	Fatty acids, acetate	Youngquist et al. (2013)
Extra-cellular (aqueous/soluble)	1,3-Propanediol	Bacteria (C. butyricum , E. Coli , K. pneumoneae)	35–80	1.5 –3	0.72 –0.88 mol/mol glycerol	Ethanol, lactic acid, succinic acid, butanediol	Zeng and Biebl (2002)

Table 2-2. Sample metrics for photoautotrophic microbial processing with details about product localization, microbial species, typical biomass titers, productivity, and potenial co-products.

Energy source		Carbon source			Biomass titer		Biomass productivity	
Light		Inorganic carbon (CO_2 and HCO_3^-)			Low (0.1 – 10 g/L)		Low (0.002 – 0.2 g/L-h)	
Localization & solubility	Product	Species	Titer (g/L)	Productivity (g/L h)	Yield	Co-products	Reference	
Intra-cellular (insoluble)	Oils, glycogen (39 –70% CDW)	Algae (C. vulgaris , B. braunii , S. acutus , P. incisa) Cyanobacteria (Synechococcus , Synechocystis)	0.1–10	0.002 –0.2	N/A	Secondary metabolites	Aikawa et al. (2014), Li et al. (2008)	
Intra-cellular (soluble)	Proteins, B phycoerythrin (2 –70% CDW)	Algae (P. cruentum), Cyanobacteria (Synechococcus , Synechocystis)	0.1–10	0.002 –0.2	N/A	Similar proteins, secondary metabolites	Ruiz Ruiz et al. (2013)	
Extra-cellular (organic/insoluble)	Fatty alcohols	Cyanobacteria (Synechocystis sp. PCC 6803)	0.002	0.000005	N/A	Fatty acids, secondary metabolites	Yao et al. (2014)	
Extra-cellular (aqueous/soluble)	1,3 Propanediol	Cyanobacteria (S. elongatus sp. PCC 7942)	0.29	0.0005	N/A	Glycerol, secondary metabolites	Hirokawa et al. (2016), Wang et al. (2001)	

Another key difference between heterotrophic and photoautotrophic bioprocesses is the concept of yield. In heterotrophic bioprocesses, both energy and carbon are provided by the organic substrate (*i. e.* sugar), so the yield of product on the organic carbon substrate is a useful metric as it determines the cost of raw material that needs to be fed into the process to achieve a desired amount of product (**Table 2-1**). For carbon limited heterotrophic bioprocesses, an upper limit on yield can be determined simply through stoichiometry. In photoautotrophic processes, energy is provided by photons and carbon is provided by CO_2. Decoupling energy and carbon complicated the concept of yield. A carbon yield is not particularly useful as the CO_2 feed requirement for a photoautotrophic bioprocess for a given amount of product is mostly affected by the rate of CO_2 leaving the system due to inefficiencies in the cultivation scheme, not by any biological process. Because photoautotrophic bioprocesses should be light-limited, yield of product on photons is a more useful metric, which will be discussed further in **Chapter 3**.

While many products have been targets for metabolic engineering, we will now consider two case studies to better understand the differences in engineering efforts for the development of heterotrophic and photoautotrophic production processes. In the first case, we will consider the development of *E. coli* and yeast production of the artemisinic acid precursor to the malaria drug artemisinin, an effort that has reached commercial production in recent years by Amyris (Paddon and Keasling 2014). In the second case, we will consider the development of cyanobacterial production of ethanol, an effort that has been industrially pursued by Joule Unlimited and Algenol, but appears to have lost appeal as Joule Unlimited merged with Red Rock Biofuels in early 2016 to focus on biomass to fuel technology (Joule 2016) and Algenol has changed focus to biomass-associated products such as pigments and nutraceuticals (Lane 2017). In each case, we will consider the metabolic engineering and cultivation strategies used to improve titers and productivities from zero to the current highest reported values. We will then highlight key differences between the two cases that are representative of the field in general.

Case Study: Artemisinic Acid in Heterotrophs

Artemisinic acid is produced from amorphadiene, one of a class of molecules called terpenoids that can be produced from isopentenyl pyrophosphate (IPP) and dimethylallyl pyrophosphate (DMAPP) which are products of the deoxyxylulose 5-phosphate (DXP) pathway in *E. coli* (Paddon and Keasling 2014). Eukaryotic organisms have an alternative mevalonate-dependent pathway (MEV) for the production of IPP and DMAPP. Martin et al. sought to produce amorphadiene in *E. coli* by expressing an amorphadiene synthase along with the non-native MEV pathway, which was hypothesized to be decoupled from regulation, unlike the native DXP pathway (Martin et al. 2003). Ro et al. built upon this result by expressing the engineered MEV pathway in baker's yeast (*S. cerevisiae*) and expressing a cytochrome P450 monooxygenase from *A. annua* to convert the resulting amorphadiene to artemisinic acid (Ro et al. 2006). Chang et al. used a similar strategy in *E. coli* to produce artemisinic acid and 8-hydroxycadinene, an alternative product using the same pathway but a different cytochrome P450 hydroxylase, showing the

general applicability of this metabolic engineering strategy to other terpenoids (Chang et al. 2007). To increase amorphadiene production, Newman et al. cultured *E. coli* in a dual phase bioreactor where the amorphadiene product was partitioned into an organic phase during cultivation, thus preventing evaporative loss of the product (Newman et al. 2006). This innovative culturing technique enabled all future improvements as all subsequent studies used this organic phase co-culturing strategy (**Table 2-3**). Lenihan et al. increased artemisinic acid production to 1.7 mg L^{-1} hr^{-1} (2.5 g L^{-1} titer) in *S. cerevisiae* by limiting flux through the competing sterol biosynthesis pathway as well as optimizing the culture medium and oxygenation (Lenihan et al. 2008). Tsuruta et al. increased amorphadiene production to 225 mg L^{-1} hr^{-1} (27 g L^{-1} titer) in *E. coli* by expressing more effective enzymes for bottleneck reactions in the MEV pathway and inducing nitrogen-limitation in a fed-batch bioreactor (Tsuruta et al. 2009). Finally, Paddon et al. increased artemisinic acid production in *S. cerevisiae* to industrially relevant levels of 179 mg L^{-1} hr^{-1} (25 g L^{-1} titer) by improving enzyme activity in bottleneck reactions in the MEV pathway and developed a chemical process for the conversion of artemisinic acid to the desired pharmaceutical product artemisinin (Paddon et al. 2013), a process which was eventually commercialized by Amyris (Paddon and Keasling 2014). This research and development process, summarized in **Table 2-3**, occurred over the course of 10 years (by publication dates), bringing the process from low production of the precursor, amorphadiene (2003), to industrially relevant production of the final product, artemisinin, with a two order of magnitude increase in product titer (2013).

Table 2-3. Overview of Heterotrophic Artemisinic Acid Process Development

Amorphadiene		Artemisinic Acid		Organism	Strategy	Equipment	Reference
Titer	Productivity	Titer	Productivity				
0.11	9	-	-	*E. coli*	Produce amorphadiene using amorphadiene synthase and the mevalonate pathway from *S. cerevisiae*	96-Well Plate	Martin, et al, 2003
0.15	1	0.12	1.3	*S. cerevisiae*	Produce artemisinic acid using mevalonate pathway and cytochrome P450 monooxygenase from *A. annua*	1 L Bioreactor	Ro et al, 2006
0.48	8	-	-	*E. coli*	Increase amorphadiene production by partitioning it into dodecane organic phase during cultivation	10 L Bioreactor with Organic Phase	Newman, et al, 2007
-	-	0.11	-	*E. coli*	Produce artemsinic acid using cytochrome P450 amorphadiene oxygenase *Produce 8-hydroxycadinene using cytochrome P450 8-cadinene hydroxylase*	Shake Flasks with Organic Phase	Chang, et al, 2007
-	-	2.5	1.7	*S. cerevisiae*	Increase artemisinic acid production by limiting competition from sterol biosynthesis pathway and optimizing media and oxygenation	Fed-batch 2 L Bioreactor	Lenihan, et al, 2008
27	225	-	-	*E. coli*	Increase amorphadiene production using improved enzymes and nitrogen-limitation	Fed-batch 2 L Bioreactor	Tsuruta, et al, 2009
13	144	25	179	*S. cerevisiae*	Increase artmesinic acid production using improved enzymes *Produce artemsinin from artemisinic acid in a chemical process*	Fed-batch 2 L Bioreactor	Paddon, et al, 2013

Titer in g L^{-1}. Productivity in mg L^{-1} hr^{-1}.

Case Study: Ethanol in Cyanobacteria

In cyanobacteria, ethanol can be produced from the central metabolite pyruvate using a pyruvate decarboxylase (pdc) to produce acetaldehyde, which can be subsequently converted to ethanol by an alcohol dehydrogenase (adh) (Dexter et al. 2015). Deng et al. expressed pdc and adh from *Z. mobilis* in the freshwater cyanobacterium *Synechococcus elongatus* sp. PCC7942 and saw slow ethanol production accumulating to a titer of 0.23 g L^{-1} (Deng and Coleman 1999). Ten years later, Dexter et al. repeated this strategy in another freshwater cyanobacterium, *Synechocystis* sp. PCC6803, this time in a photobioreactor rather than a shake flask, and saw a modest increase in productivity and titer (**Table 2-4**). Gao et al. expressed the *Z. mobilis* pdc in a strain of *Synechocystis* sp. PCC6803 overexpressing its native adh, and grew the resulting strain in a photobioreactor bubbled with 5% CO_2, achieving an order of magnitude increase in both productivity and titer of ethanol, likely due to the elimination of CO_2-limitation (Gao et al. 2012). Dienst et al. grew this same strain in a photobioreactor with 10% CO_2 where the irradiance was increased proportionally to the cell density, which resulted in only a minimal increase in productivity. They also performed a microarray transcriptomics study which could be informative for future engineering efforts (Dienst et al. 2014). Kopka et al. expressed the *Z. mobilis* pdc and the *Synechocystis* sp. PCC6803 adh in the marine cyanobacterium *Synechococcus* sp. PCC7002 and reported a productivity and titer on the same order of magnitude as previous studies, but slightly lower. Systems level analyses performed in this study could inform further engineering (Kopka et al. 2017). This research and development process, summarized in **Table 2-4**, occurred over the course of 18 years (by publication dates), increasing the productivity of ethanol by 50-fold and the titer of ethanol 25-fold, with the major breakthrough appearing to be the elimination of CO_2-limitation by supplementation with a high CO_2 gas phase.

Table 2-4. Overview of Cyanobacterial Ethanol Process Development

Ethanol		Organism	Irradiance	Strategy	Equipment	Reference
Titer	Productivity					
0.23	4	*S. elongatus* sp. PCC7942	50 (Fluorescent)	Expression of pyruvate decarboxylase and alcohol dehydrogenase from *Z. mobilis*	Flask, Ambient Air	Deng, et al, 1999
0.46	77	*Synechocystis* sp. PCC6803	200 (Fluorescent)	Expression of pyruvate decarboxylase and alcohol dehydrogenase from *Z. mobilis*	Photobioreactor (3 L), Ambient Air	Dexter, et al, 2009
5.5	212	*Synechocystis* sp. PCC6803	100 (Fluorescent)	Expression of pyruvate decarboxylase from *Z. mobilis* and overexpression of native alcohol dehydrogenase	Photobioreactor (30 mm diameter), 5% CO_2	Gao, et al, 2012
4.7	261	*Synechocystis* sp. PCC6803	100+*† (Fluorescent)	Expression of pyruvate decarboxylase from *Z. mobilis* and overexpression of native alcohol dehydrogenase, Microarray transcriptomics study	Photobioreactor (0.5 L), 10% CO2	Dienst, et al, 2014
2.0	119	*Synechococcus* sp. PCC7002	230‡ (Fluorescent)	Expression of pyruvate decarboxylase from *Z. mobilis* and overexpression of alcohol dehydrogenase from *Synechocystis* sp. PCC 6803, Systems analysis	Photobioreactor (50 mm diameter), 10% CO2	Kopka, et al, 2017

Titer in g L^{-1}. Productivity in mg L^{-1} day^{-1}. Irradiance in µmol m^{-2} s^{-1}. *In this study, the irradiance was increased with time to maintain 100 µmol m^{-2} s^{-1} OD_{730}^{-1}. ‡In these studies, CO_2 was used to control the pH of the photobioreactor.

Comparison of the Cases

I would like to highlight three key comparisons between the two cases. The first comparison is related to innovations in cultivation equipment. In the first case (artemisinic acid in heterotrophs), the researchers determined that product evaporation was a key limitation relatively early in the development process and implemented a simple solution of two-phase cultivation that enabled many of the future metabolic engineering advances (Newman et al. 2006). In the second case (ethanol in cyanobacteria), CO_2-limitation was eventually identified as a bottleneck in ethanol product, which was corrected by supplementing with a high CO_2 gas phase, accounting for the only significant improvement in ethanol production since the system was first studied in 1999 (Gao et al. 2012).

The second comparison is related to metabolic engineering strategies. In the artemisinic acid case, the researchers first attempted to maximize production of the precursor amorphadiene from the common central metabolite acetyl-CoA. This allowed the researchers to eliminate bottlenecks in a simpler system before attempting to synthesize the final product, artemisinic acid. This strategy of producing precursors to desired products and then converting these precursors to desired products has been successfully applied in other systems (Galanie et al. 2015; McKeague et al. 2016). In contrast, research on ethanol production in cyanobacteria focused on directly producing the product ethanol. While the ethanol pathway was much simpler than the artemisinic acid case, perhaps a better understanding of metabolic bottlenecks could have arisen from first increasing production of the precursor pyruvate. In addition, just as Chang et al. were able to produce an alternative product (8-hydroxycadinene) in the amorphadiene

producing strain of *E. coli*, a high pyruvate producing cyanobacterial strain could be useful for production of alternative products derived from pyruvate, such as lactic acid (Angermayr et al. 2014; Gordon et al. 2016).

The final comparison is related to process scale-up. In the artemisinic acid case, the researchers identified 25 g L^{-1} of artemisinic acid as the target density for a commercially relevant process and worked towards that goal, keeping scalability as an important consideration (Paddon and Keasling 2014). Although the researchers chose not to report product yield on sugars, it would be simple to calculate from media compositions if this were identified as an important parameter, as would be the case with most non-pharmaceutical products. In the ethanol case, a target productivity or titer for commercialization is not identified, providing no concept of proximity to a goal. Additionally, the methods sections for most studies in **Table 2-4** and most cyanobacterial metabolic engineering studies in general do not provide enough details (reactor geometry, light quality, etc.) to determine a theoretical yield of product on photons or to determine a scaled-up productivity.

2.4. Research Opportunities

Quantifying Cyanobacterial Growth and Chemical Production

As highlighted in the previous sections, there is a serious need for a standardized way to quantify cyanobacterial growth and chemical production. Because CO_2 and soluble nutrients can be provided from waste streams, a standardized cyanobacterial strain evaluation method should quantify growth and chemical production with light as the sole limiting substrate. The resulting analysis should enable prediction of scaled-up growth and chemical production from laboratory experiments as well as comparison to theoretical limits. These questions are addressed in **Chapter 3** of this work.

Understanding Cyanobacterial Growth in Excess CO_2

As mentioned previously, the most significant breakthrough in cyanobacterial chemical production came from eliminating CO_2-limitation. It is thus important to understand how cyanobacteria grow under

differing CO_2 concentrations in the context of the molecular mechanisms for CO_2 acquisition. This question is addressed in **Chapter 4** of this work.

Containment of Cyanobacteria

With any scaled-up cyanobacteria cultivation process, the containment of engineered strains is a major concern. An ideal containment mechanism would allow the engineered cyanobacteria to thrive inside of the industrial process, but be unable to propagate in the surrounding environment. A containment mechanism utilizing the difference in CO_2 concentration between an industrial process and the surrounding environment is investigated in **Chapter 5** of this work.

2.5. References

Agnew, Daniel E., Amanda K. Stevermer, J. Tyler Youngquist, and Brian F. Pfleger. 2012. "Engineering *Escherichia Coli* for Production of C12–C14 Polyhydroxyalkanoate from Glucose." *Metabolic Engineering* 14(6):705–13.

Aikawa, Shimpei et al. 2014. "Glycogen Production for Biofuels by the Euryhaline Cyanobacteria *Synechococcus* Sp. Strain PCC 7002 from an Oceanic Environment." *Biotechnology for Biofuels* 7:88.

Angermayr, S.Andreas et al. 2014. "Exploring Metabolic Engineering Design Principles for the Photosynthetic Production of Lactic Acid by *Synechocystis* Sp. PCC6803." *Biotechnology for Biofuels* 7:99.

Angermayr, S. Andreas, Aleix Gorchs Rovira, and Klaas J. Hellingwerf. 2015. "Metabolic Engineering of Cyanobacteria for the Synthesis of Commodity Products." *Trends in Biotechnology* 33(6):352–61.

Bothast, R. J. and M. A. Schlicher. 2005. "Biotechnological Processes for Conversion of Corn into Ethanol." *Applied Microbiology and Biotechnology* 67(1):19–25.

Brennan, Liam and Philip Owende. 2010. "Biofuels from microalgae—A Review of Technologies for Production, Processing, and Extractions of Biofuels and Co-Products." *Renewable and Sustainable Energy Reviews* 14(2):557–77.

Canilha, Larissa et al. 2012. "Bioconversion of Sugarcane Biomass into Ethanol: An Overview about Composition, Pretreatment Methods, Detoxification of Hydrolysates, Enzymatic Saccharification, and Ethanol Fermentation." *Journal of Biomedicine and Biotechnology* 2012.

Castanha, Rodrigo Fernandes, Lilia Aparecida Salgado de Morais, Adriano Pinto Mariano, and Regina Teresa Rosim Monteiro. 2013. "Comparison of Two Lipid Extraction Methods Produced by Yeast in Cheese Whey." *Brazilian Archives of Biology and Technology* 56(4):629–36.

Chang, Michelle C. Y., Rachel A. Eachus, William Trieu, Dae-Kyun Ro, and Jay D. Keasling. 2007. "Engineering *Escherichia Coli* for Production of Functionalized Terpenoids Using Plant P450s." *Nature Chemical Biology* 3(5):274–77.

Choi, Jong-il and Sang Yup Lee. 1997. “Process Analysis and Economic Evaluation for Poly(3-Hydroxybutyrate) Production by Fermentation.” *Bioprocess Engineering* 17(6):335–42.

Clark, Ryan L., Jeffrey C. Cameron, Thatcher W. Root, and Brian F. Pfleger. 2014. “Insights into the Industrial Growth of Cyanobacteria from a Model of the Carbon-Concentrating Mechanism.” *AIChE Journal* 60(4):1269–77.

Deng, Ming De and John R. Coleman. 1999. “Ethanol Synthesis by Genetic Engineering in Cyanobacteria.” *Applied and Environmental Microbiology* 65(2):523–28.

Dexter, Jason, Patricia Armshaw, Con Sheahan, and J.Tony Pembroke. 2015. “The State of Autotrophic Ethanol Production in Cyanobacteria.” *Journal of Applied Microbiology* 119:11–24.

Dienst, Dennis et al. 2014. “Transcriptomic Response to Prolonged Ethanol Production in the Cyanobacterium *Synechocystis* Sp. PCC6803.” *Biotechnology for Biofuels* 7:21.

Galanie, Stephanie et al. 2015. “Complete Biosynthesis of Opioids in Yeast.” *Science* 349(6252):1095–1100.

Gao, Zhengxu, Hui Zhao, Zhimin Li, Xiaoming Tan, and Xuefeng Lu. 2012. “Photosynthetic Production of Ethanol from Carbon Dioxide in Genetically Engineered Cyanobacteria.” E*nergy & Environmental Science* 5(12):9857.

Gnansounou, Edgard and Arnaud Dauriat. 2010. “Techno-Economic Analysis of Lignocellulosic Ethanol: A Review.” *Bioresource Technology* 101(13):4980–91.

Gordon, Gina C. et al. 2016. “CRISPR Interference as a Titratable, Trans-Acting Regulatory Tool for Metabolic Engineering in the Cyanobacterium *Synechococcus* Sp. Strain PCC 7002.” *Metabolic Engineering* 38:170–79.

Hahn-Hagerdal, Barbel et al. 2001. “Metabolic Engineering of *Saccharomyces Cerevisiae* for Xylose Utilization.” *Advances in Biochemical Engineering and Biotechnology* 73:53–84.

Hamelinck, Carlo N., Geertje van Hooijdonk, and André PC Faaij. 2005. “Ethanol from Lignocellulosic Biomass: Techno-Economic Performance in Short-, Middle- and Long-Term.” *Biomass and Bioenergy* 28(4):384–410.

Hatti-Kaul, R. and B. Mattiasson. 2003. *Isolation and Purification of Proteins*. New York, USA: Marcel Dekker Inc.

Herron, Jeffrey A., Jiyong Kim, Aniruddha A. Upadhye, George W. Huber, and Christos T. Maravelias. 2015. “A General Framework for the Assessment of Solar Fuel Technologies.” *Energy and Environmental Science* 8:126–57.

Hirokawa, Yasutaka, Yuki Maki, Tsuneyuki Tatsuke, and Taizo Hanai. 2016. “Cyanobacterial Production of 1,3-Propanediol Directly from Carbon Dioxide Using a Synthetic Metabolic Pathway.” *Metabolic Engineering* 34:97–103.

Huber, George W., Sara Iborra, and Avelino Corma. 2006. “Synthesis of Transportation Fuels from Biomass: Chemistry, Catalysts, and Engineering.” *Chemical Reviews* 106(9):4044–98.

Humbird, D. et al. 2011. Process Design and Economics for Biochemical Conversion of Lignocellulosic Biomass to Ethanol: Dilute-Acid Pretreatment and Enzymatic Hydrolysis of Corn Stover. National Renewable Energy Laboratory (NREL), Golden, CO.

Jones, Christopher M., Nestor J. Hernandez Lozada, and Brian F. Pfleger. 2015. "Efflux Systems in Bacteria and Their Metabolic Engineering Applications." *Applied Microbiology and Biotechnology* 99(22):9381–93.

Jones, Mark E. and William F. Banholzer. 2014. "Solar Flux, Water, and Land Impose Limits on Biology." 111(6):1059–61.

Joule. 2016. "Joule Completes Acquisition of Red Rock Biofuels | Biomassmagazine.com." *Biomass Magazine*. Retrieved June 28, 2017 (http://biomassmagazine.com/articles/12817/joule-completes-acquisition-of-red-rock-biofuels).

Jullesson, David, Florian David, Brian Pfleger, and Jens Nielsen. 2015. "Impact of Synthetic Biology and Metabolic Engineering on Industrial Production of Fine Chemicals." *Biotechnology Advances.* 33(7):1395-1402

Kato, Akihiro, Nobuyuki Takatani, Kazutaka Ikeda, Shin-ichi Maeda, and Tatsuo Omata. 2017. "Removal of the Product from the Culture Medium Strongly Enhances Free Fatty Acid Production by Genetically Engineered *Synechococcus Elongatus*." *Biotechnology for Biofuels* 10:141.

Kim, Soo Rin, Suk Jin Ha, Na Wei, Eun Joong Oh, and Yong Su Jin. 2012. "Simultaneous Co-Fermentation of Mixed Sugars: A Promising Strategy for Producing Cellulosic Ethanol." *Trends in Biotechnology* 30(5):274–82.

Knoop, Henning and Ralf Steuer. 2015. "A Computational Analysis of Stoichiometric Constraints and Trade-Offs in Cyanobacterial Biofuel Production." *Frontiers in Bioengineering and Biotechnology* 3:47.

Kopka, Joachim et al. 2017. "Systems Analysis of Ethanol Production in the Genetically Engineered Cyanobacterium *Synechococcus* Sp. PCC 7002." *Biotechnology for Biofuels* 10(1):56.

Lane, Jim. 2017. "Commercializing Algae: The Digest's 2017 Multi-Slide Guide to Algenol." *Biofuels Digest*. Retrieved June 28, 2017 (http://www.biofuelsdigest.com/bdigest/2017/03/12/commercializing-algae-the-digests-2017-multi-slide-guide-to-algenol/).

Lea-Smith, David J., Paolo Bombelli, Ravendran Vasudevan, and Christopher J. Howe. 2015. "Photosynthetic, Respiratory and Extracellular Electron Transport Pathways in Cyanobacteria." *Biochimica et Biophysica Acta* 1857(3):247–55.

Lee, Euntaek, Jérémy Pruvost, Xing He, Ramakanth Munipalli, and Laurent Pilon. 2014. "Design Tool and Guidelines for Outdoor Photobioreactors." *Chemical Engineering Science* 106:18–29.

Lenihan, Jacob R., Hiroko Tsuruta, Don Diola, Neil S. Renninger, and Rika Regentin. 2008. "Developing an Industrial Artemisinic Acid Fermentation Process to Support the Cost-Effective Production of Antimalarial Artemisinin-Based Combination Therapies." *Biotechnology Progress* 24(5):1026–32.

Li, Qiang, Wei Du, and Dehua Liu. 2008. “Perspectives of Microbial Oils for Biodiesel Production.” *Applied Microbiology and Biotechnology* 80(5):749–56.

Liao, James C., Luo Mi, Sammy Pontrelli, and Shanshan Luo. 2016. “Fuelling the Future: Microbial Engineering for the Production of Sustainable Biofuels.” *Nature Reviews Microbiology* 14:288–304.

Lynd, Lee R., Paul J. Weimer, Willem H. van Zyl, and Isak S. Pretorius. 2002. “Microbial Cellulose Utilization: Fundamentals and Biotechnology.” *Microbiology and Molecular Biology Reviews* 66(3):506–77.

Mandell, Daniel J. et al. 2015. “Biocontainment of Genetically Modified Organisms by Synthetic Protein Design.” *Nature* 518:55–60.

Martin, Vincent J. J., Douglas J. Pitera, Sydnor T. Withers, Jack D. Newman, and Jay D. Keasling. 2003. “Engineering a Mevalonate Pathway in *Escherichia Coli* for Production of Terpenoids.” *Nature Biotechnology* 21(7):796–802.

McKeague, Maureen, Yen-Hsiang Wang, Aaron Cravens, Maung Nyan Win, and Christina D. Smolke. 2016. “Engineering a Microbial Platform for de Novo Biosynthesis of Diverse Methylxanthines.” *Metabolic Engineering* 38:191–203.

Nelson, David L. and Michael M. Cox. 2008. *Lehninger Principles of Biochemistry*. 5th Edition New York: W. H. Freeman.

Newman, Jack D. et al. 2006. “High-Level Production of Amorpha-4,11-Diene in a Two Phase Partitioning Bioreactor of Metabolically Engineered *Escherichia Coli*.” *Biotechnology and Bioengineering* 95(4):684–91.

Paddon, Chris J. et al. 2013. “High-Level Semi-Synthetic Production of the Potent Antimalarial Artemisinin.” *Nature* 496(7446):528–32.

Paddon, Chris J. and Jay D. Keasling. 2014. “Semi-Synthetic Artemisinin: A Model for the Use of Synthetic Biology in Pharmaceutical Development.” *Nature Reviews Microbiology* 12(5):355–67.

Riesenberg, D. and R. Guthke. 1999. “High-Cell-Density Cultivation of Microorganisms.” *Applied Microbiology and Biotechnology* 51(4):422–30.

Ro, Dae-Kyun et al. 2006. “Production of the Antimalarial Drug Precursor Artemisinic Acid in Engineered Yeast.” *Nature* 440(7086):940–43.

Ruiz-Ruiz, Federico, Jorge Benavides, and Marco Rito-Palomares. 2013. “Scaling-up of a B-Phycoerythrin Production and Purification Bioprocess Involving Aqueous Two-Phase Systems: Practical Experiences.” *Process Biochemistry* 48(4):738–45.

Tsuruta, Hiroko et al. 2009. “High-Level Production of Amorpha-4,11-Diene, a Precursor of the Antimalarial Agent Artemisinin, in *Escherichia Coli*.” *PLoS ONE* 4(2):E4489.

Wang, Caixia et al. 2013. “Clarification of Succinic Acid Fermentation Broth by Ultrafiltration in Succinic Acid Bio-Refinery.” *Journal of Chemical Technology and Biotechnology* 88(3):444–48.

Wang, Z. X., J. Zhuge, H. Fang, and B. A. Prior. 2001. “Glycerol Production by Microbial Fermentation: A Review.” *Biotechnology Advances* 19(3):201–23.

Xue, Yong and Qingfang He. 2015. “Cyanobacteria as Cell Factories to Produce Plant Secondary Metabolites.” *Frontiers in Bioengineering and Biotechnology* 3:57.

Yao, Lun, Fengxia Qi, Xiaoming Tan, and Xuefeng Lu. 2014. “Improved Production of Fatty Alcohols in Cyanobacteria by Metabolic Engineering.” *Biotechnology for Biofuels* 7(1):94.

Yenkie, Kirti M. et al. 2016. “A Roadmap for the Synthesis of Separation Networks for the Recovery of Bio-Based Chemicals: Matching Biological and Process Feasibility.” *Biotechnology Advances* 34(8):1362–83.

Yenkie, Kirti M., Wenzhao Wu, and Christos T. Maravelias. 2017. “Synthesis and Analysis of Separation Networks for the Recovery of Intracellular Chemicals Generated from Microbial-Based Conversions.” *Biotechnology for Biofuels* 10:119.

Youngquist, J.Tyler et al. 2012. “Kinetic Modeling of Free Fatty Acid Production in *Escherichia Coli* Based on Continuous Cultivation of a Plasmid Free Strain.” *Biotechnology and Bioengineering* 109(6):1518–27.

Youngquist, J.Tyler et al. 2013. “Production of Medium Chain Length Fatty Alcohols from Glucose in *Escherichia Coli*.” *Metabolic Engineering* 20:177–86.

Zeng, A. P. and H. Biebl. 2002. “Bulk Chemicals from Biotechnology: The Case of 1,3-Propanediol Production and the New Trends.” Pp. 239–59 in *Tools and Applications of Biochemical Engineering Science*. Berlin: Springer.

Chapter 3: Light-Optimized Growth of Cyanobacterial Cultures: Growth Phases, Cellular Maintenance, and Productivity of Biomass and Secreted Molecules in Batch Growth

3.1. Background and Motivation

As discussed in **Chapter 2**, cyanobacteria have been engineered to produce many commercially relevant compounds including organic acids, alcohols, and secondary metabolites (Angermayr, Gorchs Rovira, and Hellingwerf 2015; Oliver et al. 2016; Xue and He 2015). Unlike heterotrophic conversions where yield (amount of product made per amount of substrate fed) is often the critical performance metric, cyanobacteria production strategies are evaluated by productivity (amount of product per time) and product titer (amount of product per volume). While many examples of chemical production using cyanobacterial biocatalysts have been demonstrated, few have attained product titers equivalent to those reached by heterotrophic bioconversions, most require weeks to maximize titer, and nearly all have been restricted to laboratory scale. These demonstrations have used a wide range of experimental conditions which confound comparative evaluations and scale-up projections (Schuurmans et al. 2015; Schuurmans, Matthijs, and Hellingwerf 2017). Overcoming these challenges is the goal of many ongoing metabolic and biochemical engineering studies. As researchers develop novel strains and engineering strategies, it is critical to provide a common basis for comparison and kinetic framework for evaluating cyanobacterial strains.

The key difference between cultivating cyanobacteria and heterotrophic microbes is the lack of a universal, scalable bioreactor layout due to the need to provide light to cells (*i. e.* most fermenters have a consistent geometry that can be scaled from lab to industrial scale). To maximize light delivery, photobioreactors (PBRs) are designed to maximize the surface area per culture volume. Designs for large-scale industrial reactors include open raceway ponds and closed tubular/rectangular vessels with large aspect ratios (*i. e.* depth of reactor is much smaller than its length and/or height). These photobioreactors are spread in parallel over acres of land to maximize the capture of solar irradiance required to support

the desired culture volume. In contrast, laboratory cyanobacterial cultivation systems are often built using equipment intended for cultivating heterotrophs that is augmented with exterior lighting. Common laboratory systems include tubes, flasks, bottles, flat plate PBRs, and instrumented bioreactors augmented with lighting shrouds. The different vessel geometries result in quite different photon delivery, which makes comparison of strain performance difficult. Furthermore, the difference in PBR designs between lab and industrial size provide a barrier to making accurate scale-up projections and technoeconomic assessments.

Unstructured kinetic models of heterotrophic cell growth inspired by the work of Monod, Pirt, and others (Monod 1949; Pirt 1965) have guided the design and analysis of many industrial biocatalysts (Youngquist et al. 2012). These models provide a framework to relate growth and product generation to the abundance of a limiting substrate (*i. e.* glucose) and thereby enable the simulation of cultivation schemes to predict bioprocess performance. Industrial cultivations of cyanobacteria will be provided excess nutrients (*i. e.* N-, P-, metals) and CO_2 from low-cost waste streams and rely on solar irradiance for energy to minimize operating costs. For this reason, it is prudent to characterize engineered cyanobacteria with light as the limiting nutrient. Pirt provided an overview of the energetics of photosynthetic growth that provided the foundation for modeling light-limited growth of photosynthetic organisms (Pirt 1986). Subsequent studies focused on models of light distribution inside of continuous growth experiments considering spatially varying irradiation (Evers 1991), spatially averaged irradiation (Grima et al. 1997), or measured total light absorbance (Schuurmans et al. 2015; Touloupakis, Cicchi, and Torzillo 2015). Each yielded useful information regarding light-limited growth parameters. However, continuous growth experiments are technically challenging and frequently performed with cell densities much lower than those desired for a large-scale process. Adapting the kinetic models for batch growth experiments will make this type of systematic analysis accessible to many researchers studying photosynthetic chemical production and inform process scale-up.

In this chapter, we first examine considerations for ensuring that light is the sole limiting substrate in laboratory cyanobacterial cultivation experiments by eliminating limitations from CO_2 and soluble nutrient availability. We then examine the phases of cyanobacterial batch growth with light as the sole limiting substrate while developing a theoretical framework for growth and product secretion, which enables determination of photon utilization efficiency (η) and growth associated productivity of secreted molecules (ρ) for batch growth experiments. Finally, we observe how η and ρ vary across different experimental systems for wild type and engineered strains of *Synechococcus* sp. strain PCC7002 (PCC7002) to show that: (1) photon utilization efficiency (η) is consistent across a variety of experimental conditions and can be used to compare studies performed in different experimental systems, (2) stationary phase can be achieved with light as the sole limiting substrate, and (3) the proposed framework can provide insight into metabolic engineering of cyanobacterial strains for secreted products.

3.2. Light-Limitation in Cyanobacterial Growth Experiments

The theoretical framework discussed in later sections assumes that light is the sole limiting substrate. This section considers how to eliminate other common growth limitations in laboratory systems.

CO_2 Delivery and Gas Transfer

When the CO_2 transfer rate (CTR) is lower than the inorganic carbon uptake rate (CUR) in a cyanobacterial cultivation, CO_2 can be limiting due to a CO_2 concentration (C_{CO_2}) below the saturation concentration for RuBisCO. Both modeling (Clark et al. 2014) and experimental studies (Price et al. 2004) have shown that aqueous media in equilibrium with ambient air has sufficient inorganic carbon for RuBisCO saturation in the fast-growing cyanobacterium PCC7002, a result which should hold for any photosynthetic microorganism with a similar maximal CO_2-fixation rate. Therefore, the key to avoiding a CO_2-limiting condition is to ensure that the CTR substantially exceeds the CUR. This design criterion is nearly always met at the beginning of batch cultures, but can become challenged at high cell densities.

Figure 3-1 illustrates the transport of inorganic carbon species in a cyanobacterial cultivation. The CTR depends on the mass transfer coefficient and the concentration gradient between the gas and liquid phases (**Equation 3-1**).

$$CTR = (k_L a)_{CO_2}(C^*_{CO_2} - C_{CO_2}) \quad (3\text{-}1)$$

k_L is the CO_2 transfer coefficient, a is the bubble surface area to volume ratio, and $C^*_{CO_2}$ is the saturation CO_2 concentration in the liquid. The volumetric CO_2 transfer coefficient $(k_L a)_{CO_2}$ is most often determined empirically and varies as a function of bubble size and gas flow rate. $C^*_{CO_2}$ is determined by Henry's law (**Equation 3-2**).

$$C^*_{CO_2} = k_H P_{CO_2} \quad (3\text{-}2)$$

where k_H is the Henry's law coefficient for CO_2 in the aqueous medium (0.02 M atm^{-1} in standard conditions) and P_{CO_2} is the partial pressure of CO_2 in the gas phase.

The CUR can be determined experimentally by measuring the rate of biomass accumulation as well as the production of any secreted organic molecules. A typically observed maximum CUR for PCC7002 growing linearly in laboratory cultivation vessels is on the order of 1 mM C hr^{-1}.

To increase the CTR to ensure it exceeds the CUR, P_{CO_2} and $k_L a$ can be modulated. Increasing P_{CO_2} involves the use of high CO_2 environmental chambers or delivery of elevated CO_2 gas streams to the cultivation vessel. At the high CO_2 extreme, *i. e.* when CTR >> CUR, the aqueous medium will be saturated with CO_2 in equilibrium with the elevated P_{CO_2}, resulting in decreased pH that affects cyanobacterial physiology when sufficiently low. This effect can be mitigated through modification of the buffer system in the medium or through addition of a strong base, such as NaOH.

A higher $(k_L a)_{CO_2}$ can be achieved by increasing the gas flow rate and decreasing the bubble size using a sparger. However, these methods to increase CO_2 transfer to the liquid will also lead to an increased evaporation rate. This evaporative loss can be addressed using a condenser on the gas stream exiting the cultivation vessel or through replacement of water. Additionally, the use of spargers with small

holes needed to create small bubbles can increase biofouling issues causing prohibitively high back pressure in the cultivation system.

The rate of CO_2 mass transfer is slightly less than that for molecular oxygen (*i. e.* $(k_L a)_{CO_2} = 0.9 \cdot (k_L a)_{O_2}$) for a given gas delivery system and typical $(k_L a)_{CO_2}$ values are in the range of 1-100 hr^{-1} (Boogerd et al. 1990). The maximum CTR (CTR_{MAX}) can be determined by calculating the value of CTR in **Equation 3-1** in the limit as $C_{CO_2} \rightarrow 0$. For ambient air (0.04% CO_2), CTR_{MAX} ranges from 10^{-3}-0.1 mM C hr^{-1} for typical laboratory values of $(k_L a)_{CO_2}$. Therefore, even the highest performing laboratory gas transfer apparatuses cannot achieve a CTR approaching the target of 1 mM C hr^{-1}. However, if the gas phase is changed to contain 5% CO_2, CTR_{MAX} ranges from 1-10 mM C hr^{-1}, allowing even the simplest gas transfer apparatuses to approach the target CTR. For this reason, the strategy of increasing P_{CO_2} is likely to be more effective in ensuring CO_2 is not limiting cell growth in laboratory experiments.

To demonstrate the elimination of CO_2-limitation, **Figure 3-1B** shows the linear growth rate (LGR) for PCC7002 cultures grown in laboratory bioreactors bubbled with gas phases of varying P_{CO_2} as well as CTR_{MAX} for expected values of $(k_L a)_{CO_2}$. The LGR is increased by changing from 0.01 atm CO_2 to 0.05 atm CO_2. No further increase in LGR is observed by changing the gas phase to 0.1 atm CO_2, suggesting that 0.05 atm CO_2 is sufficient to achieve excess CO_2-transfer and CO_2 is not the growth-limiting nutrient.

A

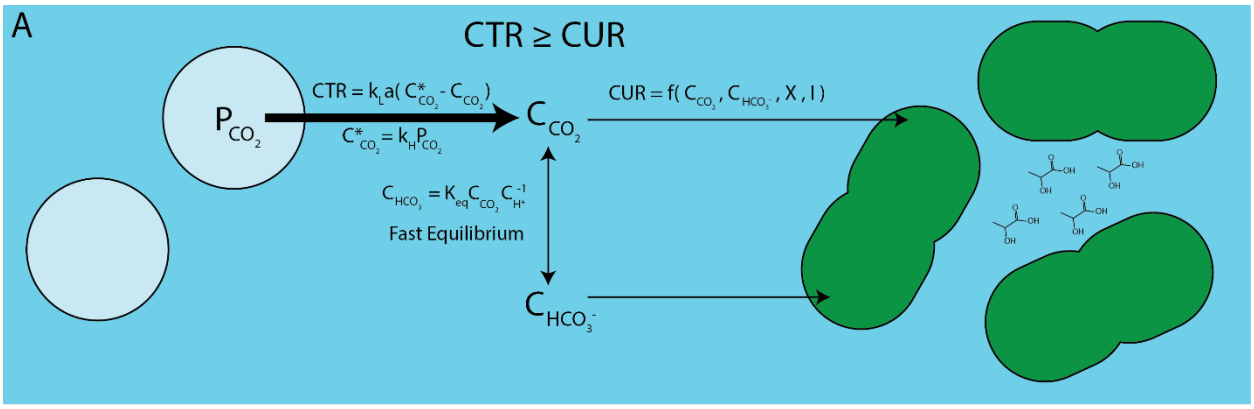

B

P_{CO_2} (atm)	Measured LGR (mg DW L^{-1} hr^{-1})	Calculated CUR (mmol C L^{-1} hr^{-1})	Max CTR (mmol C L^{-1} hr^{-1})	
			k_La=1 hr^{-1}	k_La=100 hr^{-1}
0.01	11±0.5	0.5±0.02	0.2	20
0.05	24±1	1±0.04	1	100
0.10	23±1	1±0.04	2	200

Figure 3-1. Eliminating CO_2-Limitation. To ensure CO_2 is not a limiting substrate, the CO_2 transfer rate (CTR) must be greater than the CO_2 uptake rate (CUR) for the duration of the experiment. The equations governing CO_2 transfer shown in (A) allow the optimization of CO_2 transfer in such a way that the maximum CTR (in the limit as C_{CO2} approaches zero) is greater than the empirically measured CUR. (B) CO_2-limitation was eliminated in photobioreactors cultivating PCC7002 by increasing P_{CO2} to 0.05 atm. For photobioreactor growth with a gas phase of P_{CO2}=0.01 atm, the predicted maximum CTR for a low value of k_La was insufficient to exceed the CUR. Increasing P_{CO2} to 0.05 atm increases the predicted maximum CTR to a value greater than or equal to the experimentally measured CUR for the entire expected range of k_La. Further increasing P_{CO2} to 0.10 atm caused no increase in the linear growth rate (LGR), suggesting that P_{CO2}=0.05 atm was sufficient to eliminated CO_2-limitation in the photobioreactors. CUR was calculated assuming biomass was 50 wt% C (Egli 2015). Max CTR was calculated using Equation 3-1 with C_{CO2}=0. Error in LGR is standard error of three biological replicates.

Soluble Nutrients

Depletion of soluble nutrients can cause a culture to enter stationary phase while light is still in excess. A stoichiometric analysis of two common cyanobacterial growth media (**Table 3-1**) reveals deficiencies in metabolizable nitrogen, phosphorous, sulfur, magnesium, and iron, even at cell densities below 1 g of dry cell weight per liter (g DW L^{-1}) (Egli 2015), suggesting that cultures in these media are limited by soluble nutrients. CO_2-replete cultures of PCC7002 grown in Media A enter stationary phase at a much lower cell density than cultures grown in Modified Media A (**Figure 3-2**, **Table 3-1** – Modified Media A supplemented with excess iron, nitrate, and/or phosphate). The reported media composition required per 1 g DW L^{-1} of biomass was calculated using the stoichiometric composition of typical biomass as described by Egli (Egli 2015).

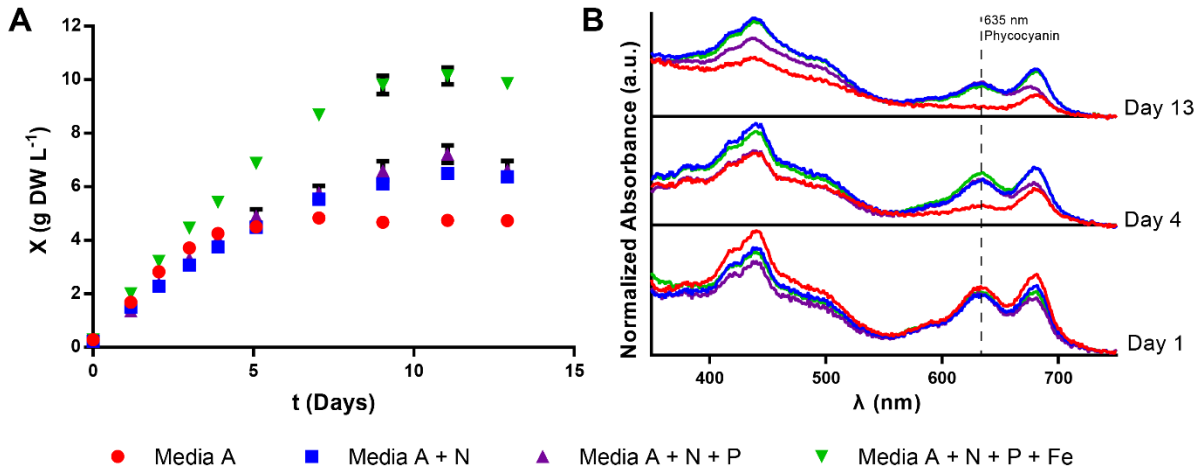

Figure 3-2. Nutrient Supplementation Allows Growth to Higher Cell Density. (A) Cell density (OD_{730} converted to g DW L^{-1} as described in methods) over time measured for cultures of PCC7002 grown in shake flasks in 1% CO_2 and 37°C in Media A with no supplement (red), supplemented with 110 mM $NaNO_3$ (blue), supplemented with 110 mM $NaNO_3$ and 31 mM KH_2PO_4 in a fed batch scheme as described in the methods (purple), or supplemented with 110 mM $NaNO_3$, 31 mM KH_2PO_4 in a fed batch scheme, and 1.1 mM $FeCl_3$ (green). Error bars are standard error of 3 biological replicates for red, blue, and purple or 2 biological replicates for green. (B) Average absorbance scans normalized to OD_{730} of samples from the flasks described in (A) are shown over time to show loss of pigmentation in nutrient deplete media and pigment persistence in nutrient sufficient media. Absorbance profiles over time are offset on the y-axis for clarity (baselines in black).

Further insight can be found in examining the absorbance spectra of the cells grown in each case. When grown in the nutrient deficient Media A, cells exhibit a nitrogen-deprivation phenotype (*i. e.* phycobilisome degradation) as they transition into stationary phase. The phenotype is observed as a decrease in absorbance around 635 nm (Jackson et al. 2015; Stevens, Balkwill, and Paone 1981). Transcriptomics analysis has shown that when PCC7002 experiences limitation in iron, nitrogen, sulfur, or phosphate, the gene *nblA* is upregulated, initiating the degradation of phycobiliproteins (Ludwig and Bryant 2012). When excess soluble nutrients are supplemented, cells continue to grow to twice the final density and maintain phycobilisomes as they eventually transition into stationary phase. For the cultures supplemented with N, P, and Fe, the culture achieved a density of 10 g DW L^{-1} at stationary phase. As can be observed in **Table 3-1**, the N, P, and Fe concentration in Modified Media A exceed the amount required for 10 g L^{-1} biomass. As shown in later sections, light can be verified as the sole limiting substrate in a cultivation by increasing the volumetric photon delivery rate of a culture that has entered stationary

phase. These observations suggest that while common historical media recipes are sufficient for growth at low cell densities (<1 g DW L^{-1}), supplementation of N, P, and Fe are necessary to eliminate limitations on growth at higher cell densities.

Table 3-1. Elemental Composition of Cyanobacteria Media

Element	Media A	BG11	Required per 1 g DW L^{-1} of Biomass[a]	Modified Media A
N	12	19	9	122
P	0.4	0.2	1	31
S	20	0.3	0.3	20
Mg	20	0.3	0.2	20
Fe	0.03	0.06	0.1	1.1

All concentrations are in mM. [a]Calculated using stoichiometric composition of typical biomass as described in reference (Egli 2015).

3.2. The Phases of Growth in Light-Limited Cyanobacterial Cultures

In the seminal work *The Growth of Bacterial Cultures*, Jacques Monod outlined distinct phases of the growth of bacterial batch cultures (Monod 1949). For heterotrophic bacteria, the most well studied phase of growth is the exponential phase, where the specific growth rate is constant, as this phase is where most biomass is produced. As the growth substrate is depleted significantly below the affinity of the rate limiting step in substrate utilization, a brief growth retardation phase begins and the specific growth rate quickly decreases to 0 at which point all substrate has been consumed and stationary phase begins.

The previous section established batch growth conditions for phototrophic bacteria in which light is the only limiting substrate. The following sections consider the light distribution and consequent growth dynamics of cyanobacteria in these differing phases of growth.

Light Quality

This work considers only accessible photons (AP), or those photons able to excite electrons for photosynthesis in the organism under study. This differs from the commonly reported photosynthetically active radiation (PAR) which considers all photons of the visible spectrum, many of which are unusable for photosynthesis by some organisms. To illustrate this, **Figure 3-3** shows emission spectra for the two

light sources used in this work as well as the solar spectrum superimposed on the absorbance spectrum of PCC7002. Wavelengths highlighted in green are included in the calculation of the irradiance of accessible photons (I_{AP}) and quality factors for converting between the irradiance of PAR (I_{PAR}) and I_{AP} as well as irradiance specifically exciting chlorophyll a (I_{ChlA}) and phycocyanin (I_{Phyc}) are given in **Table 3-2**.

Table 3-2. Light Quality Factors - Fraction of PAR Absorbed by Chlorophyll *a* or Phycocyanin

Light Source	$I_{AP}I_{PAR}^{-1}$	$I_{ChlA}I_{PAR}^{-1}$	$I_{Phyc}I_{PAR}^{-1}$
Cool White Fluorescent	0.31	0.14	0.18
White LED (4000 K)	0.40	0.23	0.17
Solar	0.44	0.27	0.17

Exponential Growth Phase in the Limit of Low Cell Density

The typical Monod growth model for microorganisms describes the phases of growth resulting from changes in the specific growth rate as a function of limiting substrate concentration (**Figure 3-4A-B**) (Monod 1949). Two differences exist in considering light as a substrate. First, a molecular substrate can be depleted, but light is provided continuously from the exterior of the culture vessel. Second, due to mixing, molecular substrate concentrations are considered constant in spatial dimensions whereas irradiance varies spatially due to absorbance by the cells, a phenomenon referred to as cell-shading (**Figure 3-4D-F**).

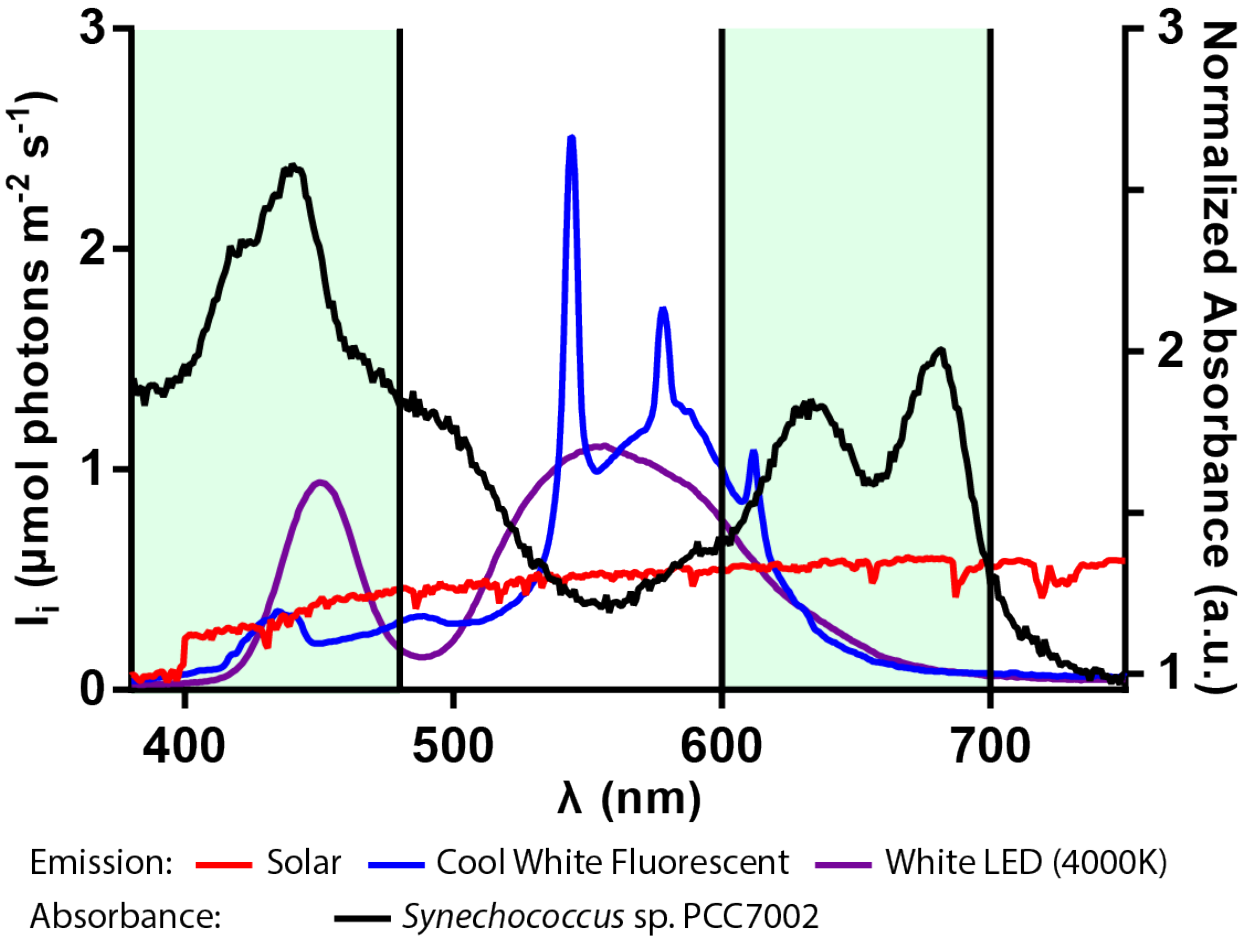

Figure 3-3. Emission Spectra and Accessibility to Photosynthetic Pigments in PCC7002. Photon wavelength distribution for solar radiation (red), cool white fluorescent light bulbs (blue), and white LEDs with a color temperature of 4000 K (purple) are given as values normalized to a total PAR flux of 200 µmol photons m^{-2} s^{-1}. I_i is the irradiance of photons of wavelength i. These are compared to the normalized absorbance spectrum of PCC7002 (black). Green regions represent accessible photons included in the calculation of the light quality factors in Table 3-2.

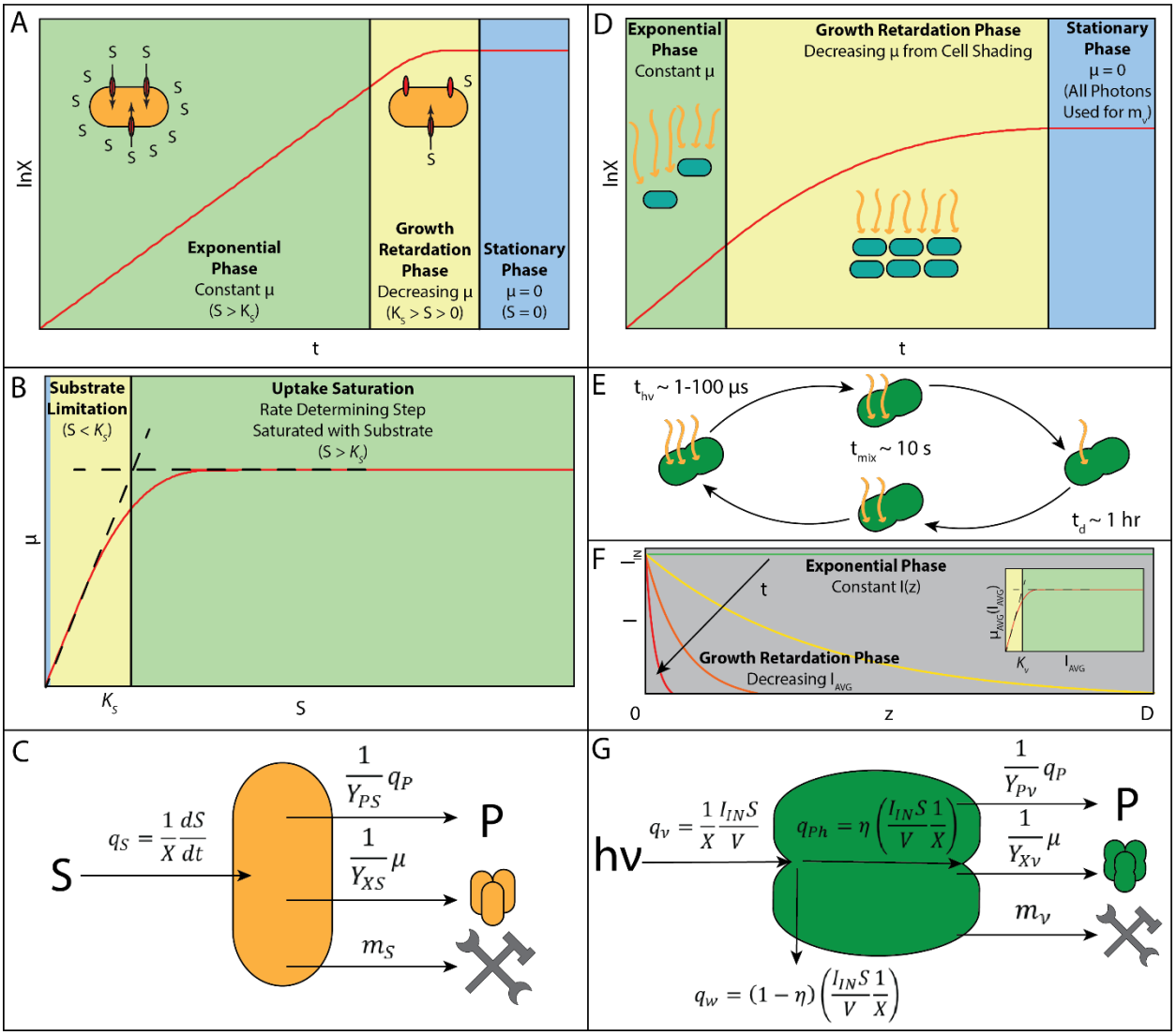

Figure 3-4. Comparison of Phenomena Driving Growth Phases for Molecular Substrate Limitation (A-C) or Light-Limitation (D-G). (A) Uptake saturation results in an exponential growth phase until substrate is depleted and the culture enters a short growth retardation phase. Once substrate is fully depleted, the culture enters stationary phase. (B) Monod kinetic model says that high substrate concentration results in uptake saturation leading to constant specific growth rate. As substrate is depleted to the region of K_s, substrate limitation begins resulting in rapidly decreasing specific growth rate. (C) Substrate balance says that substrate uptake rate (q_S) is equal to the sum of substrate utilization for product synthesis ($q_P Y_{PS}^{-1}$), growth (μY_{XS}^{-1}), and maintenance (m_S). (D) Light-Limited batch growth of cyanobacteria has a short exponential growth phase followed by a long growth retardation phase caused by cell-shading, eventually leading to stationary phase when all incident photons are used for maintenance and product synthesis. As cell density increases the biomass specific photon delivery rate decreases until all incident photons are required for cell maintenance, at which point the culture enters stationary phase. (E) The difference in order of magnitude between the characteristic times of mixing (t_{mix}), light reactions (t_{hv}), and growth (t_d) suggest that specific growth rate can be accurately estimated by I_{AVG}. (F) When cultures are at low cell density, the light intensity I(z) approximately constant across the thickness of the reactor (z). As cell density increases, I(z) is determined by Beer's law and results in decreasing I_{AVG}. (F-Inset) Using I_{AVG}, one can write a Monod growth law for μ_{AVG} (Equation 3-4). (G) Photon balance says that the specific photon uptake rate (q_v) multiplied by the photosynthetic efficiency (η) is equal to the sum of energy utilization for product synthesis ($q_P Y_{Pv}^{-1}$), growth (μY_{Xv}^{-1}), and maintenance (m_v).

The growth phases of light-limited growth are determined by changes in the spatial irradiance distribution (I(z)) inside the culture vessel (**Equation 3-3**).

$$I(z) = I_{IN}e^{-\alpha Xz} \quad (3\text{-}3)$$

I_{IN} is the irradiance of photons on the surface of the vessel, z is the path length, X is the biomass density, and α is the biomass specific absorbance of photons.

For very low X, light attenuation is minimal and I(z) is approximately constant resulting in an exponential growth phase where all cells grow with constant specific growth rate, μ. Experiments in this phase can be used to experimentally determine the Monod growth model for a given microorganism assuming I_{IN} is sufficiently low to prevent photoinhibition. The exponential growth rates of low cell density cultures of PCC7002 under various irradiances were measured and fit to the Monod growth model (**Equation 3-4**), giving the maximum specific growth rate (μ_{max}) and the saturation irradiance (K_v) (**Figure 3-5**).

$$\mu(I) = \frac{\mu_{max}I}{K_v+I} \quad (3\text{-}4)$$

For irradiances significantly higher than those used in this work, photoinhibition negatively influences the growth rate and **Equation 3-4** overpredicts μ.

Growth Retardation Phase Driven by Light Attenuation

As cell density increases, light attenuation significantly affects I(z). In most laboratory culture vessels, the mixing time occurs on the order of 10-100 s (Barbosa et al. 2003; Shuler and Kargi 1992). Therefore, a cell will visit all spaces in a photobioreactor many times over the course of one cell cycle, which occurs on the order of hours. Time constants for excitation and relaxation of a photosynthetic unit through photochemical quenching are on the order of 100 μs and 1 μs, respectively (García-Camacho et al. 2012). Therefore, photosystems cycle through the light reactions many times at each location (**Figure 3-4E**). Taking these considerations into account, a simplifying assumption is made such that the cells experience

a spatially average irradiance (I_{AVG}). Thus, the average specific growth rate is determined by the specific growth rate for I_{AVG} (**Equation 3-5**).

$$\mu_{AVG} = \mu(I_{AVG}) \tag{3-5}$$

A differential expression for the growth of bacteria neglecting cellular maintenance and secreted products can be written based on the work of Monod and Pirt, and others (**Equation 3-6**) (Monod 1949; Pirt 1965).

$$\frac{1}{X}\frac{dX}{dt} = \mu_{AVG} \tag{3-6}$$

A photon balance accounting for the distribution of energy produced from absorbed photons can be used to study the effects of cellular maintenance and secreted product synthesis on growth (**Equation 3-7**) (Evers 1991; Pirt 1986).

$$\eta\left(\frac{1}{X}\frac{I_{IN}S}{V}\right) = \frac{1}{Y_{Xv}}\mu_{AVG} + \frac{1}{Y_{Pv}}q_P + m_v \tag{3-7}$$

In **Equation 3-7**, η is the photon utilization efficiency, I_{IN} is the irradiance at the surface of the vessel, S is the irradiated surface area of the vessel, V is the culture volume, q_P is the biomass specific rate of synthesis of a secreted product, m_v is the biomass specific photon utilization for maintenance, Y_{Xv} is the theoretical maximum yield of biomass on photons, and Y_{Pv} is the theoretical maximum yield of product on photons. In the growth retardation phase, cell density is sufficient for all photons entering the culture vessel to be absorbed by the biomass. Thus, the photons used for energy production can be determined by multiplying the volumetric photon delivery rate ($I_{IN}SV^{-1}$) by the photon utilization efficiency (η). The energy produced from these photons is then used for growth, secreted products, and cellular maintenance (**Figure 3-4G**). In this work, η, m_v, Y_{Xv} and Y_{Pv} are considered constant in time.

The maximum theoretical yield on photons of either biomass (Y_{Xv}) or a product (Y_{Pv}) can be readily calculated using genome-scale metabolic models. These models are mathematical representations of metabolic networks and are genomic and biochemical knowledge bases of an organism's metabolism (Lewis, Nagarajan, and Palsson 2012). In this work, Y_{Xv} and Y_{Pv} were calculated with the

PCC7002 genome-scale metabolic model, *i*Syp708, and used to fit batch growth data and L-lactate and L-lysine production data (Vu et al. 2013). Additionally, the Y_{Pv} for a variety of other compounds were determined and are reported in **Table 3-3**. These compounds are potential metabolic engineering targets and many of them have previously been produced in cyanobacteria.

Table 3-3. Theoretical Yields in PCC7002 for Various Compounds

Product Name	Y_{Pv} (nmol product per μmol photons)	Product Name	Y_{Pv} (nmol product per μmol photons)
Ethanol	41.7	Sucrose	10.3
Acetone	29.4	Isoprene (MEP Pathway)	17.9
Isopropanol	27.4	Isoprene (MVA Pathway)	16.9
1-Butanol	20.8	Limonene (MEP Pathway)	8.93
Isobutyraldehyde	22.7	Limonene (MVA Pathway)	8.48
Isobutanol	20.8	Bisabolene (MEP Pathway)	5.95
2-Methyl-1-Butanol	16.7	Bisabolene (MVA Pathway)	5.65
1,2-Propanediol	31.3	Squalene (MEP Pathway)	2.94
2,3-Butanediol	22.7	Squalene (MVA Pathway)	2.81
L-Lactate	41.7	Octanoic Acid	11.4
3-Hydroxybutyrate	27.2	Octanol	10.4
Glycerol	35.7	Dodecanoic Acid	7.35
D-Mannitol	19.2	Dodecanol	6.94
L-Lysine (Nitrate media)	11.4	Hexadecanoic Acid	5.44
L-Lysine (Ammonia media)	17.9	Hexadecanol	5.21

If **Equation 3-7** is rearranged to solve for μ_{AVG}, it can be substituted into **Equation 3-6** to generate **Equation 3-8**.

$$\frac{dX}{dt} = Y_{Xv}X(\eta \frac{I_{IN}S}{V}\frac{1}{X} - \frac{1}{Y_{Pv}}q_P - m_v) \tag{3-8}$$

For an organism with negligible product secretion ($q_P \rightarrow 0$), the initial growth rate in growth retardation phase appears linear as defined by **Equation 3-8** in the limit of low X (**Equation 3-9**).

$$\left.\frac{dX}{dt}\right|_{X \rightarrow X_0} = Y_{Xv}\eta \frac{I_{IN}S}{V} \tag{3-9}$$

The left side of **Equation 3-9** is the linear growth rate (LGR) measured at the beginning of the growth retardation phase.

For comparison, we will now consider a differential equation for growth produced by inserting the Monod model for specific growth rate into the differential equation for bacterial growth under the assumption of $I_{AVG} << K_v$ (**Equation 3-10**).

$$\frac{dX}{dt} = \frac{\mu_{MAX} I_{AVG}}{K_v} X \tag{3-10}$$

I_{AVG} can be determined by averaging I(z) (**Equation 3-3**) across the volume of the vessel (**Equation 3-11**, See Supplementary Note for derivation).

$$I_{AVG} = \frac{I_{IN} S}{V} \frac{1}{\alpha X} \tag{3-11}$$

Inserting **Equation 3-11** into **Equation 3-10** produces another equation predicting a linear growth rate (**Equation 3-12**).

$$\frac{dX}{dt} = \frac{\mu_{MAX}}{\alpha K_v} \frac{I_{IN} S}{V} \tag{3-12}$$

Comparing **Equations 3-8 and 3-9** reveals a relationship between η and the Monod kinetic parameters (**Equation 3-13**).

$$\eta = \frac{\frac{\mu_{MAX}}{K_v} I(z)}{\alpha Y_{Xv} I(z)} \tag{3-13}$$

The numerator of **Equation 3-13** is the expected specific growth rate from the Monod growth model. The denominator is the theoretical maximum specific growth rate if all energy from photons absorbed are used to produce biomass. Using μ_{max} and K_v from **Figure 3-5**, Y_{Xv} calculated as described later, and α measured for accessible photon wavelengths, the expected value of η is in the range of 0.5-0.7, consistent with the results presented in **Table 3-4** (See Supplementary Note for derivation).

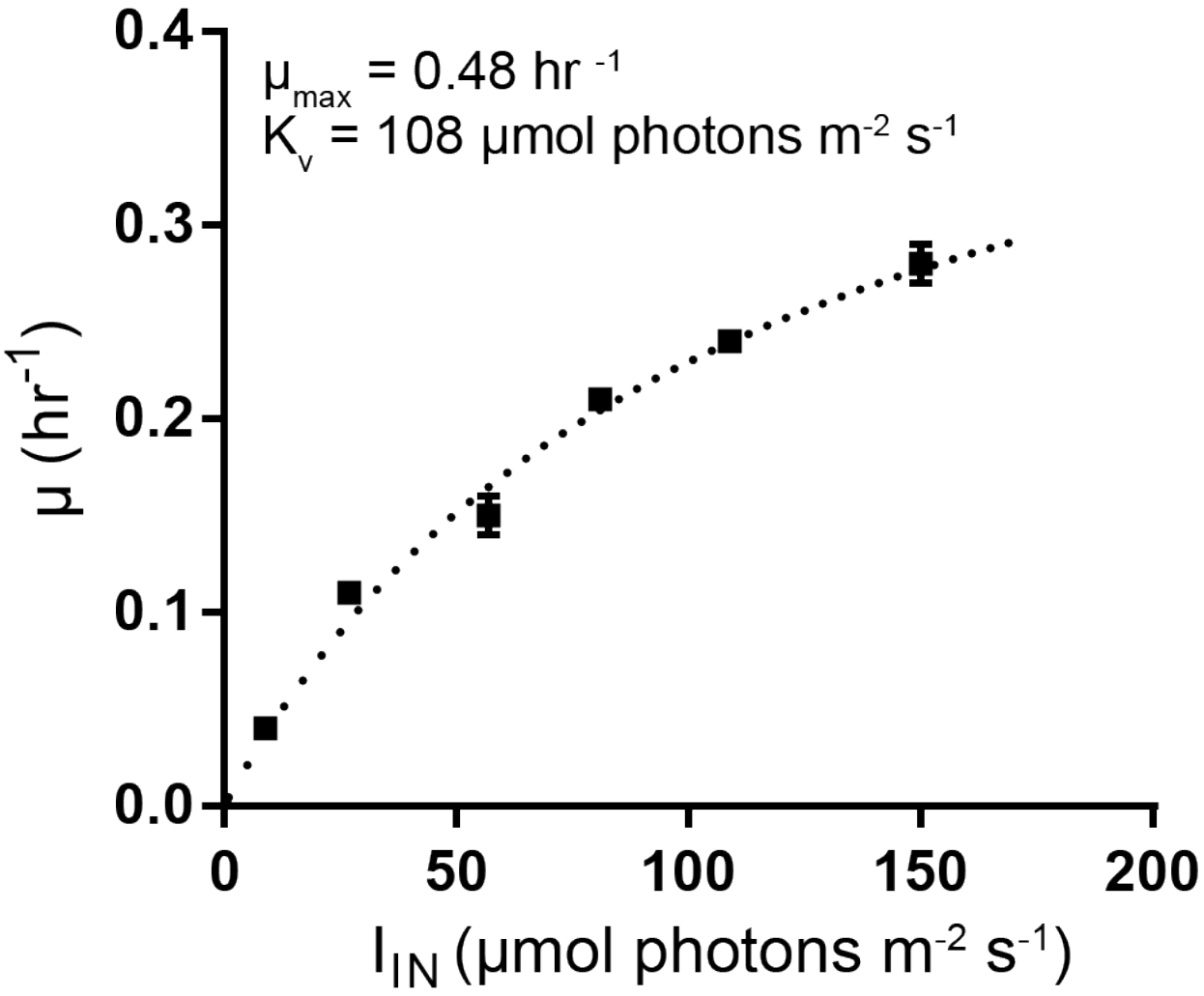

Figure 3-5. Photonic Monod Growth Model Fit from Exponential Phase Batch Cultures of PCC7002. μ values are calculated from the exponential growth rate of cultures grown in the specified I_{IN} with all cell density measurements made at OD730 less than 0.1 to limit the effect of cell shading on I_{AVG}. Error bars represent the standard error of at least three biological replicates.

The photon balance described in **Equation 3-8** includes a term for secreted products, allowing analysis of cyanobacteria engineered for production of secreted molecules. This analysis considers a growth associated product such that the specific productivity of P is proportional to the specific growth rate (**Equation 3-10**).

$$q_P = \rho \mu_{AVG} \tag{3-14}$$

Here, ρ is the growth-associated productivity parameter (mol P (g DW)$^{-1}$). This model should be applicable to most molecules of interest as chemical production is often tied to growth in cyanobacteria.

However, a similar analysis could easily be performed for cases where this does not apply through careful choice of productivity model.

Combining the productivity model with the photon balance and differential growth equation (**Equation 3-8**) produces **Equation 3-15**.

$$\frac{dX}{dt} = \frac{Y_{X\nu} X\left(\frac{1}{X}\eta\frac{I_{IN}S}{V} - m_\nu\right)}{\left(1+\frac{Y_{X\nu}}{Y_{P\nu}}\rho\right)} \tag{3-15}$$

The corresponding product balance expression is given in **Equation 3-16**.

$$\frac{dP}{dt} = \rho\frac{dX}{dt} = \rho\frac{Y_{X\nu} X\left(\frac{1}{X}\eta\frac{I_{IN}S}{V} - m_\nu\right)}{\left(1+\frac{Y_{X\nu}}{Y_{P\nu}}\rho\right)} \tag{3-16}$$

An analytical solution to **Equations 3-15 and 3-16** yields expressions for cell density and product concentration as a function of time, given in **Equation 3-17 to 3-20** (See Supplementary Note for derivation).

$$X(t) = X(0)\mathrm{e}^{-\kappa t} + X_S[1 - \mathrm{e}^{-\kappa t}] \tag{3-17}$$

$$P(t) = P(0) + \rho[X_S - X(0)][1 - \mathrm{e}^{-\kappa t}] \tag{3-18}$$

$$\kappa = \frac{Y_{X\nu} m_\nu}{1+\rho\frac{Y_{X\nu}}{Y_{P\nu}}} \tag{3-19}$$

$$X_S = \frac{\eta\frac{I_{IN}S}{V}}{m_\nu} \tag{3-20}$$

Here, X_S is the stationary phase cell density predicted by model parameters and κ is a characteristic time constant for transition to stationary phase. **Equation 3-17 to 3-20** provide a theoretical framework for characterizing the productivity of cyanobacteria cultures with the key parameters η, ρ, and m_ν.

3.3. Experimental Validation and Predictive Capabilities of Theoretical Framework

Photon Utilization Efficiency for Scaling

Table 3-4 gives values of η calculated from the LGR of cultures of Wild Type PCC7002 grown across different vessel geometries, I_{IN}, temperature, and salinity. η varied only slightly in the range of 0.55-0.76 for all experiments performed in this work except for excessive salinity (72 g L^{-1} NaCl) where η was severely

decreased. η was similar for experiments performed with *Synechococcus elongatus* UTEX 2973, another fast-growing cyanobacterium. Calculated values of η from yields determined in chemostat experiments with *Synechocystis sp.* PCC6803 and the algae *Chlorella sorokiniana* 211-8K were comparable to those determined from LGR experiments in this work (Schuurmans et al. 2015).

To further illustrate the usefulness of $I_{IN}SV^{-1}$ as a scaling factor for predicting cyanobacterial growth rate in different experimental systems, **Figure 3-6A** gives the LGR plotted vs. $I_{IN}SV^{-1}$ for three different vessel geometries (culture tubes, shake flasks, and 1 L culture bottles). As shown in **Figure 3-6B**, η is an easily calculated and useful parameter for identifying changes in culture conditions that cause deviations in photon utilization efficiency from standard conditions. In these experiments measuring LGR of PCC7002 in cultures in which temperature and salinity were varied, the only significant negative deviation in η occurred with 4x the salinity of standard Media A, or approximately twice the salinity of seawater. This approach is useful in quantifying how variations in culture conditions in a scaled-up process that differ from standard experimental conditions can affect photon utilization efficiency.

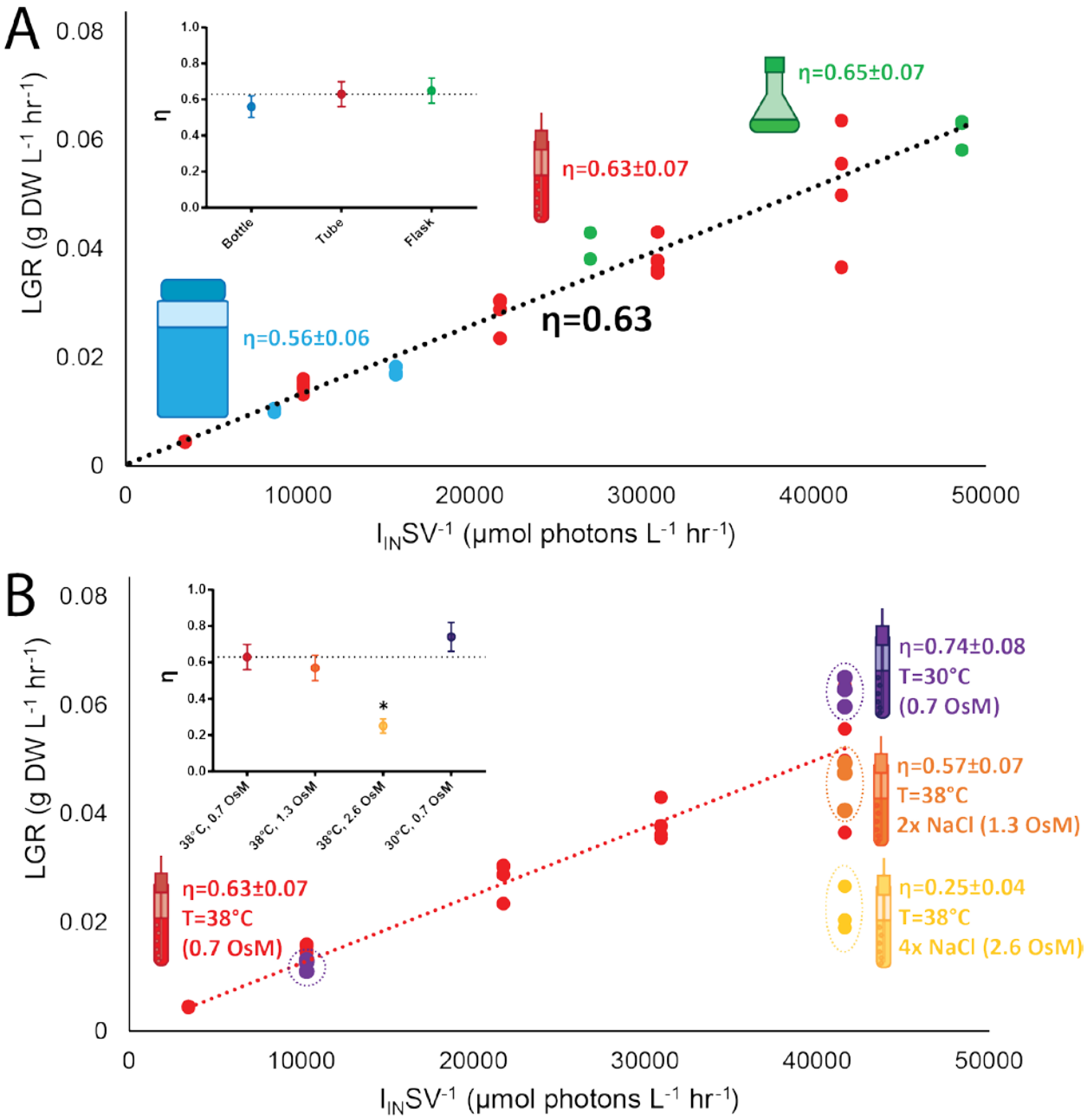

Figure 3-6. Linear Growth Rate Scales with Volumetric Photon Delivery Rate but Varies with Osmolarity. (A) LGR of PCC7002 increases with volumetric photon delivery rate. This result holds between three vessel geometries. Inset: η does not differ significantly from the average value for different geometries. (B) Decreasing temperature to 30°C has minimal effect on photon utilization efficiency in PCC7002. PCC7002 is salt tolerant, but extreme increase in osmolarity to approximately 2x the osmolarity of seawater (2.6 OsM) by the addition of NaCl significantly decreases photon utilization efficiency. Inset: 2.6 OsM is the only experimental treatment where η varied significantly from the average (p-value<0.05).

Table 3-4. Photon Utilization Efficiency Under Various Experimental Conditions

Vessel	Osmolarity (OsM)	T (°C)	SV^{-1} (m^{-1})	I_{IN}[a]	($I_{IN}SV^{-1}$)[b]	LGR[c]	Yield[d]	η
Synechococcus sp. PCC7002								
Flask A[e]	0.7	37	180	75	48600	62±4	1.3	0.63±0.07
Tube	0.7	38	100	110	41400	51±6	1.2	0.62±0.10
Tube	0.7	38	100	80	31000	38±2	1.2	0.61±0.07
Flask B[f]	0.7	37	100	75	27000	41±4	1.5	0.75±0.10
Tube	0.7	38	100	60	21900	28±2	1.3	0.64±0.08
Liter Bottle	1	30	40	110	15700	17±0.5	1.1	0.55±0.06
Tube	0.7	38	100	30	10200	15±0.8	1.5	0.73±0.08
Liter Bottle	1	30	40	60	8600	10±0.2	1.2	0.59±0.06
Tube	0.7	38	100	10	3500	4.5±0.2	1.3	0.65±0.07
Tube[g]	0.7	38	NA	~600	NA	NA	NA	**~0.1**
Lower Temperature								
Tube	0.7	**30**	100	110	41400	63±3	1.5	0.76±0.08
Tube	0.7	**30**	100	30	10200	12±0.8	1.2	0.60±0.07
Higher Salinity								
Tube	**1.3**	38	100	110	41400	47±3	1.1	0.57±0.07
Tube	**2.6**	38	100	110	41400	21±3	0.5	**0.25±0.04**
Synechocystis sp. PCC6803								
Chemostat[h]	0.04	30	NA	76	NA	NA	1.7	0.85
Chemostat[i]	0.04	28	NA	45	NA	NA	1.2	0.60
Chlorella sorokiniana 211-8K								
Chemostat[h]	0.04	30	NA	76	NA	NA	1.8	0.88

[a][µmol photons m^{-2} s^{-1}] Standard error is 10% of measured value. [b][µmol photons L^{-1} hr^{-1}] [c][mg DW L^{-1} hr^{-1}] [d][g DW (mol photons)$^{-1}$] [e]250 mL Flask with 25 mL culture volume. [f]250 mL Flask with 45 mL culture volume. [g]Experiment from Xiong, et al. found an 80% decrease in linear growth rate when I_{IN} was increased from 15 umol m^{-2} s^{-1} to 600 umol m^{-2} s^{-1} (estimated I_{AP}/I_{PAR} of 0.3) (Xiong et al. 2015). This was used to estimate η under very high light intensity from the experiments performed in this work. [h]Experiments from Schuurmans, et al. (Schuurmans et al. 2015). [i]Experiments from Touloupakis, et al. (Touloupakis et al. 2015). Error values are standard error of the mean propagated from LGR and I_{IN} measurements of at least three biological replicates. Bold text to emphasize variables of interest.

Transition to Stationary Phase in Batch Growth

Stationary phase is characterized by a net growth rate of zero. In **Equation 3-8**, this occurs when the biomass specific rate of photon utilization ($q_{Ph}=\eta I_{IN}SV^{-1}X^{-1}$, **Figure 3-4G**) has decreased to the point where all photons are being used for maintenance. No further increase in cell density is observed after this point without perturbation in the volumetric photon delivery rate. In practice, the onset of stationary phase

occurs abruptly and at cell densities significantly lower than predicted by the model in **Equation 3-8**. This is likely due to regulatory changes induced by low biomass-specific photon delivery rate.

While η can be calculated from the initial LGR, m_v requires information about growth rate at cell densities approaching X_S. To accomplish this, cultures of PCC7002 were grown in photobioreactors with Media A supplemented with $NaNO_3$, $FeCl_3$, and KH_2PO_4 until stationary phase under two different I_{IN} (**Figure 3-7**). The average value of η for these cultures was 0.55±0.06 or 0.59±0.06 for 110 or 60 µmol photons m^{-2} s^{-1}, respectively, as determined by initial rate analysis (LGR calculated from first 3 days of growth). Using these values of η in **Equation 3-17** and fitting the resulting equation to growth data gave an average m_v of 1100±110 or 420±30 µmol photons (g DW)$^{-1}$ hr^{-1} for 110 or 60 µmol photons m^{-2} s^{-1}, respectively. A sensitivity analysis looking at the goodness of fit of the model given in **Equation 3-17** while varying the parameters shows that the fit is much less sensitive to changes in m_v than to changes in η or ρ (**Figure 3-8**). This analysis suggests that the batch culture method for determination of m_v is accurate only in order of magnitude and continuous cultures study is necessary for more accurate quantification of cellular maintenance. The m_v values calculated here are on the same order of magnitude as the values of 900 µmol photons (g DW)$^{-1}$ hr^{-1} for *Synechocystis* sp. PCC6803 (Touloupakis et al. 2015) and 1250 µmol photons (g DW)$^{-1}$ hr^{-1} for *Oscillatoria agardhii* (Evers 1991), both determined by continuous culture experiments.

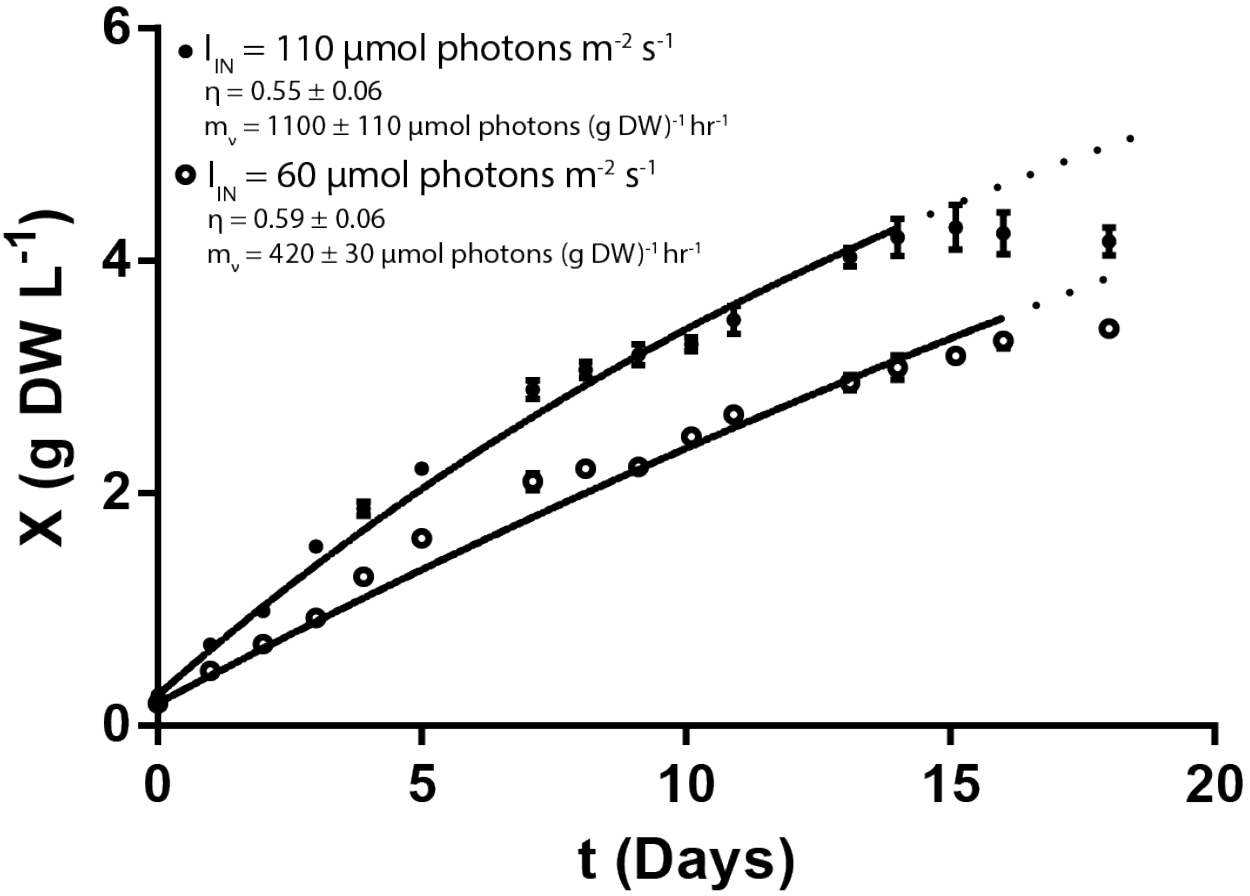

Figure 3-7. Batch Growth of Wild Type PCC7002 to Light-Limited Stationary Phase with Varying Irradiance. PCC7002 was grown to stationary phase under light limitation in photobioreactors at I_{IN} of 110 (closed circles) or 60 (open circles) µmol photons m^{-2} s^{-1}. Cell density was measured approximately every 24 hours and the growth retardation phase model was fit to the resulting data set for the first 14 days or 16 days for 110 or 60 µmol photons m^{-2} s^{-1} respectively. Growth deviated significantly from predictions (dotted line) after these periods, so subsequent data points were not included in the fit. The initial rate method was used to determine η and then m_v was determined using the best fit of Equation 3-15. Error bars and parameter errors represent the standard error of three biological replicates.

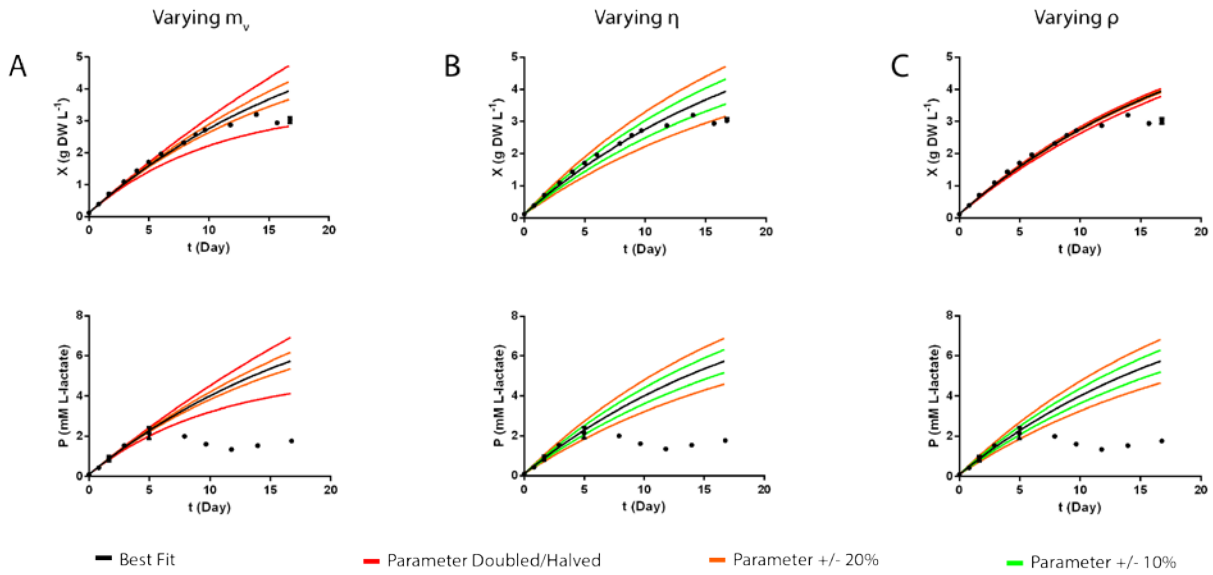

Figure 3-8. Sensitivity Analysis for Light-Limited Growth Model (Described by Equation 3-17 to 3-20). Data is from experiment described in Figure 3-9. Black line for each plot is the best fit parameter set and colored lines represent fits if m_v (A), η (B), or ρ (C) are varied from the best fit by the specified amount while holding the other parameters constant. (A) X and P have low sensitivity to m_v as doubling or halving the value of m_v has minimal effect on the goodness of fit. (B) X and P have high sensitivity to η as even a 20% variation in this parameter has significant effect on the goodness of fit. (C) P has a high sensitivity to ρ while X has a low sensitivity to ρ.

Initial Rate Analysis for Determination of η and ρ

Initial rate analysis is useful for expediting experimentation as measuring an initial linear growth rate is less time consuming than measuring an entire batch growth into stationary phase.

Equation 3-21 gives the derivative of **Equation 3-18** with respect to time.

$$\frac{dX}{dt} = \kappa[X_s - X(0)]\exp(-\kappa t) \tag{3-21}$$

Equation 3-22 gives **Equation 3-21** in the limit as time goes to zero (beginning of growth retardation phase) with the assumption that $\frac{X(0)}{X_s}$ is small.

$$\left.\frac{dX}{dt}\right|_{t\to 0} = \kappa X_s = \frac{Y_{Xv}\eta\frac{I_{IN}S}{V}}{1+\rho\frac{Y_{Xv}}{Y_{Pv}}} \tag{3-22}$$

A similar analysis for P produces **Equation 3-23.**

$$\left.\frac{dP}{dt}\right|_{t\to 0} = \kappa\rho X_s = \frac{Y_{Xv}\eta\frac{I_{IN}S}{V}\rho}{1+\rho\frac{Y_{Xv}}{Y_{Pv}}} \tag{3-23}$$

This result allows η and ρ to be determined from the initial linear rates of growth (LGR) and product secretion (LPR).

Predicting Scale-Up for PCC7002 Strains Engineered for L-lactate Secretion

In previous work, the PCC7002 strain CC131 was engineered for secretion of L-lactate through heterologous expression of an L-lactate dehydrogenase mutated to co-utilize NADPH and NADH as reducing agents to convert pyruvate to L-lactate and through introduction of a CRISPRi system targeted to the metabolic regulator *glnA* (Gordon et al. 2016). In that work, CC131 cultures were grown in tubes in 1% CO_2 with 100 µmol photons m^{-2} s^{-1} ($I_{IN}SV^{-1}$=38,200 µmol photons L^{-1} hr^{-1}) with a resulting LGR of 35±1 mg DW L^{-1} hr^{-1} and a LPR of 92±1 µM L-lactate hr^{-1} (Note that in (Gordon et al. 2016), cell pellets were washed with Tris-buffered saline before determining dry weight rather than distilled water, as was done in this work. To correct for this, dry weight measurements were multiplied by 0.75, the ratio of the dry weight of a distilled water washed pellet to a Tris-buffered saline washed pellet). Using **Equations 3-22 and 3-23**, the photon utilization efficiency (η) was calculated to be 0.52±0.06 and the growth associated productivity (ρ) was calculated to be 2.61±0.09 mmol L-lactate (g DW)$^{-1}$. Using these values, we predicted the scaled-up LGR and LPR of CC131 in 1 L culture bottles ($I_{IN}SV^{-1}$=15,700 µmol photons L^{-1} hr^{-1}) to be 16±2 mg DW L^{-1} hr^{-1} and 43±6 µM L-lactate hr^{-1}, respectively (**Table 3-5**).

To test these predictions, cultures of CC131 were grown in 1 L bottle photobioreactors with Media A supplemented with $NaNO_3$, $FeCl_3$, and KH_2PO_4 until stationary phase and the cell density and L-lactate concentration were measured over time (**Figure 3-8**). The LGR and LPR were 14±0.3 mg DW L^{-1} hr^{-1} and 21±0.9 µM L-lactate hr^{-1}, respectively (calculated from the first 3 days of growth an L-lactate production). While the LGR was close to the predicted value, the LPR was substantially lower than expected. The average values of η and ρ for these cultures were 0.48±0.04 and 1.5±0.07 µmol L-lactate (mg DW)$^{-1}$ determined by initial rate analysis. This significant decrease in growth associated productivity (ρ) suggests

that the ability of cells to convert pyruvate into L-lactate is reduced in the condition of lower q_{Ph} ($\eta I_{IN} SV^{-1} X^{-1}$, **Figure 3-4G**) where cellular energy content is lower.

Using these values of η and ρ in **Equations 3-17 and 3-18** and fitting the resulting equations to growth and L-lactate secretion data for 14 days of growth yielded an average m_v of 1060±100 µmol photons $(g\ DW)^{-1}\ hr^{-1}$, which is similar to that determined for Wild Type PCC7002 (**Figure 3-7**). It is interesting to note that the L-lactate production rate significantly deviated from the model fit after 5 days of growth (approximately 2 g DW L^{-1} and 2 mM L-lactate) and the growth rate significantly deviated from the model fit after 14 days of growth (approximately 3 g DW L^{-1}), suggesting significant changes in metabolism with decreasing q_{Ph}. Data after 14 days were not included in the fit to determine m_v as the model does not adequately describe this result.

Table 3-5. Scale-Up Predictions for Engineered L-lactate and L-lysine Producing Cyanobacteria

CC131 L-lactate Production				
	Tube[a]	Bioreactor		Flask (Perturbation)
$I_{IN}SV^{-1}$ (µmol photons $L^{-1}\ hr^{-1}$)	38200	15700		41000
		Predicted	Measured	
LGR (mg DW $L^{-1}\ hr^{-1}$)	35±1	16±2	14±0.3	
LPR (µM L-lactate hr^{-1})	92±1	43±6	21±0.9	
Best Fit Parameters				
η	0.52±0.06	0.48±0.04		0.41±0.01
ρ (mmol L-lactate $(g\ DW)^{-1}$)	2.6±0.09	1.5±0.07		4.4±0.03
m_v (µmol photons $(g\ DW)^{-1}\ hr^{-1}$)		1060±100		
TK.032 L-lysine Production				
	Flask[b]	Bioreactor		Flask (Perturbation)
$I_{IN}SV^{-1}$ (µmol photons $L^{-1}\ hr^{-1}$)	24300	15700		41000
		Predicted	Measured	
LGR (mg DW $L^{-1}\ hr^{-1}$)	20±2	17±4	10±0.4	
LPR (µM L-lysine hr^{-1})	31±4	26±7	13±0.5	
Best Fit Parameters				
η	0.53±0.11	0.38±0.03		0.34±0.05
ρ (mmol L-lysine $(g\ DW)^{-1}$)	1.6±0.25	1.4±0.08		0.38±0.2
m_v (µmol photons $(g\ DW)^{-1}\ hr^{-1}$)		1150±100		

[a]Experiments from reference (Gordon et al. 2016). [b]Experiments from reference (Korosh et al. 2017).

When the cultures achieved stationary phase and maintained the same cell density for 7 days, the effect of a perturbation in the volumetric photon delivery rate was studied by transferring a 30 mL sample of each culture from the photobioreactor ($I_{IN}SV^{-1}$=15,700 µmol photons L^{-1} hr^{-1}) to a shake flask ($I_{IN}SV^{-1}$=41,000 µmol photons L^{-1} hr^{-1}) (**Figure 3-8**). An immediate restoration of growth and L-lactate production was observed and a model fit (**Equations 3-17 and 3-18**) using m_v=1060 µmol photons $(g\ DW)^{-1}$ hr^{-1} yielded values for the constants η=0.41±0.01 and ρ=4.38±0.03 mmol L-lactate $(g\ DW)^{-1}$. This result suggests that the stationary phase observed in the photobioreactors before the perturbation was due to light limitation as hypothesized. The value of η determined after the perturbation was similar in value to that determined before the perturbation, but the value of ρ was significantly higher after the perturbation. This suggests that the metabolism of CC131 converts fixed carbon to L-lactate more effectively in the condition of higher q_{Ph} in agreement with our previous observations.

At the time of perturbation, samples were taken from each reactor and the spent media was isolated by centrifugation and decanting. Fresh cultures of CC131 were unable to grow in 25 mL of this supernatant in shake flasks ($I_{IN}SV^{-1}$=49,000 µmol photons L^{-1} hr^{-1}) even when supplemented with vitamin B12 or KH_2PO_4. This result in comparison to the robust growth of directly cultured samples discussed previously suggests that the cultures had either sequestered at least one essential nutrient (other than vitamin B12 and phosphate) into their biomass leaving the extracellular medium depleted. Alternatively, the culture accumulated some molecule that is toxic at low cell densities (high biomass specific photon delivery rate), but not high cell densities (low biomass specific photon delivery rate).

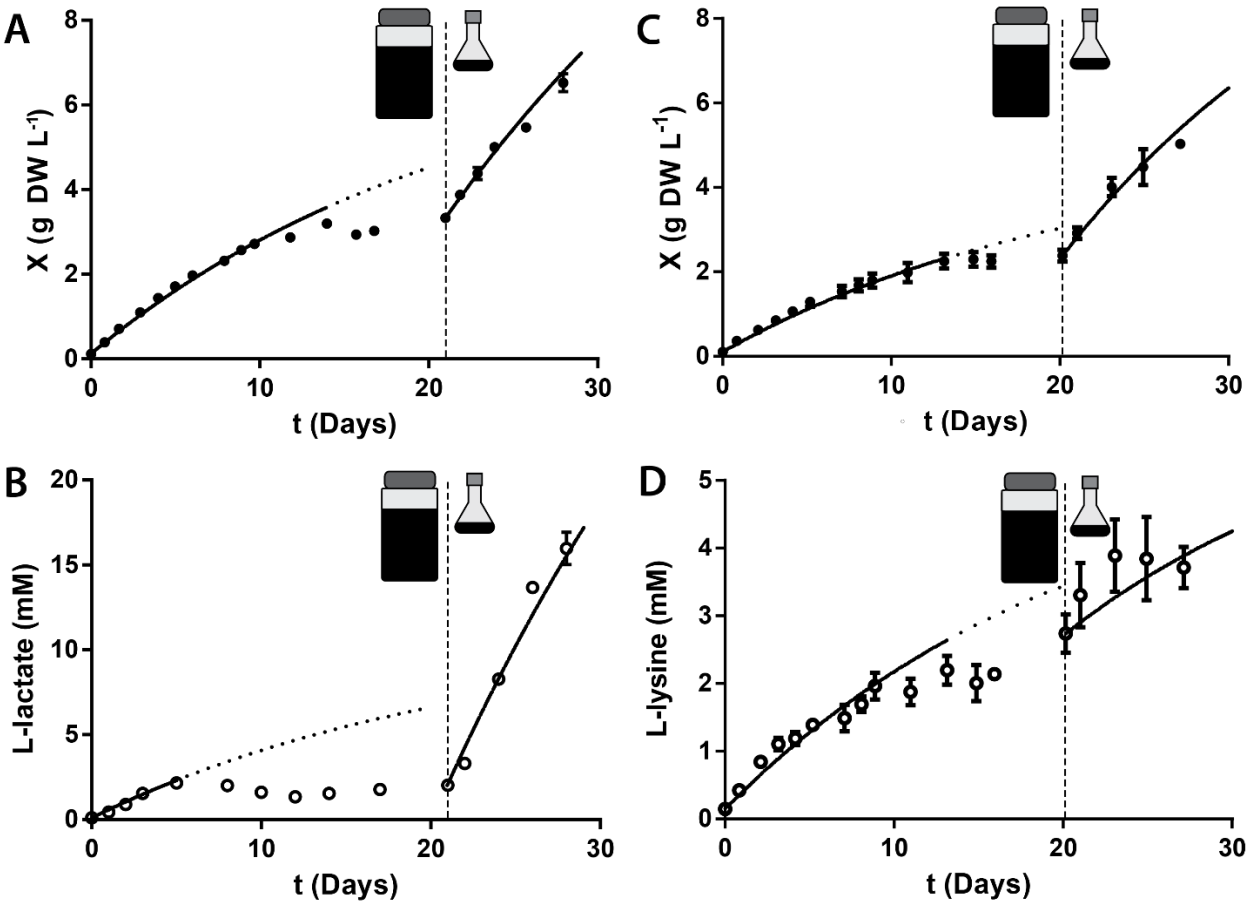

Figure 3-9. Growth and Production of L-lactate and L-lysine in Engineered Cyanobacteria. CC131 growth (A) and L-lactate production (B) and TK.032 growth (C) and L-lysine production (D) were measured in photobioreactors to stationary phase. Subsequently, light limitation was verified by transfer of culture to flasks in which $I_{IN}SV^{-1}$ was significantly higher. Samples were obtained for cell density measurement approximately every 24 hours and L-lactate or L-lysine concentration was determined. The growth retardation phase model was fit to the first 14 days of growth and the first 5 days of L-lactate or L-lysine production after which values deviated significantly from predictions (dotted line). The initial rate method was used to determine η and ρ and then m_v was determined using the best fit of Equations 3-17 and 3-18. After ~21 days (vertical dashed line), samples from each photobioreactor were transferred to shake flasks. η and ρ were determined for this new growth condition by a best fit of Equations 3-17 and 3-18 using the value of m_v determined in the photobioreactors. Parameter values are given in Table 3-5. Error bars represent the standard error of at least two biological replicates.

Predicting Scale-Up for PCC7002 Strains Engineered for L-lysine Secretion

In previous work, the PCC7002 strain TK.032 was engineered for secretion of L-lysine through heterologous expression of an *E. coli* amino acid transporter ybjE and an aspartate kinase insensitive to feedback regulation (Korosh et al. 2017). In that work, TK.032 cultures were grown in shake flasks in 1% CO_2 with 75 µmol photons m^{-2} s^{-1} ($I_{IN}SV^{-1}$=24,300 µmol photons L^{-1} hr^{-1}) with a resulting LGR of 20±2 mg DW L^{-1} hr^{-1} and LPR of 31±4 µM L-lysine hr^{-1}. Using **Equations 3-22 and 3-23**, the photon utilization

efficiency (η) was calculated to be 0.53±0.1 and the growth associated productivity (ρ) was calculated to be 1.56±0.25 mmol L-lysine (g DW)$^{-1}$. Using these values, we predicted the scaled-up LGR and LPR of TK.032 in 1 L culture bottles ($I_{IN}SV^{-1}$=15,700 µmol photons L^{-1} hr^{-1}) to be 17±4 mg DW L^{-1} hr^{-1} and 26±7 µM L-lysine hr^{-1}, respectively (**Table 3-5**).

To test these predictions, cultures of TK.032 were grown in 1 L bottle photobioreactors with Media A supplemented with $NaNO_3$, $FeCl_3$, and KH_2PO_4 until stationary phase and the cell density and L-lysine concentration were measured over time (**Figure 3-7**). The LGR and LPR were 10±0.4 mg DW L^{-1} hr^{-1} and 13±0.5 µM L-lysine hr^{-1}, respectively (calculated from the first 3 days of growth and L-lactate production), both significantly lower than the predicted values. The average values of η and ρ for the photobioreactor cultures were 0.38±0.03 and 1.35±0.08 mmol L-lysine (g DW)$^{-1}$. In this experiment, the change in growth associated productivity (ρ) was minimal relative to the experiments in shake flasks, but photon utilization efficiency (η) decreased by approximately 30% which caused the significant difference between the predicted and actual growth and L-lysine productivity. This contrasts with the scale-up of CC131 where photon utilization efficiency did not change, but a decrease in growth associated productivity accounted for the difference between predicted and actual L-lactate productivity.

The decrease in η for TK.032 observed after moving to the photobioreactors was likely due to osmotic stress associated with nutrient supplementation. We suspect that TK.032 may be less robust to osmotic changes than other strains of PCC7002 due to high expression of the membrane protein *ybjE*. This hypothesis is supported by the observation that TK.032 required approximately 48 hours after reactor inoculation to enter growth retardation phase, significantly longer than observed for other strains of PCC7002, which could be a result of reduced ability to adapt to the higher osmolarity.

Using η and ρ in **Equations 3-17 and 3-18** and fitting the resulting equations to growth and L-lysine secretion data for 13 days of growth yielded an average m_v of 1150±100 µmol photons (g DW)$^{-1}$ hr^{-1}, which is similar to that determined for Wild Type PCC7002 (**Figure 3-7**). It is interesting to note that the growth

rate significantly deviated from the model fit after 13 days of growth (approximately 2 g DW L^{-1}), suggesting significant changes in metabolism with very low I_{AVG}. Data after 13 days were not included in the fit to determine m_v as the model does not adequately describe this result.

The same perturbation in volumetric photon delivery rate described earlier for cultures of CC131 was performed on the TK.032 cultures (**Figure 3-8**). An immediate restoration of growth was observed, but L-lysine secretion was minimal. A model fit (**Equations 3-17 and 3-18**) using m_v=1150 µmol photons (g DW)$^{-1}$ hr^{-1} yielded values for the constants η=0.34±0.05 and ρ=0.38±0.23 mmol L-lysine (g DW)$^{-1}$. The value of η determined after the perturbation was similar in value to that determined before the perturbation, but the value of ρ was significantly lower after the perturbation. This suggests that some irreversible change in metabolism occurred during stationary phase that significantly decreased the L-lysine production potential.

3.4. Discussion

For the purposes of engineering cyanobacteria for fuel and chemical production, it is preferable to study behavior under light-limitation as this is the desired limitation in an industrial process where CO_2 and soluble nutrients can be provided in excess from waste sources (Yenkie et al. 2016). Failure to eliminate other limitations in laboratory cyanobacterial cultivation experiments can lead to confounding results. For example, overexpression of RuBisCO has been studied as a strategy for increased photosynthetic production of fatty acids (Ruffing 2014), isobutyraldehyde (Atsumi, Higashide, and Liao 2009), and sucrose (Ducat et al. 2012) by engineered cyanobacteria, suggesting carbon fixation could be rate-limiting. In subsequent studies, several genes in carbon-fixation were overexpressed in *Synechocystis* sp. PCC6803, some of which caused large increases in O_2-evolution (Liang and Lindblad 2016, 2017). Despite these promising phenotypes, observed increases in growth rate were minimal. A key difference between this study and the previously mentioned successful RuBisCO overexpression studies is that growth experiments were performed in ambient air rather than environments in which inorganic carbon

was supplemented in the form of gas phases with elevated CO_2 or addition of $NaHCO_3$. Thus, eliminating CO_2-limitation in these growth experiments could elucidate why increased O_2-evolution did not translate into increased CO_2-fixation.

Similarly, glycogen accumulation in cyanobacteria has been studied for potential applications as alternative feedstocks for biofuels (Aikawa et al. 2015; Möllers et al. 2014; Song et al. 2016). However, all experiments have been performed in nutrient limiting media where nitrogen limitation triggers the accumulation of glycogen. In practice, nitrogen limitation would limit biomass titer, significantly increasing downstream processing costs (Yenkie et al. 2016). Increasing glycogen accumulation without nutrient limitation is an interesting engineering challenge that will have major implications on the feasibility of this biotechnological pursuit.

In evaluating candidate cyanobacterial species as hosts for photosynthetic chemical production, specific growth rate or doubling time are often reported as the defining growth parameters for which organism is "best", often ignoring the transition to linear phase in this calculation (Schuurmans et al. 2017). The short duration of the exponential growth phase practically necessitates the use of a different parameter to compare strains. We propose that η calculated from the LGR is a better means of comparison between different cyanobacterial species. This suggests that the primary advantage of PCC7002 in the context of photosynthetic chemical production is not the often-lauded high exponential growth rate, but rather its ability to maintain a high η across a wide range of osmolarities, temperatures, and irradiances as shown in **Table 3-4** and **Figure 3-6**. Improving the ability to maintain such efficiencies at irradiances approaching peak solar irradiance is a key engineering challenge for the field.

Productivities of secreted molecules are often reported in units of mg L^{-1} OD^{-1} hr^{-1}, a quantity that describes the biomass specific productivity of a molecule given that the biomass is irradiated with excess photons (Oliver and Atsumi 2014). In addition to ignoring differences in OD to dry cell weight measurements from different laboratories, this method of reporting is not useful for predicting

productivities in a scaled-up process where light is limiting and the biomass specific productivity varies over the course of a batch as shown in this and other work (Kopka et al. 2017). We propose that the standard method of reporting for cyanobacteria engineered for product secretion should include LGR (g DW L^{-1} hr^{-1}) and LPR (mM Product hr^{-1}) as well as the volumetric accessible photon delivery rate ($I_{IN}SV^{-1}$, µmol photons m^{-2} s^{-1}). η and ρ can be determined from these measurements allowing easy comparison across experimental systems for future researchers to build on previous results. While the simple model for q_P used in this work does not capture all the dynamics of product secretion, it does provide some information about how productivity changes over the course of a batch and across different experimental systems. More rigorous studies will consider how q_P varies in time and under relevant process conditions, providing interesting insight into the dynamics of metabolism in engineered cyanobacteria.

Biomass titer and product titer at stationary phase are key factors affecting process economics (Yenkie et al. 2016). As demonstrated in this work, biomass titer is largely determined by specific maintenance, but significant deviations from predicted biomass accumulation occur at high cell densities as observed in **Figures 3-6 and 3-7**. Physiological changes during the transition from growth retardation phase to stationary phase could elucidate the biological mechanisms limiting the achievable biomass titer. Transcriptional changes for light-dark transitions in cyanobacteria have been shown to be regulated by the stringent response (Hood et al. 2016), so it is possible that light-limited stationary phase is triggered due to buildup of (p)ppGpp as the biomass specific photon delivery rate decreases to a point of starvation.

3.5. Conclusions

This work identified conditions for batch growth of cyanobacteria under which light-limitation can be maintained through stationary phase. Theoretical descriptions of the phases of growth provided insight into key factors that limit the productivity and achievable titer of cyanobacterial cultures, including high irradiance, high salinity, and cellular maintenance. Experimental and data analysis methods outlined in this work provide a framework for quantification of bioenergetics of cyanobacteria engineered to secrete

molecules in simple batch culture experiments. Utilization of this framework by researchers of metabolic engineering in cyanobacteria will improve comparisons of experiments performed under different conditions to improve understanding of key factors for photosynthetic chemical production.

3.6. Methods

Culturing Cyanobacteria

Wild Type PCC7002, TK.032, and CC131 were maintained on Media A adapted from Stevens et al (Stevens, Patterson, and Myers 1973) (308 mM NaCl, 20 mM $MgSO_4$, 0.08 mM Na_2EDTA, 8 mM KCl, 3 mM $CaCl_2$, 12 mM $NaNO_3$, 0.37 mM KH_2PO_4, 8 mM Tris Base, 30 µM Ferric Ammonium Citrate, 554 µM H_3BO_3, 22 µM $MnCl_2$, 2.3 µM $ZnCl_2$, 208 nM MoO_3, 12 nM $CuSO_4$, 51 nM $CoCl_2$, 3 nM cobalamin) with 1.5% (w/v) Bacto-Agar (Fisher). CC131 was acquired from Gordon, et al (Gordon et al. 2016) and was maintained with the addition of 100 µg mL^{-1} kanamycin and 30 µg mL^{-1} gentamicin. TK.032 was obtained from (Korosh et al. 2017) and was maintained with the addition of 100 µg mL^{-1} kanamycin. *Synechococcus elongatus* UTEX 2973 was maintained on BG11 medium (Rippka 1988) with 1.5% (w/v) Bacto-Agar (Fisher). Inoculum for experiments was prepared by transferring biomass from solid media to 250 mL shake flasks containing 50 mL of the appropriate medium with a sterile loop and incubating the resulting culture in a Kuhner Climo-Shaker ISF1-X outfitted with a white LED (1% (v/v) CO_2, 37°C, 75 µmol photons m^{-2} s^{-1} from 4000 K White LED). This apparatus was contained in a chemical safety hood to prevent CO_2 accumulation in the laboratory. Optical density at 730 nm was measured in a Genesys 20 spectrophotometer (Thermo Scientific) in 1 cm cuvettes. All samples were diluted into the linear range of OD730 between 0.01-0.30. For cultures in which excess nutrients were added, the dilutions used were sufficient to dissolve any precipitates such that they did not contribute significantly to light scattering. An OD730 to g DW L^{-1} conversion was determined to be 0.26 g DW L^{-1} $OD730^{-1}$ by weighing cell pellets washed three times with MilliQ filtered water and then lyophilized.

Light Quality Calculations

Luminous flux was determined with a Traceable Dual-Range Light Meter (Fisher Scientific). Total PAR radiant intensity was calculated using a conversion factor for the light source used to calibrate the meter. A normalized radiant intensity spectrum for a given light source was measured with a GoDirect SpectroVis Plus Spectrophotometer (Vernier). The total radiant intensity was combined with this radiant flux spectrum to determine the radiant intensity distribution, which was converted to a photonic flux distribution using the photonic energy. I_{AP} was determined to be the sum of all photonic flux between 380-480 nm and 600-700 nm. I_{Chla} was determined to be the sum of all photonic flux between 380-480 nm and 660-700 nm. I_{Phyc} was determined to be the sum of all photonic flux between 600-660 nm. All values of I_{IN} in this work are reported in terms of accessible photons.

Photobioreactor Cultivation

The photobioreactors used in this work are described in **Appendix A**. Briefly, the reactor vessels were 1 L Corning glass wide mouth bottles with modified caps for instrumentation (SV^{-1}=40 m^{-1}). The gas phase was mixed to the specified P_{CO2} using two mass flow controllers, one for air and one for pure industrial grade CO_2, before being delivered to the reactors at approximately 0.3 L min^{-1}. Light was provided by cool white fluorescent bulbs with average I_{IN} of 110 µmol photons m^{-2} s^{-1}. The temperature was maintained at the specified value by a cooling fan (heat provided by the fluorescent bulbs).

The initial working volume for all photobioreactor experiments was 900 mL. For CO_2 transfer optimization, photobioreactors were inoculated with Wild Type PCC7002 to an initial OD730 of 0.05 (three biological replicates per condition). Samples were taken approximately every 24 hours after adjusting the reactor volume with sterile MilliQ to make up for evaporation and OD730 was measured. The first sample taken (approximately 24 hours after inoculations) was determined to be time zero for determination of LGR by fitting a line to the cell density measurements for the first 72 hours.

Nutrient Supplementation in Shake Flasks

40 mL cultures of PCC7002 in Media A were prepared in 250 mL shake flasks inoculated to a final OD730 of 0.05. Media A + N cultures were supplemented with 110 mM $NaNO_3$. Media A + N + P cultures were supplemented with 110 mM $NaNO_3$ and 5.2 mM KH_2PO_4. Media A + N + P + Fe cultures were supplemented with 110 mM $NaNO_3$, 5.2 mM KH_2PO_4, and 1.1 mM $FeCl_3$ and then adjusted to a pH of 7 by addition of NaOH. Samples to which KH_2PO_4 was added were supplemented with additional aliquots of 5.2 mM KH_2PO_4 These flasks were place in the shaking incubator (1% (v/v) CO_2, 37°C, 75 µmol photons m^{-2} s^{-1} from 4000 K White LED) and time zero for growth retardation was taken to be approximately 24 hours after inoculation (OD730~1). + P cultures were supplemented with additional aliquots of 5.2 mM KH_2PO_4 on days 0, 1, 2, 3, and 4 for a total addition of 31 mM KH_2PO_4. Approximately every 24 hours sterile MilliQ water was added to make up for evaporation and OD730 was measured. The samples that were diluted for OD730 measurement were then analyzed for their absorbance spectrum of light from 350-750 nm (1 nm band) in an Infinite M1000 plate reader (Tecan). The resulting spectrum was normalized by dividing by the average OD measurement in the range of 730-750 nm and inserting a baseline at this average value.

Exponential Growth Rate Measurements

Cultures were grown in glass tubes (2x15 cm) containing 20 mL of Media A inoculated to an initial OD730 of 0.01. Tubes were placed in a custom plexiglass water bath maintained at 38°C and illuminated from one side by a White (4000 K) LED Panel with the specified I_{IN}. OD730 measurements were made at time intervals less than the doubling time for a given condition and all measurements were made below OD730=0.1. Exponential growth rate was determined by the slope of a plot of ln(OD730) over time for each sample.

Linear Growth Rate Measurements

Cultures were treated as described in “Exponential Growth Rate Measurements”, but samples were taken in the range of OD730 0.5-5. The water bath temperature was adjusted for varying temperature

samples. High osmolarity cultures were grown in Media A supplemented with NaCl to the specified osmolarity. LGR was determined by the slope of a plot of OD730 over time for each sample. Yields were calculated by the ratio of LGR to the volumetric photon delivery rate ($I_{IN}SV^{-1}$).

Photobioreactor I_{IN} Variation Experiments

Photobioreactors were inoculated with Wild Type PCC7002 to an OD730 of 0.05 with a working volume of 900mL of Media A. The temperature controller was set to maintain the reactors at 30°C. Reactors with I_{IN}=60 µmol photons m^{-2} s^{-1} had 4 of the 8 fluorescent bulbs removed. Time zero for growth retardation was taken to be 24 hours after inoculation (OD730~1). Nutrients were added in aliquots containing 18.3mM $NaNO_3$, 183µM $FeCl_3$, and 5.2mM KH_2PO_4 on Days 0, 2, 4, 7, and 10 for reactors with I_{IN}=110 µmol photons m^{-2} s^{-1} and on Days 0, 3, 5, and 10 for reactors with I_{IN}=60 µmol photons m^{-2} s^{-1}. Samples were taken approximately every 24 hours after adjusting the reactor volume with sterile MilliQ to make up for evaporation and the OD730 was measured.

Photobioreactor L-lactate Production Experiments

Photobioreactors were inoculated with CC131 or TK.032 to an OD730 of 0.05 with a working volume of 930mL of Media A supplemented with 110mM $NaNO_3$, 1.1mM $FeCl_3$, and 5.2mM KH_2PO_4. Reactors with CC131 were supplemented with 100 µg/mL kanamycin, 30 µg/mL gentamicin, and 1mM IPTG. Reactors with TK.032 were supplemented with 100 µg/mL kanamycin, 1mM IPTG, and 100 ng/mL anhydrous tetracycline. The temperature controller was set to maintain the reactors at 37°C. A gas phase containing 5% CO_2 was introduced at a flow rate of 0.3 L min^{-1} and the system was given 1 hour to equilibrate, at which point the pH of each culture was adjusted to 7 by adding approximately 1.7mL of 5M NaOH. Time zero for growth retardation phase was taken to be 24 hours after inoculation for CC131 and 48 hours after inoculation for TK.032 (OD730~1). Samples were taken approximately every 24 hours after adjusting the reactor volume with sterile MilliQ to make up for evaporation and the pH and OD730 were measured. Samples were centrifuged and the supernatant was saved for L-lactate or L-lysine quantification (stored

at -20°C until measurement). Additional KH_2PO_4 was added in 5.2mM aliquots on days 3, 6, and 8 for CC131 and days 2 and 6 for TK.032 (pH fluctuated between 6.7 and 7.2 as KH_2PO_4 was added and subsequently consumed).

Once stationary phase was achieved and maintained for 4 days (21 days after start of experiment), 30 mL samples were transferred from each reactor to 250 mL shake flasks and placed into the shaking incubator (1% (v/v) CO_2, 37°C, 75 µmol photons m^{-2} s^{-1} from 4000 K White LED) where sampling was continued similarly to the photobioreactors for 7 days. Additional samples were taken from the reactors at the same time and centrifuged to remove biomass. The resulting supernatant was inoculated to an OD730 of 0.05 with fresh CC131 culture, but no growth was observed.

L-lactate Quantification

L-lactate concentrations were determined using a L-lactate assay kit (Sigma Aldrich) where an enzymatic reaction results in a colorimetric (450 nm) product. Measurements were made using the protocol contained in the kit. Briefly, standards containing 0, 2, 4, 6, 8, or 10 nmol of L-lactate in 100uL of reaction buffer with the provided enzyme mix and substrate were placed into wells of a 96-well plate. Samples to be quantified were diluted to be within the range of standards (≤2.5 µL of each sample) into reaction buffer with the provided enzyme mix and substrate and placed into wells of a 96-well plate. The same process was repeated for standards and samples excluding the enzyme mix to control for background florescence. The plates were incubated at ambient temperature in the dark for 30 minutes and the absorbance at 450nm was measured with an Infinite M1000 plate reader (Tecan). The absorbance of the control plates was subtracted from the reaction plates and a standard curve was determined from the standards by fitting a line to all samples. This standard curve was used to determine the L-lactate concentration of the samples.

L-lysine Quantification

L-lysine quantification was performed using HPLC (Shimadzu Co., Columbia, MD, USA) equipped with a quaternary pump, autosampler, vacuum degasser, photodiode array and fluorescence detector. HPLC separations were performed using a Xbridge C18 column (2.1 X 150 mM, 3.5 µm, Waters) as described previously (Korosh et al. 2017). The method employed a 20-minute linear gradient starting with 100% Buffer A: [925 ml of 100 mM Acetate (pH 6.95); 50 ml of HPLC Grade Methanol: 25 ml of HPLC Grade Tetrahydrofuran] to 100% Buffer B: [975 ml of HPLC Grade Methanol: 25 ml of HPLC Grade Tetrahydrofuran] before returning to the initial conditions for 10 mins. The flow rate was 0.400 mL/min, column temperature 40°C, and injection volume 10 µL. Amino acid samples and standards were quantified by comparison with peaks generated by monitoring the fluorescence (Ex 320 nm/ Em 450 nm) of known amounts of standards in Media A^+, after precolumn derivatization with 3 mg/ml o-phthalaldehyde with 3-mercaptopropionic acid in 0.4 M borate buffer.

Theoretical Yield Calculations

Theoretical maximum yields on photons of both biomass and the products in **Table 3-3** were calculated using a genome-scale metabolic model of PCC7002, *i*Syp708. Within the model, the total photon uptake flux (*i. e.* r_EX_PHOTONPSII_E + r_EX_PHOTONPSI_E) was constrained to be less than or equal to 1 mmol photons $(g\ DW)^{-1}\ hr^{-1}$. The uptake fluxes of carbon dioxide, nitrate, water, oxygen, phosphate, sulfate, magnesium, and protons were unconstrained. The bidirectional hydrogenase and pyruvate synthase reactions were disabled as those reactions are known to be inactive in the presence of oxygen. For simulations maximizing the yields of non-native compounds, the appropriate biosynthesis pathways were added to the model. Additionally, when simulating terpenes produced via the non-native mevalonate pathway, the native MEP pathway in the model was inactivated by disabling flux through the 2-C-methyl-D-erythritol-2,4-cyclodiphosphate dehydratase reaction. “Demand” reactions were added to the model to remove the products of interest from the cytosol. Given these constraints, flux balance

analysis (FBA) was performed with the objective of maximizing the production of biomass or the specific product of interest (Orth, Thiele, and Palsson 2010). Yields were determined by dividing this maximum production flux by the photon uptake flux. For all yield calculations, it was verified that the total photon uptake flux was unique given the maximized objective. All simulations were performed in GAMS (GAMS Development Corporation, Washington, DC) using the CPLEX solver.

It should be noted that there is a small degree of uncertainty in these Y_{Pv} values stemming from uncertainty in the exact H^+/ATP ratio utilized by the ATP synthase in PCC7002 (the published *i*Syp708 model uses a ratio of 4). To examine the magnitude of this uncertainty on the yields reported in **Table 3-3**, the H^+/ATP ratio in the metabolic model was varied from 3 to 5 and the percent change in each product yield across this range was calculated. The largest percent decrease in Y_{Pv} from H^+/ATP=3 to H^+/ATP=5 was ~15% for acetone, with most compounds having a percent decrease well below 10%. As such, it seems that the uncertainties in the calculated Y_{Pv} should have relatively little impact on the accuracy of the models developed in this work.

Model Fits

Model fits were determined using the Solver tool in Microsoft Office Excel 2016. For each data point the normalized square error was normalized by the theoretical yield on photons using the following expression:

$$\frac{|X_{Data}-X_{Model}|}{Y_{Xv}} \; or \; \frac{|P_{Data}-P_{Model}|}{Y_{Pv}} \tag{3-24}$$

The normalized square error was summed for all data point included in the fit and this sum divided by the number of data points was used as the objective function. The fit was optimized using the Microsoft Excel Solver tool by setting the objective function to zero and changing the specified parameters.

3.7. References

Aikawa, Shimpei et al. 2015. “Improving Polyglucan Production in Cyanobacteria and Microalgae via Cultivation Design and Metabolic Engineering.” *Biotechnology Journal* 10(6):886–98.

Angermayr, S.Andreas, Aleix Gorchs Rovira, and Klaas J. Hellingwerf. 2015. “Metabolic Engineering of Cyanobacteria for the Synthesis of Commodity Products.” *Trends in Biotechnology* 33(6):352–61.

Atsumi, Shota, Wendy Higashide, and James C. Liao. 2009. “Direct Photosynthetic Recycling of Carbon Dioxide to Isobutyraldehyde.” *Nature Biotechnolog*y 27(12):1177–80.

Barbosa, Maria J., Marcel Janssen, Nienke Ham, Johannes Tramper, and René H. Wijffels. 2003. “Microalgae Cultivation in Air-Lift Reactors: Modeling Biomass Yield and Growth Rate as a Function of Mixing Frequency.” *Biotechnology and Bioengineering* 82(2):170–79.

Boogerd, F. C., P. Bos, J. G. Kuenen, J. J. Heijnen, and R. G. van der Lans. 1990. “Oxygen and Carbon Dioxide Mass Transfer and the Aerobic, Autotrophic Cultivation of Moderate and Extreme Thermophiles: A Case Study Related to the Microbial Desulfurization of Coal.” *Biotechnology and Bioengineering* 35(11):1111–19.

Clark, Ryan L., Jeffrey C. Cameron, Thatcher W. Root, and Brian F. Pfleger. 2014. “Insights into the Industrial Growth of Cyanobacteria from a Model of the Carbon-Concentrating Mechanism.” *AIChE Journal* 60(4):1269–77.

Ducat, Daniel C., J. Abraham Avelar-Rivas, Jeffrey C. Way, and Pamela a Silver. 2012. “Rerouting Carbon Flux to Enhance Photosynthetic Productivity.” *Applied and Environmental Microbiology* 78(8):2660–68.

Egli, Thomas. 2015. “Microbial Growth and Physiology: A Call for Better Craftsmanship.” *Frontiers in Microbiology* 6:287.

Evers, E. G. 1991. “A Model for Light-Limited Continuous Cultures: Growth, Shading, and Maintenance.” *Biotechnology and Bioengineering* 38(3):254–59.

García Camacho, F., A. Sánchez Mirón, E. Molina Grima, F. Camacho Rubio, and J. C. Merchuck. 2012. “A Mechanistic Model of Photosynthesis in Microalgae Including Photoacclimation Dynamics.” *Journal of Theoretical Biology* 304:1–15.

Gordon, Gina C. et al. 2016. “CRISPR Interference as a Titratable, Trans-Acting Regulatory Tool for Metabolic Engineering in the Cyanobacterium *Synechococcus* Sp. Strain PCC 7002.” *Metabolic Engineering* 38:170–79.

Grima, E. Molina, F. García Camacho, J. A. Sánchez Pérez, F. G. Acién Fernéndez, and J. M. Fernández Sevilla. 1997. “Evaluation of Photosynthetic Efficiency in Microalgal Cultures Using Averaged Irradiance.” *Enzyme and Microbial Technology* 21(5):375–81.

Hood, Rachel D., Sean A. Higgins, Avi Flamholz, Robert J. Nichols, and David F. Savage. 2016. “The Stringent Response Regulates Adaptation to Darkness in the Cyanobacterium *Synechococcus Elongatus*.” *Proceedings of the National Academy of Sciences of the United States of America* 113(33):E4867–76.

Jackson, Simon A., Julian J. Eaton-Rye, Donald A. Bryant, Matthew C. Posewitz, and Fiona K. Davies. 2015. “Dynamics of Photosynthesis in a Glycogen-Deficient glgC Mutant of *Synechococcus* Sp. Strain PCC 7002.” *Applied and Environmental Microbiology* 81(18):6210–22.

Kopka, Joachim et al. 2017. “Systems Analysis of Ethanol Production in the Genetically Engineered Cyanobacterium *Synechococcus* Sp. PCC 7002.” *Biotechnology for Biofuels* 10(1):56.

Korosh, Travis C., Andrew L. Markley, Ryan L. Clark, Laura L. McGinley, and Brian F. Pfleger. 2017. “Engineering Photosynthetic Production of L-Lysine.” *Biotechnology for Biofuels* In Preparation

Lewis, Nathan E., Harish Nagarajan, and Bernhard O. Palsson. 2012. “Constraining the Metabolic Genotype–phenotype Relationship Using a Phylogeny of in Silico Methods.” *Nature Reviews Microbiology* 10(4):291–305.

Liang, Feiyan and Peter Lindblad. 2016. “Effects of Overexpressing Photosynthetic Carbon Flux Control Enzymes in the Cyanobacterium *Synechocystis* PCC 6803.” *Metabolic Engineering* 38:56–64.

Liang, Feiyan and Peter Lindblad. 2017. “*Synechocystis* PCC 6803 Overexpressing RuBisCO Grow Faster with Increased Photosynthesis.” *Metabolic Engineering Communications* 4:29–36.

Ludwig, Marcus and Donald A. Bryant. 2012. “Acclimation of the Global Transcriptome of the Cyanobacterium *Synechococcus* Sp. Strain PCC 7002 to Nutrient Limitations and Different Nitrogen Sources.” *Frontiers in Microbiology* 3:145.

Möllers, K.Benedikt, David Cannella, Henning Jørgensen, and Niels-Ulrik Frigaard. 2014. “Cyanobacterial Biomass as Carbohydrate and Nutrient Feedstock for Bioethanol Production by Yeast Fermentation.” *Biotechnology for Biofuels* 7:64.

Monod, Jacques. 1949. “The Growth of Bacterial Cultures.” *Annual Review of Microbiology* 3(1):371–94.

Oliver, John W. K. and Shota Atsumi. 2014. “Metabolic Design for Cyanobacterial Chemical Synthesis.” *Photosynthesis Research* 120(3):249–61.

Oliver, Neal J. et al. 2016. “Cyanobacterial Metabolic Engineering for Biofuel and Chemical Production.” *Current Opinion in Chemical Biology* 35:43–50.

Orth, Jeffrey D., Ines Thiele, and Bernhard Ø. Palsson. 2010. “What Is Flux Balance Analysis?” *Nature Biotechnology* 28(3):245–48.

Pirt, S. J. 1965. “The Maintenance Energy of Bacteria in Growing Cultures.” *Proceedings of the Royal Society of London. Series B, Biological Sciences* 163(991):224–31.

Pirt, S. J. 1986. “The Thermodynamic Efficiency (Quantum Demand) and Dynamics of Photosynthetic Growth.” *New Phytologist* 102(4):3–37.

Price, G.Dean, Fiona J. Woodger, Murray R. Badger, Susan M. Howitt, and Loraine Tucker. 2004. “Identification of a SulP-Type Bicarbonate Transporter in Marine Cyanobacteria.” *Proceedings of the National Academy of Sciences of the United States of America* 101(52):18228–33.

Rippka, Rosmarie. 1988. “Isolation and Purification of Cyanobacteria.” *Methods in Enzymology* 167:3–27.

Ruffing, Anne M. 2014. “Improved Free Fatty Acid Production in Cyanobacteria with *Synechococcus* Sp. PCC 7002 as Host.” *Frontiers in Bioengineering and Biotechnology* 2:17.

Schuurmans, R. M., J. C. P. Matthijs, and K. J. Hellingwerf. 2017. “Transition from Exponential to Linear Photoautotrophic Growth Changes the Physiology of *Synechocystis* Sp. PCC 6803.” *Photosynthesis Research* 132(1):69–82.

Schuurmans, R.Milou, Pascal Van Alphen, J.Merijn Schuurmans, Hans C. P. Matthijs, and Klaas J. Hellingwerf. 2015. “Comparison of the Photosynthetic Yield of Cyanobacteria and Green Algae: Different Methods Give Different Answers.” *PLoS ONE* 10(9):1–17.

Shuler, Michael L. and Fikret Kargi. 1992. *Bioprocess Engineering: Basic Concepts*. Prentice Hall.

Song, Kuo, Xiaoming Tan, Yajing Liang, and Xuefeng Lu. 2016. “The Potential of *Synechococcus Elongatus* UTEX 2973 for Sugar Feedstock Production.” *Applied Microbiology and Biotechnology* 100:7865.

Stevens, S. E., D. L. Balkwill, and D. A. M. Paone. 1981. “The Effects of Nitrogen Limitation on the Ultrastructure of the Cyanobacterium *Agmenellum Quadruplicatum*.” *Archives of Microbiology* 130:204–12.

Stevens, S. E., C. O. P. Patterson, and J. Myers. 1973. “The Production of Hydrogen Peroxide by Blue-Green Algae: A Survey.” *Journal of Phycology* 9:427–30.

Touloupakis, Eleftherios, Bernardo Cicchi, and Giuseppe Torzillo. 2015. “A Bioenergetic Assessment of Photosynthetic Growth of *Synechocystis* Sp. PCC 6803 in Continuous Cultures.” *Biotechnology for Biofuels* 8(1):133.

Vu, Trang T. et al. 2013. “Computational Evaluation of *Synechococcus* Sp. PCC 7002 Metabolism for Chemical Production.” *Biotechnology Journal* 8(5):619–30.

Xiong, Qian et al. 2015. “Integrated Transcriptomic and Proteomic Analysis of the Global Response of *Synechococcus* Sp . PCC 7002 to High Light Stress.” *Molecular and Cellular Proteomics* 14(4):1038–53.

Xue, Yong and Qingfang He. 2015. “Cyanobacteria as Cell Factories to Produce Plant Secondary Metabolites.” *Frontiers in Bioengineering and Biotechnology* 3:57.

Yenkie, Kirti M. et al. 2016. “A Roadmap for the Synthesis of Separation Networks for the Recovery of Bio-Based Chemicals: Matching Biological and Process Feasibility.” *Biotechnology Advances* 34(8):1362–83.

Youngquist, J.Tyler et al. 2012. “Kinetic Modeling of Free Fatty Acid Production in *Escherichia Coli* Based on Continuous Cultivation of a Plasmid Free Strain.” *Biotechnology and Bioengineering* 109(6):1518–27.

Chapter 4: Insight into the Industrial Growth of Cyanobacteria from a Model of the CO_2-Concentrating Mechanism

This chapter is adapted from *AIChE Journal*, Vol. 60, No. 4, Clark, Ryan L; Cameron, Jeffrey C; Root, Thatcher W; Pfleger, Brian F; Insights into the Industrial Growth of Cyanobacteria from a Model of the Carbon-Concentrating Mechanism, p. 1269-1277, Copyright 2014, with permission from John Wiley and Sons.

4.1. Background and Motivation

In cyanobacteria, the light reactions of photosynthesis are carried out in the thylakoid membrane, where the light-driven oxidation of H_2O produces molecular O_2, electrons transferred to plastiquinones, and protons in the thylakoid lumen (Lea-Smith et al. 2015). The resulting proton gradient is used for ATP production and the electrons are transferred along the photosynthetic electron transport chain to terminal electron acceptors, the most significant of which is $NADP^+$ to generate NADPH. ATP and NADPH are subsequently utilized by the Calvin-Benson-Bassham cycle (CBB cycle) for the fixation of CO_2 into organic molecules, while O_2 acts as a competitive inhibitor of carbon fixation because of the dual substrate specificity of ribulose 1,5-bisphosphate carboxylase/oxygenase (RuBisCO), the key carbon fixing enzyme (Tcherkez, Farquhar, and Andrews 2006).

The slow catalytic turnover and lack of specificity of RuBisCO between CO_2 and O_2 were sufficient for growth under the high concentrations of CO_2 and low concentrations of O_2 in the Earth's early atmosphere. However, over millions of years photosynthetic organisms significantly increased atmospheric O_2 levels and consumed CO_2, shifting their relative abundance (Badger and Price 2003). Under current atmospheric conditions (21% O_2 and 0.039% CO_2), CO_2 concentration is a limiting factor for photosynthesis; the photosynthetic capacity of the cell is directly correlated with the availability of CO_2. During the transition from abundant to limiting CO_2 concentrations, cyanobacteria evolved an elaborate CO_2-concentrating mechanism (CCM) comprised of inorganic carbon sequestration systems and the carboxysome, a protein-based organelle for carbon fixation (Price et al. 2008). The CCM functions to concentrate CO_2 at the site of carbon fixation, where it is consumed by RuBisCO. While the CCM is essential for viability in current atmospheric CO_2 concentrations, this requirement can be overcome in

laboratory conditions through enrichment of the growth environment in CO_2. In industrial applications using high CO_2 streams from combustion flue gases, feed enrichment could be as high as 15% CO_2.

In the aqueous environments where cyanobacteria are typically found, HCO_3^- is the predominant form of inorganic carbon (C_i) (Butler 1982). HCO_3^- is actively transported across the cell by a suite of membrane bound transporters. Three classes of HCO_3^- transporters have been shown to be important for C_i acquisition in cyanobacteria. BCT1 is a high affinity ATP binding cassette (ABC) transporter that is induced under low C_i conditions (Omata et al. 2002). SbtA is a high affinity, Na^+-dependent transporter that is also induced under low C_i conditions (Shibata et al. 2002). BicA is a Na^+-dependent, low affinity, high-flux transporter (Price et al. 2004). In *Synechococcus* sp. PCC7002, BicA is present during carbon-replete conditions but is upregulated during carbon limitation. In contrast, the BicA homolog in *Synechocystis* sp. PCC6803 has been reported to be constitutively expressed (Wang, Postier, and Burnap 2004). Different species of cyanobacteria express some or all of these HCO_3^- uptake systems. *Synechocystis* sp. PCC6803 contains all three systems, while *Synechococcus elongatus* PCC7942 lacks BicA, and *Synechococcus* PCC7002 lacks BCT1 (Price et al. 2004). Moreover, differences in transport activity have been reported for the BicA homologs (Price et al. 2004). In contrast to HCO_3^-, CO_2 can diffuse across the cell membrane. Two CO_2 uptake protein complexes, NDH-1_4 and NDH-1_3, are involved in the hydration of CO_2 into HCO_3^- in the cytoplasm (Ohkawa et al. 2000). NDH-1_4 is a constitutively expressed, low-affinity system that may be located on the plasma membrane (Maeda, Badger, and Price 2002; Shibata et al. 2001). NDH-1_3 is a high-affinity, low C_i inducible system located on the thylakoid membrane (Klughammer et al. 1999; Maeda et al. 2002; Shibata et al. 2001). The concerted activity of these transporters allows the cells to accumulate high internal levels of HCO_3^-.

In addition to the C_i acquisition system, the CCM also requires the carboxysome, which is a protein-based bacterial microcompartment (BMC) that resembles an icosahedral viral capsid (Tanaka et al. 2008). It is composed of a semi-permeable shell containing hexameric and pentameric proteins surrounding

RuBisCO and carbonic anhydrase (CA) (Yeates et al. 2008). The shell has been proposed to be permeable to HCO_3^-, but not O_2 or CO_2 due to the electrostatic properties of the residues lining the pore of each shell protein (Kinney, Axen, and Kerfeld 2011). However, a recent modelling study suggests that the diffusion barrier provided by the carboxysome need not be specific to function (Mangan et al. 2016). Once HCO_3^- enters the carboxysome, it is dehydrated to CO_2 by CA, known to be one of the most active enzymes (Shingles and Moroney 1997). RuBisCO catalyzes the carboxylation of ribulose-1,5-bisphosphate (RuBP) to form two molecules of 3-phosphoglycerate (3-PGA). 3-PGA diffuses out of the carboxysome, where it is consumed by the CBB-cycle, providing the major sink for photosynthetically derived ATP and NADPH. Carboxysomes are found in all free-living cyanobacteria and are essential for survival in ambient CO_2 concentrations. However, they are dispensable at high CO_2 (*i. e.* 10%) concentrations. Thus, strains lacking a carboxysome have a high CO_2 requiring (HCR) phenotype (Price and Badger 1989b). It is critical to the formation of the intracellular HCO_3^- pool that CA activity is localized exclusively to the carboxysome. It has been shown that expression of an extra-carboxysomal human CA in *Synechococcus elongatus* PCC7942 results in an HCR phenotype (Price and Badger 1989a). Evidence suggests that this locational specificity is accomplished through deactivation of carboxysomal CA before it is oxidized during carboxysome biogenesis (Peña et al. 2010).

The CCM provides significant fitness benefits to the cell during natural, low-CO_2 conditions. However, it is not clear whether the CCM will be beneficial in an industrial setting for photosynthetic production of fuels and chemicals where a high CO_2 environment could be provided using CO_2 from waste streams. Previously, several groups have investigated the maximum CO_2-fixation rates in cyanobacteria and the role of the CCM (Mangan et al. 2016; Mangan and Brenner 2014; Price et al. 2004; Rae et al. 2012; Westermark and Steuer 2016). However, equivalent models have not been used to investigate the maximum CO_2-fixation rates in carboxysome-less strains exposed to different C_i concentrations. In this work, we investigate the effects of diffusion, size and number of carboxysomes, and the active carbon

uptake system on rates of photosynthesis. Our results provide insight into the limitations of carbon fixation and strategies for increased carbon fixation in industrially relevant conditions.

4.2. Definition of Model

Simplifying assumptions that eliminate unimportant parameters and emphasize the question at hand are at the heart of any transport analysis in the style of Bird, Stewart, and Lightfoot. In this study, we wished to determine the impact of the carbon-concentrating mechanism evolved by cyanobacteria on the rate of carbon-fixation by RuBisCO over a range of industrially relevant CO_2 concentrations. The simplifications imposed upon this problem address geometry, kinetics, and mass transport. To demonstrate the importance and impact of the CO_2-concentrating mechanism, two cases were considered: a wild type cyanobacterium and a mutant lacking the carboxysome unit of the CCM. Quantitative results were obtained by applying this analysis to two different species of cyanobacteria: (1) the industrially attractive *Synechococcus sp.* PCC7002 and (2) the model strain for studies of β-carboxysomes, *Synechococcus elongatus* PCC7942.

For modeling purposes, the geometry of the cyanobacterial cell was idealized to a sphere in a well-mixed medium as shown in **Figure 4-1**, resulting in a problem analogous to the classic "Diffusion and Chemical Reaction Inside a Porous Catalyst" problem (Bird, Stewart, and Lightfoot 2007). The membranes of the cell were assumed to be negligible in thickness relative to the radius of the cell and form the outer boundary of the sphere. The permeability of lipid bilayers to CO_2 is six orders of magnitude higher than to HCO_3^-, so the cell membrane was assumed HCO_3^--impermeable (Gutknecht, Bisson, and Tosteson 1977).

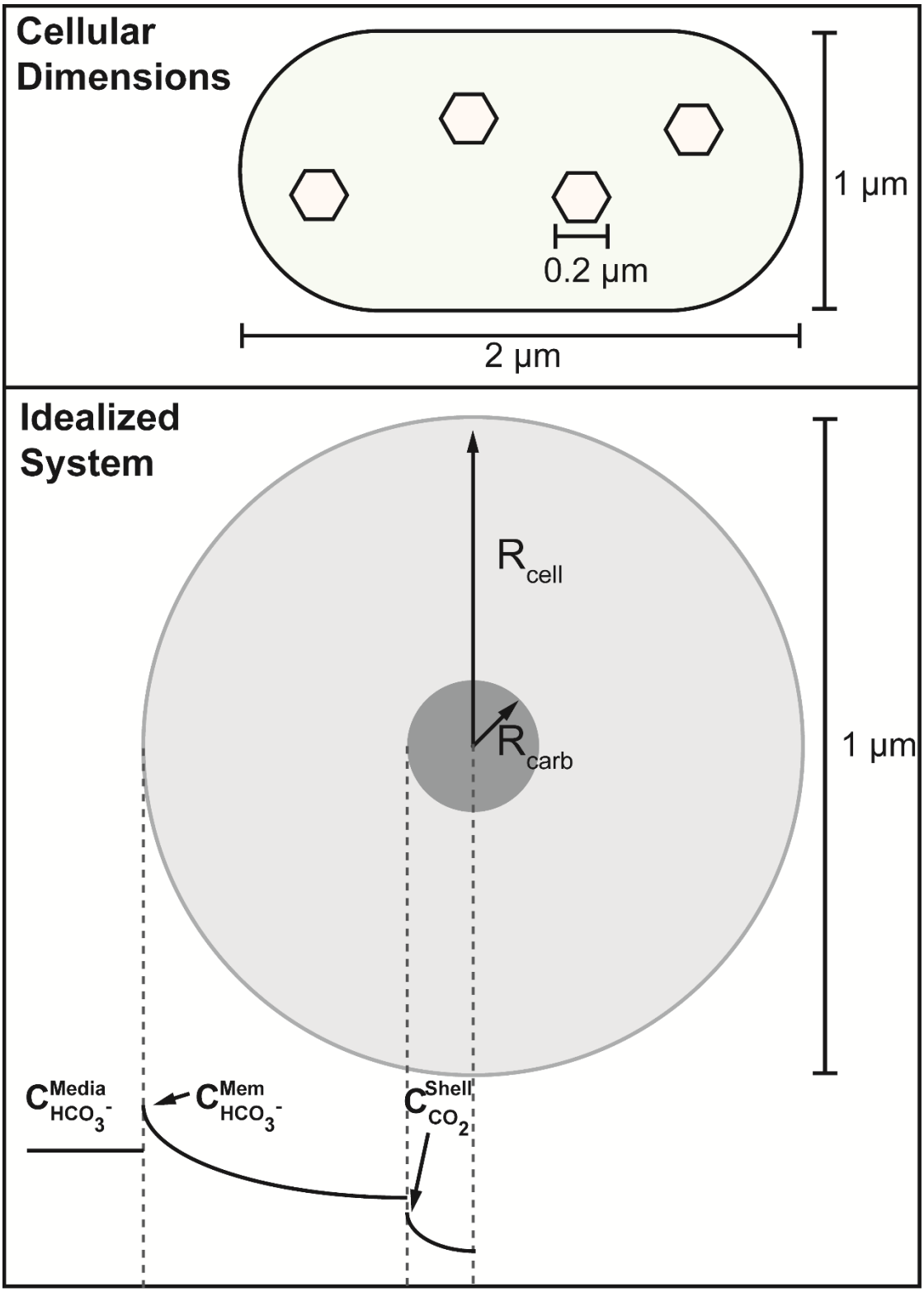

Figure 4-1. Spherical Approximation for the Model of Wild Type Cyanobacteria. The $HCO3^-$ profile is exaggerated to emphasize any concentration gradients needed to produce diffusive flux to the carboxysome. The same spherical boundary at the membrane was used in the model of the carboxysome-lacking mutant.

For the wild type case, the cell was divided into two distinct phases: the carboxysome and the cytoplasm. Convective velocities within the cell were assumed to be negligible, leaving mass transport to occur only through diffusion. BicA is the most relevant active carbon transporter in PCC7002 in the CO_2 concentration range studied in this analysis and was therefore the only transporter considered. PCC7942 does not have a BicA transporter so we chose to estimate its HCO_3^- flux as a fraction of that of PCC7002 determined from the literature(Price et al. 2004). The consumption of CO_2 and HCO_3^- in the cytoplasm by non-carbon-fixation related metabolic processes were considered negligible relative to carbon-fixation catalyzed by RuBisCO. At the inner boundary of the cytoplasm phase located at the carboxysome wall, a Fick's Law constant flux boundary condition was imposed. The flux into the carboxysome was the integrated CO_2 consumption rate inside the carboxysome per unit surface area of the carboxysome.

The cell was modeled with one concentric spherical carboxysome within which the consumption of CO_2 occurred through a homogeneous reaction catalyzed by uniformly packed RuBisCO. The O_2-inhibited Michaelis-Menten kinetic model (Ku and Edwards 1978) was used for the carbon fixation rate of RuBisCO:

$$v = \frac{k_{cat}[R]C_{CO_2}^{Carb}}{C_{CO_2}^{Carb} + K_{m,CO_2}\left(1+\frac{C_{O_2}^{Carb}}{K_{m,O_2}}\right)} \qquad (4\text{-}1)$$

The k_{cat} for carbonic anhydrase(Shingles and Moroney 1997) present in the carboxysome is four orders of magnitude larger than that of RuBisCO (Badger et al. 1998), so HCO_3^- was treated as instantaneously equilibrated with CO_2 within the carboxysome. Therefore, the concentration of CO_2 directly inside the carboxysome wall was proportional to the HCO_3^- concentration directly outside of the wall in the cytoplasm phase. The proportionality constant incorporated both the CO_2-HCO_3^- equilibrium constant and a barrier to HCO_3^- transport across the carboxysome wall. Evidence suggesting a mechanism to prevent the leakage of CO_2 from the carboxysome exists, so the carboxysome wall was approximated as impermeable to CO_2 (Price et al. 2008).

The second case considered a mutant cyanobacterial cell lacking the carboxysomes and active bicarbonate transporters, with a mutant model simplified by two primary differences from the wild type. First, RuBisCO was considered to be distributed homogeneously throughout the single cytoplasm phase. Second, the CO_2 concentration was determined only by direct diffusion across the cell membrane.

4.3. Transport Analysis

To determine the importance of diffusion in the carbon fixation process, the differential mass balances for the various phases in question were examined. The balances were non-dimensionalized and the reactive flux was compared to the diffusive flux. The resulting dimensionless group, referred to as the Damköhler number, is defined as the ratio of the characteristic reaction rate to the characteristic diffusion rate for each case (Bailey and Ollis 1986). This analysis focuses on fluxes of CO_2 and HCO_3^- as key species controlling the RuBisCO carbon fixation kinetics. This step also involves consumption of co-reactants and generation of products, including RuBP, 3-PGA, ATP, and NADH. These need not be modeled explicitly because they are also small molecules that would be present at excess concentrations as provided by other processes and would be expected to have diffusive properties (Kao, Abney, and Verkman 1993; Mastro et al. 1984) almost as fast as CO_2. Further, these species have not been observed to affect RuBisCO reaction rates under nutritionally rich conditions.

CO_2 in Carboxysome

In considering the CO_2 profile inside the carboxysome, the differential mass balance equation for a sphere with homogeneous reaction following oxygen-inhibited Michaelis-Menten kinetics was used with constant surface concentration and spherical symmetry boundary conditions:

$$\frac{D_{CO_2}^{Carb}}{r^2}\frac{\partial}{\partial r}\left(r^2\frac{\partial C_{CO_2}^{Carb}}{\partial r}\right)=\frac{k_{cat}[R]C_{CO_2}^{Carb}}{C_{CO_2}^{Carb}+K_{m,CO_2}\left(1+\frac{C_{O_2}^{Carb}}{K_{m,O_2}}\right)} \tag{4-2}$$

$$BC1: C_{CO_2}^{Carb}=C_{CO_2}^{Shell} \text{ at } r=R_{Carb} \tag{4-3}$$

$$BC2: \frac{\partial C_{CO_2}^{Carb}}{\partial r}=0 \text{ at } r=0 \tag{4-4}$$

where $C_{CO_2}^{Shell}$ is related to the HCO_3^- concentration in the cytoplasm by a function unimportant for the transport analysis. This relationship was revisited in the kinetic analysis of the localization of CO_2 to the carboxysome for carbon fixation.

For further simplification, two situations were considered for the rate expression of the RuBisCO catalyzed reaction: one in which $C_{CO_2}^{Carb} \gg K_{m,CO_2}$, resulting in zero-order kinetics, and one in which $C_{CO_2}^{Carb} \ll K_{m,CO_2}$, resulting in first-order kinetics. For non-dimensionalizing these equations, the characteristic length used was the carboxysome radius and the characteristic concentration used was the CO_2 concentration at the carboxysome surface. The following Damköhler numbers were determined:

$$C_{CO_2}^{Carb} \gg K_{m,CO_2}: Da = \frac{k_{cat}[Ru]_{Carb}R_{Carb}^2}{D_{CO_2}^{Carb}C_{CO_2}^{Shell}} \quad (4\text{-}5)$$

$$C_{CO_2}^{Carb} \ll K_{m,CO_2}: Da = \frac{k_{cat}[Ru]_{Carb}R_{Carb}^2}{D_{CO_2}^{Carb}K_{m,CO_2}\left(1+\frac{C_{O_2}^{Carb}}{K_{m,O_2}}\right)} \quad (4\text{-}6)$$

The inorganic carbon flux at the carboxysome shell was needed for transport analysis of the cytoplasm phase. Expressions for J^* were determined for zero- and first-order kinetics by integrating the rate expressions over the volume of the carboxysome and dividing by the surface area of the carboxysome, resulting in the following expressions:

$$C_{CO_2}^{Carb} \gg K_{m,CO_2}: J^* = \frac{k_{cat}[Ru]_{Carb}R_{Carb}}{4} \quad (4\text{-}7)$$

$$C_{CO_2}^{Carb} \ll K_{m,CO_2}: J^* = \frac{k_{cat}[Ru]_{Carb}R_{carb}C_{CO_2}^{Shell}}{3K_{m,CO_2}} \quad (4\text{-}8)$$

HCO_3^- in Cytoplasm

The HCO_3^- profile within the cytoplasm of the wild type cell was calculated from the spherical differential mass balance equation with no generation or consumption term. A constant concentration boundary condition was applied at the cell membrane boundary and a constant flux boundary condition was applied at the carboxysome boundary:

$$\frac{\partial}{\partial r}\left(r^2\frac{\partial C_{HCO_3^-}^{Cyt}}{\partial r}\right)=0 \quad (4\text{-}9)$$

$$BC1: C_{HCO_3^-}^{Cyt}=C_{HCO_3^-}^{Mem} \text{ at } r=R_{Cell} \quad (4\text{-}10)$$

$$BC2: \frac{\partial C_{HCO_3^-}^{Cyt}}{\partial r}=\frac{-J^*}{D_{HCO_3^-}^{Cyt}} \text{ at } r=R_{Carb} \quad (4\text{-}11)$$

where $C_{HCO_3^-}^{Mem}$ is related to the HCO_3^- concentration in the media by a flux balance unimportant for the transport analysis. This relationship was revisited in the kinetic analysis of the formation of the intracellular HCO_3^- pool.

For the cytoplasm phase, the characteristic length was the radius of the cell and the characteristic concentration was the HCO_3^- concentration at the inside of the cell membrane interface. The solution to this non-dimensionalized differential mass balance and its boundary conditions resulted in the following Damköhler number relating the rate of reaction to the rate of diffusive flux:

$$Da=\frac{J^*R_{Carb}^2}{D_{HCO_3^-}^{Cyt}C_{HCO_3^-}^{Mem}R_{cell}} \quad (4\text{-}12)$$

The expressions for J^* determined in the analysis of the carboxysome phase were used to determine the final Damköhler numbers for the cases of $C_{CO_2}^{Carb} \gg K_{m,CO_2}$ and $C_{CO_2}^{Carb} \ll K_{m,CO_2}$.

No-Carboxysome Case

The differential mass balance and boundary conditions for the mutant case of a cell with no carboxysomes were analogous to the carboxysome phase of the previous case. The characteristic length for this case was the radius of the cell and the characteristic concentration was the CO_2 concentration at the cell membrane interface, which was equal to the CO_2 concentration in the media. The resulting Damköhler numbers were as follows:

$$C_{CO_2}^{Cyt} \gg K_{m,CO_2}: Da=\frac{k_{cat}[Ru]_{Cyt}R_{Cell}^2}{D_{CO_2}^{Cyt}C_{CO_2}^{Mem}} \quad (4\text{-}13)$$

$$C_{CO_2}^{Cyt} \ll K_{m,CO_2}: Da = \frac{k_{cat}[Ru]_{Cyt}R_{Cell}^2}{D_{CO_2}^{Cyt}K_{m,CO_2}\left(1+\frac{C_{O_2}^{Cyt}}{K_{m,O_2}}\right)} \quad (4\text{-}14)$$

Determination of Controlling Phenomena

The numerical values of the Damköhler numbers allow assessment of relative importance of transport and reaction rates in limiting overall carbon fixation. If *Da* ≈ 1, both reaction and diffusion are comparable, and as *Da* differs more from unity then the slower process completely controls the overall rate. A range of parameter values can be found in the literature, and preliminary evaluation showed *Da* << 1 to indicate reaction is generally slow compared to diffusion. To test how close the Damköhler numbers approached the *Da* ≈ 1 regime in which diffusion is not rapid, extreme high and low parameter values were chosen to maximize the Damköhler number. The values used in the calculation as well as their rationale can be found in **Table 4-1**. The constants associated with the RuBisCO kinetics specific to PCC7002 were used in this analysis. However, many other species have k_{cat} and K_m values within an order of magnitude of these values so the result was applied to PCC7942 and may be applied in a somewhat general way (Badger et al. 1998). The expressions and extremal values associated with each Damköhler number can be seen in **Table 4-2** and each was of an order of magnitude smaller than 10^{-3}.

Because these *Da* values are all so small, diffusive processes are all fast compared to reaction rates and the HCO_3^- and CO_2 concentrations can be treated as constant across each phase. Therefore, the carbon fixation rate is independent of the number or size of carboxysomes at a fixed total number of RuBisCO units per cell. In the no-carboxysome case, rapid diffusion will provide a constant CO_2 concentration inside the cell independent of the HCO_3^- concentration or the kinetics of the conversion between HCO_3^- and CO_2. Thus, the presence or absence of active HCO_3^- transporters in the no-carboxysome cell has no effect and the activity of the carbonic anhydrase, which has been postulated to be inactive outside of the carboxysome environment(Peña et al. 2010), does not affect these calculations.

Table 4-1. Values Used to Calculate Damköhler Numbers

Variable	Value/Estimate	Rationale	Citation
Specified Values			
k_{cat}	$11.4\ s^{-1} \cdot site^{-1}$	Value for RuBisCO isolated from PCC 7002	Badger, Andrew, and Whitney, 1998
K_{m,CO_2}	$185\ \frac{\mu mol}{L}$	Value for RuBisCO isolated from PCC 7002	Badger, Andrew, and Whitney, 1998
K_{m,O_2}	$1300\ \frac{\mu mol}{L}$	Value for RuBisCO isolated from PCC 7002	Badger, Andrew, and Whitney, 1998
R_{Carb}	$100\ nm$	Radius of a carboxysome in PCC 7942	Rae, et al., 2012
Values in the Numerator of Damköhler Numbers (Maximum Limit)			
$[Ru]_{Carb}$	$10^{-3}\ \frac{site}{nm^3}$	Wild Type: The inverse volume of one unit of RuBisCO	Liu, et al., 2010
$[Ru]_{Cyt}$	$10^{-6}\ \frac{site}{nm^3}$	No Carboxysome: RuBisCO from carboxysome distributed uniformly throughout cytoplasm	Liu, et al., 2010
$\frac{C_{CO_2}^{Shell}}{C_{HCO_3^-}^{Mem}}$	0.01	Equilibrium concentration is $\frac{10^{-pH}}{K_a}$ at pH=8, Temperature= 38°C	Butler, 1982
R_{Cell}	$1000\ nm$	Approximated spherical radius of a PCC 7942 cell (Larger than PCC 7002)	Moronta-Barrios, et al., 2013 Xu, et al., 2012
Values in the Denominator of Damköhler Numbers (Minimum Limit)			
D_i^j	$3\times10^{-6}\ \frac{cm^2}{s}$	Diffusivity of a small molecule in cytoplasm	Mastro, et al., 1984
$C_{CO_2}^{Mem}$ or $C_{CO_2}^{Shell}$	$185\ \frac{\mu mol}{L}$	For excess carbon, concentration must be at least equal to the affinity constant	Badger, Andrew, and Whitney, 1998
C_{O_2}	$0\ \frac{\mu mol}{L}$	Rate is maximized in absence of O_2 inhibition	-
$C_{HCO_3^-}^{Mem}$	$10\ \frac{\mu mol}{L}$	1000 times lower than equilibrium concentration at atmospheric conditions.	Butler, 1982

Table 4-2. Summary of Damköhler Numbers

Case	Phase	Conditions	Damköhler Number	Estimated Value
Wild Type	Cyt	$C_{CO_2}^{Cyt} \gg K_{m,CO_2}$	$\frac{k_{cat}[Ru]_{Carb}R_{Carb}^3}{4D_{HCO_3^-}^{Cyt}C_{HCO_3^-}^{Mem}R_{Cell}}$	2×10^{-3}
Wild Type	Carb	$C_{CO_2}^{Carb} \gg K_{m,CO_2}$	$\frac{k_{cat}[Ru]_{Carb}R_{Carb}^2}{D_{CO_2}^{Carb}C_{CO_2}^{Shell}}$	3×10^{-3}
Wild Type	Cyt	$C_{CO_2}^{Cyt} \ll K_{m,CO_2}$	$\frac{k_{cat}[Ru]_{Carb}R_{Carb}^3\left(\frac{C_{CO_2}^{Shell}}{C_{HCO_3^-}^{Mem}}\right)}{3K_{m,CO_2}D_{HCO_3^-}^{Cyt}R_{Cell}}$	1×10^{-6}
Wild Type	Carb	$C_{CO_2}^{Carb} \ll K_{m,CO_2}$	$\frac{k_{cat}[Ru]_{Carb}R_{Carb}^2}{D_{CO_2}^{Carb}K_{m,CO_2}\left(1+\frac{C_{O_2}^{Carb}}{K_{m,O_2}}\right)}$	3×10^{-3}
No Carboxysome	Cyt	$C_{CO_2}^{Cyt} \gg K_{m,CO_2}$	$\frac{k_{cat}[Ru]_{Cyt}R_{Cell}^2}{D_{CO_2}^{Cyt}C_{CO_2}^{Mem}}$	3×10^{-4}
No Carboxysome	Cyt	$C_{CO_2}^{Cyt} \ll K_{m,CO_2}$	$\frac{k_{cat}[Ru]_{Cyt}R_{Cell}^2}{D_{CO_2}^{Cyt}K_{m,CO_2}\left(1+\frac{C_{O_2}^{Cyt}}{K_{m,O_2}}\right)}$	3×10^{-4}

4.4. Kinetic Analysis

A kinetic approach was utilized to determine a quantitative explanation of carbon fixation in cyanobacterial cells. **Figure 4-2** shows a schematic diagram of the processes occurring during steady-state carbon uptake and **Table 4-3** gives the equations used to model these processes. These processes can be divided into three different stages: (1) external CO_2 equilibrium, (2) inorganic carbon uptake, and (3) carbon fixation.

External CO_2 Equilibrium

The first stage of carbon uptake is concerned with the transfer of carbon from the gas phase to the liquid phase. The CO_2 concentration in the liquid phase was determined from a Henry's Law relationship with a gas phase at 1 atm and variable CO_2 concentration. The liquid phase was considered well-mixed so that CO_2 and HCO_3^- were at chemical equilibrium (Butler 1982) in the liquid phase. The equilibrium inorganic carbon concentrations calculated for any gas-phase concentration are the maximum possible achievable. This ideality may not hold in the laboratory for most situations and this stage could be adjusted to fit various bioreactor geometries and transport scenarios.

HCO_3^- Uptake

The second stage in carbon uptake is concerned with the formation of an intracellular bicarbonate pool through the transfer of carbon from the liquid media to the cytoplasm of the cell. This stage has the largest interspecies variation as the active transport systems utilized by β-cyanobacteria vary from species to species. In PCC7002, the primary HCO_3^- transporter BicA has a flux that is orders of magnitude higher than any of the other transporters, and as these processes are parallel they do not contribute significantly to the carbon flux (Price et al. 2004). PCC7942 lacks this BicA transporter and thus has significantly lower flux of carbon into the cell. In a study by Price et al, the BicA transporter from PCC7002 was introduced into PCC7942 and an approximately tenfold increase in maximum carbon flux was observed (Price et al.

2004). Therefore, in the model for PCC7942, the HCO_3^- flux expression from the PCC7002 model was used with a V_{max} equal to 10% of that used for PCC7002.

Once inside the cell, HCO_3^- is only slowly dehydrated to CO_2 in an uncatalyzed process due to the absence of carbonic anhydrase in the cytoplasm (Wang et al. 2010). The slow rate of this conversion is crucial to the formation of the inorganic carbon pool. As the cell membrane is essentially impermeable to HCO_3^-, a high concentration of HCO_3^- is trapped inside the cell. The cell membrane presents no barrier to the transfer of the uncharged CO_2 species, so any HCO_3^- that is converted to CO_2 leaks out of the cell into the media, equilibrating the outer and inner CO_2 concentrations.

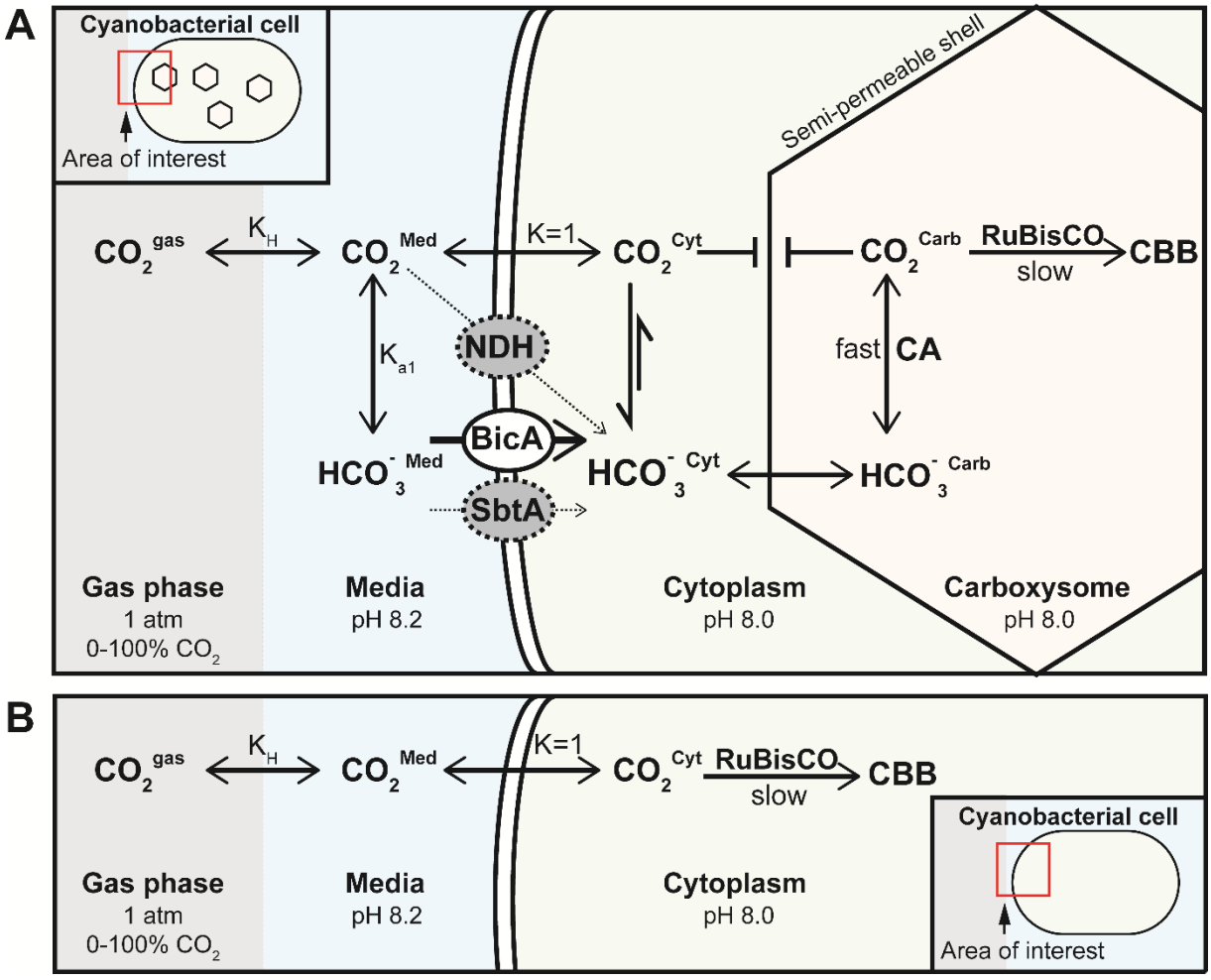

Figure 4-2. Kinetic Model Used to Calculate Carbon Fixation Rate. (A) The schematic for the wild type cell containing the entire CCM. The NDH and SbtA inorganic carbon transporters have small flux compared to BicA and were neglected. (B) the schematic for the carboxysome-lacking mutant. The equations used to model the reactions in these schematics are given in Table 4-3.

Table 4-3. Kinetic Model of Carbon Fixation

Process	Equation	Literature Values	Citation
Wild Type Cyanobacteria			
$CO_2^{Gas} \overset{K_H}{\leftrightarrow} CO_2^{Med}$	$C_{CO_2}^{Med} = P_{CO_2} K_H$	$K_H = 0.02\ \frac{mol}{L \cdot atm}$	Butler, 1982
$H_2O + CO_2^{Med} \overset{K_a}{\leftrightarrow} HCO_3^{-Med} + H^{+Med}$	$C_{H^+}^{Med} C_{HCO_3^-}^{Med} = K_a C_{CO_2}^{Med}$	$K_a = 0.9\ \frac{\mu mol}{L}$	Butler, 1982
$CO_2^{Med} \leftrightarrow CO_2^{Cyt}$	$C_{CO_2}^{Cyt} = C_{CO_2}^{Med}$	Permeability CO_2 >> HCO_3^-	Gutknecht, et al., 1977
$HCO_3^{-Med} \overset{BicA}{\longrightarrow} HCO_3^{-Cyt}$	$v_{in} = \frac{v_{max} C_{HCO_3^-}^{Med}}{K_m + C_{HCO_3^-}^{Med}}$	$v_{max} = 0.4 \frac{\mu mol}{mg\ Chl\ a \cdot s} = 4\times10^9 \frac{molecules}{cell \cdot hr}$ $K_m = 217 \frac{\mu mol}{L}$	Price, et al., 2004
$CO_2^{Cyt} + OH^{-Cyt} \overset{k_f, k_r}{\leftrightarrow} HCO_3^{-Cyt}$	$v_f = k_f C_{CO_2}^{Cyt} C_{OH^-}^{Cyt}$ $v_r = k_r C_{HCO_3^-}^{Cyt}$	$k_f = 3\times10^4 \frac{L}{mol \cdot s}$ $k_r = 1\times10^{-3} s^{-1}$	Wang, et al., 2010
$HCO_3^{-Cyt} \overset{Q}{\leftrightarrow} HCO_3^{-Carb}$	$C_{HCO_3^-}^{Carb} = Q C_{HCO_3^-}^{Cyt}$	Q ~ 1	-
$HCO_3^{-Carb} + H^{+Carb} \overset{CA}{\leftrightarrow} H_2O + CO_2^{Carb}$	$K_a C_{CO_2}^{Carb} = C_{H^+}^{Carb} C_{HCO_3^-}^{Carb}$	$k_{cat}^{CA} \sim 10^4 \cdot k_{cat}^{Rub}$, Fast Equilibrium	Shingles and Moroney, 1997
$CO_2^{Carb} \xrightarrow{RuBisCO} CBB\ Cycle$	$v_{fix} = \frac{k_{cat} N_{sites} C_{CO_2}^{Carb}}{C_{CO_2}^{Carb} + K_{m,CO_2}\left(1 + \frac{C_{O_2}^{Carb}}{K_{m,O_2}}\right)}$	$k_{cat} = 11.4\ \frac{molecules}{site \cdot s}$ $K_{m,CO_2} = 185\ \frac{\mu mol}{L}$ $K_{m,O_2} = 1300\ \frac{\mu mol}{L}$, $[O_2] = 400 \frac{\mu mol}{L}$ $N_{sites} = \left(4 \frac{carboxysomes}{cell}\right)\left(3351 \frac{sites}{carboxysome}\right)$	Price, et al., 1998 Long, et al., 2007 Savage, et al., 2010
No Carboxysome Mutant			
$CO_2^{Gas} \overset{K_H}{\leftrightarrow} CO_2^{Med}$	$C_{CO_2}^{Med} = P_{CO_2} K_H$	$K_H = 0.02\ \frac{mol}{L \cdot atm}$	Butler, 1982
$CO_2^{Med} \leftrightarrow CO_2^{Cyt}$	$C_{CO_2}^{Cyt} = C_{CO_2}^{Med}$	Permeability CO_2 >> HCO_3^-	Gutknecht, et al., 1977
$CO_2^{Carb} \xrightarrow{RuBisCO} CBB\ Cycle$	$v_{fix} = \frac{k_{cat} N_{sites} C_{CO_2}^{Carb}}{C_{CO_2}^{Carb} + K_{m,CO_2}\left(1 + \frac{C_{O_2}^{Carb}}{K_{m,O_2}}\right)}$	$k_{cat} = 11.4\ \frac{molecules}{site \cdot s}$ $K_{m,CO_2} = 185\ \frac{\mu mol}{L}$ $K_{m,O_2} = 1300\ \frac{\mu mol}{L}$, $[O_2] = 400 \frac{\mu mol}{L}$ $N_{sites} = \left(4 \frac{carboxysomes}{cell}\right)\left(3351 \frac{RuBisCo}{carboxysome}\right)$	Price, et al., 1998 Long, et al., 2007 Savage, et al., 2010
*Chlorophyll content of PCC 7002 cells were measured to be $5\times10^{-12} \frac{mg\ Chl\ a}{cell}$ during exponential growth phase as in Lichtenthaler[38]			

Carbon Fixation

The third stage in carbon uptake is the localization of carbon to the carboxysome where it can be consumed by RuBisCO. This is the most controversial of the steps studied in the carbon-concentrating mechanism. It is not known how HCO_3^- passes into carboxysome or if there is a barrier to this flux. To approximate the concentration of HCO_3^- in the carboxysome relative to that in the cytoplasm, a proportionality relationship was established between the HCO_3^- inside and outside of the carboxysome. The proportionality constant Q was initially set to 1 to evaluate the upper limit of the carbon fixation rate, and the sensitivity of the model to decreases in this parameter was examined. The model was not overly sensitive to the value of Q within an order of magnitude, so the original value of 1 was used for further analysis.

The HCO_3^- inside the carboxysome was treated as quickly equilibrated with CO_2 by carbonic anhydrase (Badger et al. 1998; Shingles and Moroney 1997). The carboxysome was considered

impermeable to CO_2 as it has been generally hypothesized that that the protein shell prevents its escape (Price et al. 2008). The RuBisCO catalyzed reaction in which CO_2 flux is directed into the Calvin Cycle was used as the rate determining step in the reaction scheme, based on the *Da* analysis above. There was postulated to be an excess of ribulose-1,5-bisphosphate, the co-substrate required for carbon fixation by RuBisCO. The kinetic parameters of RuBisCO for PCC7002 were also for PCC7942 in expectation that the unknown values were within an order of magnitude of each other, as is the trend with other strains of cyanobacteria (Badger et al. 1998).

Solving the Reaction System

To determine the carbon uptake rate of the cell, the rate equation for RuBisCO catalyzed fixation of CO_2 was used as the rate-limiting step with the rapid diffusion and active transport steps proceeding as outlined above. The key to solving the reaction system was equating the flux into and out of the cell's HCO_3^- pool. This expression is as follows:

$$\begin{pmatrix} Active\ HCO_3^- \\ Pump\ Flux \end{pmatrix} = \begin{pmatrix} Carbon\ Consumption \\ by\ RuBisCo \end{pmatrix} + \begin{pmatrix} Net\ Conversion\ of \\ HCO_3^-\ to\ CO_2 \end{pmatrix}$$

$$\left(\frac{v_{max} C_{HCO_3^-}^{Media}}{K_{m,HCO_3^-} + C_{HCO_3^-}^{Media}}\right) = \left(\frac{k_{cat} N_{sites} C_{CO_2}^{Carb}}{C_{CO_2}^{Carb} + K_{m,CO_2}\left(1 + \frac{C_{O_2}^{Carb}}{K_{m,O_2}}\right)}\right) + [(k_r C_{HCO_3^-}^{Cyt} - k_f C_{CO_2}^{Cyt} C_{OH^-}^{Cyt}) V_{cell}] \quad (4\text{-}15)$$

The first term represents the flux into the cell due to active HCO_3^- transport, the second term represents the forward reaction of CO_2 into HCO_3^-, the third term represents the flux of carbon into the CBB-cycle, and the final term represents the reverse reaction of HCO_3^- into CO_2. This expression was solved analytically for the CO_2 concentration inside the carboxysome and the carbon fixation rate as a function of $C_{HCO_3^-}^{Media}$ can be seen in **Figure 4-3** for each cyanobacterial species. The resulting curves were compared to oxygen evolution data obtained from literature (Price et al. 2004; Rae et al. 2012) for wild type strains of each species with good agreement in trend. Oxygen evolution rate is proportional to carbon fixation

rate because the CBB-cycle acts as a sink for energy and reducing power generated during photosynthesis (Tcherkez et al. 2006).

No-Carboxysome Case

The reaction scheme for the hypothetical case of a cell with no carboxysomes, depicted in **Figure 4-2**, was much simpler than that of the wild type case. This model was solved analytically and the resulting carbon fixation rate as a function of $C_{HCO_3^-}^{Media}$ can be seen in **Figure 4-3** for comparison to the wild type case. As expected, the model predicts that both cyanobacterial species have little or no carbon fixation activity at present ambient CO_2 levels, and shows the clear necessity of the CCM in wild type species. However, CO_2 transport without HCO_3^- pumping allows significant CCM at gas phase CO_2 compositions of 10% or greater. Thus, the carboxysome may become unnecessary at sufficient CO_2 levels. Indeed, PCC7942 models show the carboxysome-free variant predicted to have a higher carbon fixation rate over a range of enriched CO_2 levels.

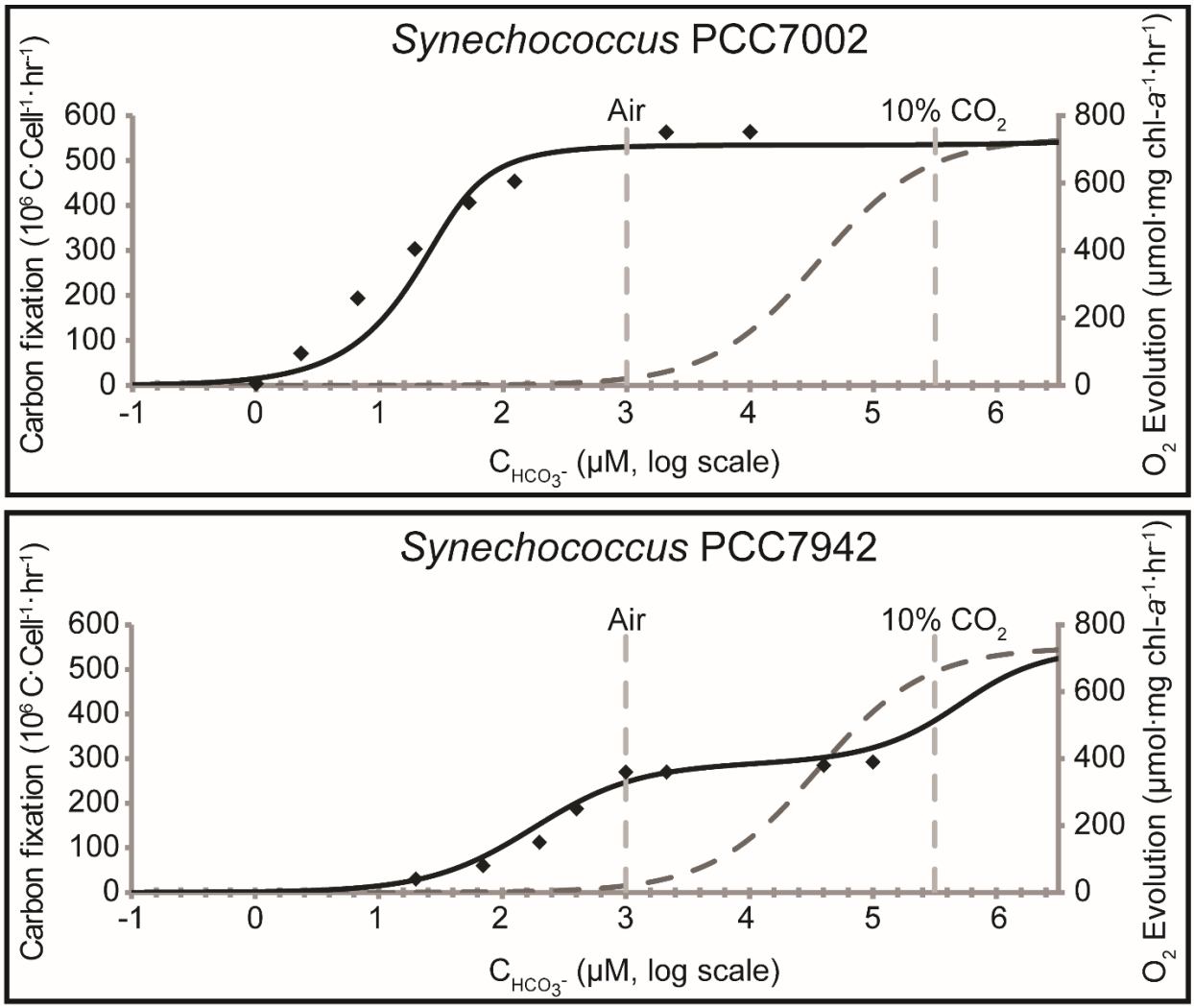

Figure 4-3. Carbon Fixation Model Results. Plots of potential carbon fixation rate as a function of the inorganic carbon concentration in the media for the wild type (solid line) and carboxysome-lacking mutant (dashed line) for both PCC7002 and PCC7942. The vertical lines indicate HCO_3^- concentrations achievable in the media through equilibrium with a gas phase containing CO_2 at concentrations of 400 ppm (air) and 10% (flue gas). Points (♦) represent data from the literature (Price et al. 2004; Rae et al. 2012) showing O_2 evolution in wild type cultures of each species as a function of media HCO_3^- concentration with corresponding values on the right-hand y-axis.

4.5. Discussion

Three important conclusions can be drawn from this study. First, carbon uptake is not diffusion limited, so the number, size, shape, and intracellular location of the carboxysomes have a negligible effect on carbon fixation rate with a given number of RuBisCO units and these details need not be considered further. Second, large interspecies variations in the carbon fixation landscape are largely due to the difference in the kinetics of the active HCO_3^- transporters present in the cell. Finally, the potential carbon

fixation rate of the no-carboxysome cell approaches and can even surpass that of the wild type when grown at CO_2 concentrations of 10% or higher. These conclusions were considered in their implications on future research paths.

Carboxysome Engineering

At gas phase CO_2 concentrations approaching that of flue gas, there is not a large carbon fixation benefit in a cell containing carboxysomes. In the low HCO_3^- flux case of PCC7942, there was even a carbon fixation deficit as the cytoplasmic CO_2 concentration due to a high media concentration overcomes that achievable by the carbon concentrating mechanism and the carboxysome serves only as a barrier to the localization of CO_2 to RuBisCO. Because the carboxysome shell proteins are very large with a final structure diameter on the order of 10% of that of the cell, there would be a metabolic benefit in redirecting the energy used to make these proteins as well as others involved in the CCM into other processes, such as the production of more RuBisCO units (Moronta-Barrios, Espinosa, and Contreras 2013; Rae et al. 2012). This would be an interesting area of research to increase a cell's affinity to the high CO_2 environments relevant to industrial processes. The natural elimination of carboxysomes at high CO_2 concentrations has been observed in at least one wild type cyanobacterium (Stöckel et al. 2013). Another benefit of the removal of carboxysome from a genetically modified cyanobacterial strain would be to reduce its fitness in nature so it is unable to grow in ambient CO_2 levels, mitigating the possibility of inadvertent release of a genetically modified organism resulting in potential biological contamination of the environment.

HCO_3^- Transporter Engineering

As the carbon-fixation rate of RuBisCO reaches saturation at low concentrations for high HCO_3^- flux species such as PCC7002, increasing the affinity or flux of these transporters will not provide a benefit. However, in low HCO_3^- flux species such as PCC7942, a great carbon fixation benefit at all CO_2 levels should be achieved by the introduction of a higher flux HCO_3^- transporter. The potential magnitude of this benefit is especially evident when comparing the typical doubling times of 4 hours for PCC7002 to 10 hours for

PCC7942 (Price et al. 2004; Rae et al. 2012). The benefit of the implementation of the high flux HCO_3^- transporter BicA from PCC7002 in PCC7942 has been observed (Price et al. 2004).

RuBisCO Engineering

The modification of RuBisCO for increased performance has long been a goal of researchers who desire to increase the efficiency of photosynthesis (Liu et al. 2010). There are two targets relevant to this model for increasing the performance of RuBisCO: k_{cat}, and affinity. Increasing the k_{cat} of RuBisCO will naturally increase the carbon fixation rate of a cell. This rate of increase will be approximately linear in the case of a high flux cell or the hypothetical no-carboxysome cell as the enzyme will be saturated until the k_{cat} is increased by an order of magnitude. In the case of a low flux cell, increases to the k_{cat} of RuBisCO do not have as large of a carbon fixation benefit as the saturation of the active bicarbonate transporters prevents RuBisCO saturation.

Increasing the affinity of RuBisCO for CO_2 can greatly improve the carbon fixation rate of the no-CCM case by allowing for RuBisCO saturation at lower CO_2 concentrations. This same benefit could be achieved in the low HCO_3^- flux PCC7942 cell, but this effect is not additive when compared to the effect of improved active HCO_3^- transport. Little benefit will be achieved by this affinity increase in the high HCO_3^- flux PCC7002 cell, as the RuBisCO is already saturated by the significantly higher CO_2 concentration at industrially relevant CO_2 concentrations.

4.6. Conclusions

A mass transport model considering the uptake of inorganic carbon by cyanobacteria showed that diffusion was fast compared to kinetic conversion by RuBisCO yielding flat CO_2 and HCO_3^- concentration profiles within the cell. As a result, the number, size, shape, and intracellular location of carboxysomes have a negligible effect on carbon fixation rate with a given number of RuBisCO units. A kinetic model of the fluxes of inorganic carbon in the carbon uptake systems of wild type and hypothetical carboxysome-lacking mutant cyanobacteria was developed. The wild type case for both PCC7002 and PCC7942 matched

the trend of experimental oxygen-evolution data from the literature. Interspecies variations in the potential carbon-fixation rate are largely due to differences in active HCO_3^- transporters. The models showed that the potential steady-state carbon-fixation rate of a carboxysome-lacking mutant approaches that of the wild type at inorganic carbon concentrations achievable using a gas feed containing 10% CO_2. Future research towards increasing the fitness of cyanobacteria in an industrial setting should focus on the metabolic benefits of the elimination of the energy-intensive proteins associated with the CCM that are not necessary at high CO_2 concentrations.

4.7. Notation

Variable	Meaning	Units
C_i^j	Variable concentration of species i in phase j	$\frac{mol}{L}$
D_i^j	Diffusivity of species i in phase j	$\frac{m^2}{s}$
Da	Damköhler number	None
J^*	HCO_3^- flux at carboxysome surface	$\frac{mol}{m^2 \cdot s}$
k_{cat}	Carbon fixation rate constant for RuBisCO	s^{-1}
k_f	Rate constant for $CO_2 + OH^- \rightarrow HCO_3^-$	$\frac{L}{mol \cdot s}$
k_r	Rate constant for $HCO_3^- \rightarrow CO_2 + OH^-$	s^{-1}
$K_{m,\mathrm{i}}$	RuBisCO Michaelis-Menten constant for species i	$\frac{mol}{L}$
N_{sites}	Total number of RuBisCO sites per cell	$sites$
r	Variable Radius	m
R_{Cell}	Cell Radius	m
R_{Carb}	Carboxysome Radius	m
$[Ru]_j$	RuBisCO concentration in phase j	$\frac{sites}{m^3}$
V_j	Volume of phase j	m^3
v_{max}	Maximum active HCO_3^- uptake rate	$\frac{mol}{L \cdot s}$

4.8. References

Badger, M. R. and G. Dean Price. 2003. "CO_2 Concentrating Mechanisms in Cyanobacteria: Molecular Components, Their Diversity and Evolution." *Journal of Experimental Botany* 54(383):609–22.

Badger, Murray R. et al. 1998. "The Diversity and Coevolution of Rubisco , Plastids , Pyrenoids , and Chloroplast-Based CO_2-Concentrating Mechanisms in Algae 1." *Canadian Journal of Botany* 1071:1052–71.

Bailey, James and David F. Ollis. 1986. *Biochemical Engineering Fundamentals*. McGraw-Hill.

Bird, Robert Byron, Warren E. Stewart, and Edwin N. Lightfoot. 2007. “Diffusion and Chemical Reaction Inside a Porous Catalyst.” Pp. 563–67 in Transport Phenomena, Second Edition.

Butler, James N. 1982. *Carbon Dioxide Equilibria and Their Applications*, *First Edition* Reading, Massachusetts: Addison-Wesley Publishing Company Inc.

Gutknecht, J., M. a Bisson, and F. C. Tosteson. 1977. “Diffusion of Carbon Dioxide through Lipid Bilayer Membranes: Effects of Carbonic Anhydrase, Bicarbonate, and Unstirred Layers.” *The Journal of General Physiology* 69(6):779–94.

Kao, H. P., J. R. Abney, and a S. Verkman. 1993. “Determinants of the Translational Mobility of a Small Solute in Cell Cytoplasm.” *The Journal of Cell Biology* 120(1):175–84.

Kinney, James N., Seth D. Axen, and Cheryl A. Kerfeld. 2011. “Comparative Analysis of Carboxysome Shell Proteins.” *Photosynthesis Research* 109:21–32.

Klughammer, Barbara, Dieter Sultemeyer, Murray R. Badger, and G.Dean Price. 1999. “The Involvement of NAD(P)H Dehydrogenase Subunits, NdhD3 and NdhF3, in High-Affinity CO_2 Uptake in *Synechococcus* Sp. PCC7002 Gives Evidence for Multiple NDH-1 Complexes with Specific Roles in Cyanobacteria.” *Molecular Microbiology* 32(6):1305–15.

Ku, S. B. and G. E. Edwards. 1978. “Oxygen Inhibition of Photosynthesis.” *Planta* 991–99.

Lea-Smith, David J., Paolo Bombelli, Ravendran Vasudevan, and Christopher J. Howe. 2015. “Photosynthetic, Respiratory and Extracellular Electron Transport Pathways in Cyanobacteria.” *Biochimica et Biophysica Acta* 1857(3):247–55.

Lichtenthaler, HK. 1987. “Chlorophylls and Carotenoids: Pigments of Photosynthetic Biomembranes.” *Methods in Enzymology* 148:350–82.

Liu, Cuimin et al. 2010. “Coupled Chaperone Action in Folding and Assembly of Hexadecameric Rubisco.” *Nature* 463(7278):197–202.

Long, Benedict M., Murray R. Badger, Spencer M. Whitney, and G.Dean Price. 2007. “Analysis of Carboxysomes from *Synechococcus* PCC7942 Reveals Multiple Rubisco Complexes with Carboxysomal Proteins CcmM and CcaA.” *The Journal of Biological Chemistry* 282(40):29323–35.

Maeda, Shin-ichi, Murray R. Badger, and G. Dean Price. 2002. “Novel Gene Products Associated with NdhD3/D4-Containing NDH-1 Complexes Are Involved in Photosynthetic CO_2 Hydration in the Cyanobacterium, *Synechococcus* Sp. PCC7942.” Molecular Microbiology 43(2):425–35.

Mangan, Niall and Michael Brenner. 2014. “Systems Analysis of the CO_2 Concentrating Mechanism in Cyanobacteria.” *eLife* 2014(3):1–17.

Mangan, Niall, Avi Flamholz, Rachel D. Hood, Ron Milo, and David Savage. 2016. “pH Determines the Energetic Efficiency of the Cyanobacterial CO_2 Concentrating Mechanism.” *Proceedings of the National Academy of Sciences of the United States of America* 113(36):E5354–62.

Mastro, A. M., M. A. Babich, W. D. Taylor, and a D. Keith. 1984. “Diffusion of a Small Molecule in the Cytoplasm of Mammalian Cells.” *Proceedings of the National Academy of Sciences of the United States of America* 81(11):3414–18.

Moronta-Barrios, Félix, Javier Espinosa, and Asunción Contreras. 2013. “Negative Control of Cell Size in the Cyanobacterium *Synechococcus Elongatus* PCC 7942 by the Essential Response Regulator RpaB.” *FEBS letters* 587(5):504–9.

Ohkawa, H., G. D. Price, M. R. Badger, and T. Ogawa. 2000. “Mutation of Ndh Genes Leads to Inhibition of CO_2 Uptake Rather than HCO_3^- Uptake in *Synechocystis* Sp. Strain PCC 6803.” *Journal of Bacteriology* 182(9):2591–96.

Omata, Tatsuo, Yukari Takahashi, Osamu Yamaguchi, and Takashi Nishimura. 2002. “Structure, Function and Regulation of the Cyanobacterial High-Affinity Bicarbonate Transporter, BCT1.” *Functional Plant Biology* 29(3):151–59.

Peña, Kerry L., Stephane E. Castel, Charlotte de Araujo, George S. Espie, and Matthew S. Kimber. 2010. “Structural Basis of the Oxidative Activation of the Carboxysomal Gamma-Carbonic Anhydrase, CcmM.” *Proceedings of the National Academy of Sciences of the United States of America* 107(6):2455–60.

Price, G. D. and M. R. Badger. 1989a. “Expression of Human Carbonic Anhydrase in the Cyanobacterium *Synechococcus* PCC7942 Creates a High CO_2-Requiring Phenotype : Evidence for a Central Role for Carboxysomes in the CO_2 Concentrating Mechanism.” *Plant Physiology* 91:505–13.

Price, G. D. and M. R. Badger. 1989b. “Isolation and Characterization of High CO_2-Requiring Mutants of the Cyanobacterium *Synechococcus* PCC7942.” *Plant Physiology* 91:514–25.

Price, G. D., Murray R. Badger, Fiona J. Woodger, and Ben M. Long. 2008. “Advances in Understanding the Cyanobacterial CO_2-Concentrating-Mechanism (CCM): Functional Components, C_i Transporters, Diversity, Genetic Regulation and Prospects for Engineering into Plants.” *Journal of Experimental Botany* 59(7):1441–61.

Price, G. D., Fiona J. Woodger, Murray R. Badger, Susan M. Howitt, and Loraine Tucker. 2004. “Identification of a SulP-Type Bicarbonate Transporter in Marine Cyanobacteria.” *Proceedings of the National Academy of Sciences of the United States of America* 101(52):18228–33.

Rae, Benjamin D., Benedict M. Long, Murray R. Badger, and G. D. Price. 2012. “Structural Determinants of the Outer Shell of β-Carboxysomes in *Synechococcus Elongatus* PCC 7942: Roles for CcmK2, K3-K4, CcmO, and CcmL.” *PloS ONE* 7(8):e43871.

Savage, David F., Bruno Afonso, Anna H. Chen, and Pamela A. Silver. 2010. “Spatially Ordered Dynamics of the Bacterial Carbon Fixation Machinery.” *Science* 327(5970):1258–61.

Shibata, M. et al. 2001. “Distinct Constitutive and Low-CO_2-Induced CO_2 Uptake Systems in Cyanobacteria: Genes Involved and Their Phylogenetic Relationship with Homologous Genes in Other Organisms.” *Proceedings of the National Academy of Sciences of the United States of America* 98(20):11789–94.

Shibata, Mari et al. 2002. “Genes Essential to Sodium-Dependent Bicarbonate Transport in Cyanobacteria: Function and Phylogenetic Analysis.” *The Journal of Biological Chemistry* 277(21):18658–64.

Shingles, R. and J. V Moroney. 1997. “Measurement of Carbonic Anhydrase Activity Using a Sensitive Fluorometric Assay.” *Analytical Biochemistry* 252:190–97.

Stöckel, Jana, Thanura R. Elvitigala, Michelle Liberton, and Himadri B. Pakrasi. 2013. “Carbon Availability Affects Diurnally Controlled Processes and Cell Morphology of *Cyanothece* 51142.” *PLoS ONE* 8(2):e56887.

Tanaka, Shiho et al. 2008. “Atomic-Level Models of the Bacterial Carboxysome Shell.” *Science* 319(5866):1083–86.

Tcherkez, Guillaume G. B., Graham D. Farquhar, and T. John Andrews. 2006. “Despite Slow Catalysis and Confused Substrate Specificity, All Ribulose Bisphosphate Carboxylases May Be Nearly Perfectly Optimized.” *Proceedings of the National Academy of Sciences of the United States of America* 103(19):7246–51.

Wang, Hong-Liang, Bradley L. Postier, and Robert L. Burnap. 2004. “Alterations in Global Patterns of Gene Expression in *Synechocystis* Sp. PCC 6803 in Response to Inorganic Carbon Limitation and the Inactivation of ndhR, a LysR Family Regulator.” *The Journal of Biological Chemistry* 279(7):5739–51.

Wang, Xiaoguang, William Conway, Robert Burns, Nichola McCann, and Marcel Maeder. 2010. “Comprehensive Study of the Hydration and Dehydration Reactions of Carbon Dioxide in Aqueous Solution.” *The Journal of Physical Chemistry A* 114(4):1734–40.

Westermark, Stefanie and Ralf Steuer. 2016. “Toward Multiscale Models of Cyanobacterial Growth: A Modular Approach.” *Frontiers in Bioengineering and Biotechnology* 4:95.

Yeates, Todd O., Cheryl A. Kerfeld, Sabine Heinhorst, Gordon C. Cannon, and Jessup M. Shively. 2008. “Protein-Based Organelles in Bacteria: Carboxysomes and Related Microcompartments.” *Nature Reviews Microbiology* 6(9):681–91.

Chapter 5: High CO_2 Requirement as a Mechanism for the Containment of Genetically Modified Cyanobacteria

5.1. Background and Motivation

Many researchers have genetically engineered cyanobacteria for the photosynthetic production of fuels and commodity chemicals directly from CO_2 and sunlight (Angermayr, Gorchs Rovira, and Hellingwerf 2015; Liao et al. 2016; Oliver et al. 2016). Systems level analysis has begun to assess the viability of so-called "photosynthetic biorefinery" processes for their feasibility to create replacements for chemicals sourced from non-renewable sources (Yenkie et al. 2016). Large scale production of any fuel or chemical requires cultivation across large surface areas, greatly increasing the risk of contamination of surrounding natural ecosystems by genetically modified or non-native cyanobacteria. A biocontainment mechanism could be introduced in genetically modified cyanobacteria to alleviate this risk.

Previous research into biocontainment mechanisms has focused on the use of toxin and antitoxin kill switches (Cai et al. 2015; Chan et al. 2015; Li and Wu 2009; Molin et al. 1987) or the establishment of auxotrophies to natural (Curtiss 1978) or synthetic (Malyshev et al. 2014; Mandell et al. 2015; Rovner et al. 2015) metabolites. Despite increasingly robust circuits, kill switch mechanisms are susceptible to deactivation through genetic drift and require the development of sensing systems to trigger the switch (Chan et al. 2015; Schmidt and de Lorenzo 2016). Auxotrophies to natural metabolites can be circumvented through natural sources of the required metabolite (Moe-Behrens, Davis, and Haynes 2013; Schmidt and de Lorenzo 2016). Auxotrophies to synthetic metabolites eliminate this escape mechanism, but current methods require supplementation with non-standard amino acids (Mandell et al. 2015; Rovner et al. 2015) or nucleic acids (Malyshev et al. 2014) that are not readily available or cost-effective.

Due to the low abundance of CO_2 in aquatic systems, cyanobacteria and eukaryotic algae have evolved CO_2-concentrating mechanisms (CCM) to increase the local concentration of CO_2 near the ribulose-1,5-

bisphosphate carboxylase oxygenase (RuBisCO) enzyme inside of cellular protein microcompartments called carboxysomes (Raven, Beardall, and Sánchez-Baracaldo 2017). Disrupting this mechanism in cyanobacteria through deletion of carboxysome shell proteins (Price and Badger 1989) or inorganic carbon transporters (Orf et al. 2015) imposes a high CO_2 concentration requirement (HCR) for growth. HCR through CCM disruption has been suggested as a potential containment mechanism for photoautotrophic microorganisms where an industrial cultivation environment could be supplemented with waste CO_2, while the relatively CO_2-deplete natural environment would be unable to support the growth of CCM-lacking photoautotrophs (Clark et al. 2014; Gee and Niyogi 2017).

In this work, we experimentally validate a containment system for genetically modified cyanobacteria using the model cyanobacterium *Synechococcus* sp. PCC7002 (PCC7002) in which the CCM was disrupted, resulting in a high CO_2 requirement for growth. Because this containment mechanism involves only gene deletions it is robust to the issues of genetic drift encountered by kill switch mechanisms. Natural environments containing CO_2 concentrations sufficient for growth of CCM-lacking cyanobacteria do not exist, so environmental supplementation is not a possible escape mechanism. One potentially likely escape mechanism is through horizontal gene transfer. PCC7002 has a high natural competence and CCM-related genes are highly conserved in cyanobacteria (Scanlan et al. 2009), so the risk of escape through horizontal gene transfer was investigated and mitigated through the deletion of natural competence-related genes. This containment mechanism was then implemented in a previously characterized strain of PCC7002 engineered to produce L-lactate and observed no negative impact on growth or L-lactate production.

5.2. Results and Discussion

Carboxysome Knockout Mutants Have a High CO_2 Requirement

To investigate the survival of CCM-lacking cyanobacteria under differing CO_2 concentrations, we deleted the ccmK2K1LMN operon from PCC7002 using a kanamycin resistance marker as described

previously (Gordon et al. 2016). The resulting strain, PCC7002 ΔccmK2K1LMN (7002_RLC01), as well as Wild Type PCC7002 were grown in cultures tubes bubbled with various concentrations of CO_2 and their exponential growth rates were measured at cell densities low enough for light attenuation to be minimal (OD_{730}<0.1) (**Chapter 3**). The resulting exponential growth data as a function of CO_2 concentration were fit to a Monod Model (Equation 1).

$$\mu(P_{CO_2}) = \frac{\mu_{MAX} P_{CO_2}}{K_{CO_2} + P_{CO_2}} \quad (5\text{-}1)$$

μ is the specific growth rate, P_{CO2} is the partial pressure of CO_2 in the gas phase, μ_{MAX} is the maximum specific growth rate, and K_{CO2} is the half-maximum growth rate constant for CO_2. The exponential growth data and Monod Model fits are shown in **Figure 5-1** for Wild Type PCC7002 and PCC7002 ΔccmK2K1LMN. PCC7002 ΔccmK2K1LMN exhibited negligible growth after 72 hours in ambient air, but grew at the same rate as Wild Type PCC7002 in 5% CO_2 (0.05 atm CO_2) or greater, verifying the expected high CO_2 requirement for PCC7002 ΔccmK2K1LMN.

Unsurprisingly, μ_{MAX} did not differ by much between Wild Type PCC7002 and PCC7002 ΔccmK2K1LMN as RuBisCO saturation should result in similar growth rates assuming similar RuBisCO content. It is interesting to note that the previously measured K_{CO2} for RuBisCO in PCC7002 was 185 μM CO_2, the concentration of a liquid phase in equilibrium with a gas phase containing 0.09% CO_2 ($9*10^{-3}$ atm CO_2) (Badger et al. 1998), a value almost double the K_{CO2} measured for PCC7002 ΔccmK2K1LMN (0.05% CO_2, $5*10^{-3}$ atm CO_2, **Figure 5-1**). The kinetics of CO_2-fixation in CCM-lacking mutants is thought to be controlled by RuBisCO kinetics as the cytoplasmic CO_2 concentration is equal to the media CO_2 concentration (Clark et al. 2014). This discrepancy could be due to differences in temperature between the in vitro RuBisCO kinetic assay (25°C) and the in vivo experiments in this work (38°C).

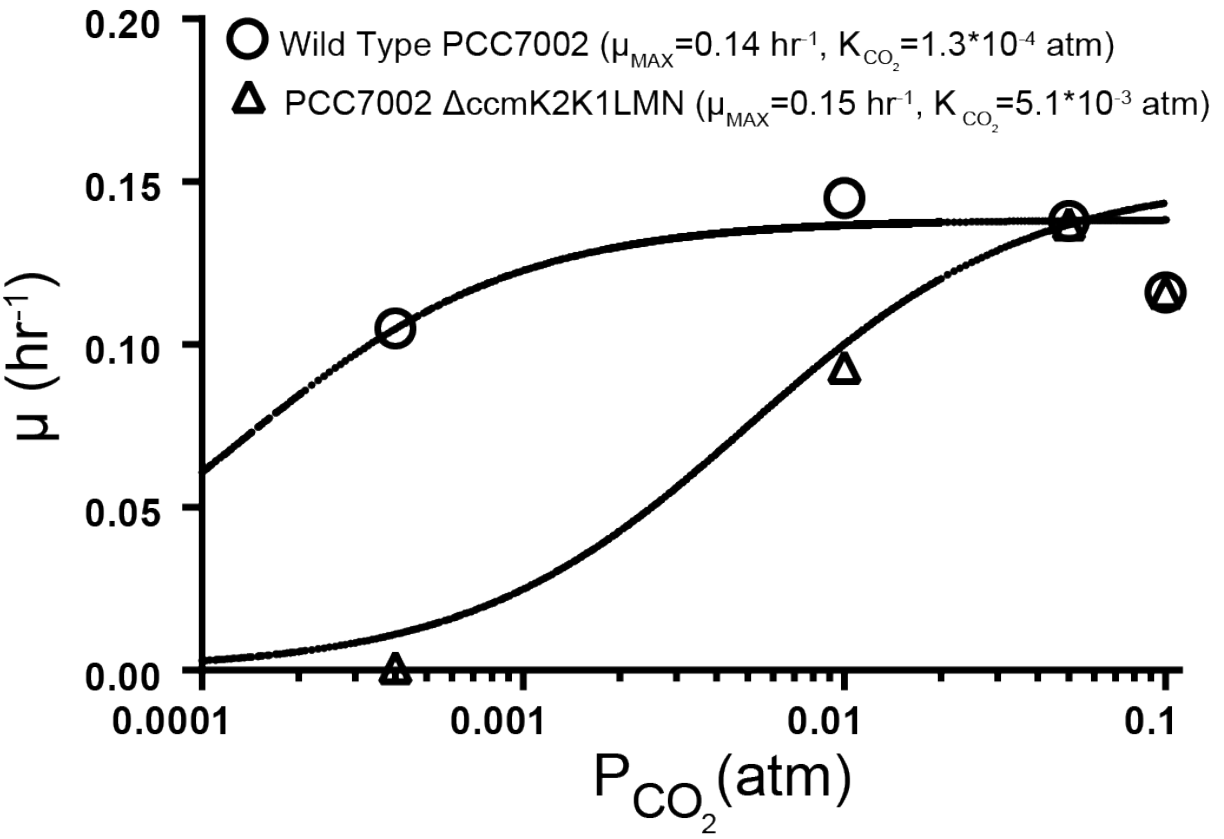

Figure 5-1. Growth of Wild Type PCC7002 (circles) and PCC7002 ΔccmK2K1LMN (triangles) at Varying CO_2 Concentration. Data is given as the average specific growth rate of three replicates (error bars smaller than the data symbols). Values in parentheses are the best fit parameters of the model in Equation 5-1.

Table 5-1. Colony Forming Units per mL for Culture Plated in 5% CO_2 or Ambient Air

Plating Condition	5% CO_2	Ambient Air
Wild Type PCC7002	$5*10^8$	$5*10^8$
PCC7002 ΔccmK2K1LMN	$5*10^8$	<1 in $2*10^9$

To test the effectiveness of the HCR containment mechanism, we grew cultures of Wild Type PCC7002 and PCC7002 ΔccmK2K1LMN in 10% CO_2 to an OD_{730} of approximately 3 and then plated cells on non-selective Media A in ambient air or 5% CO_2. For Wild Type PCC7002 an equivalent number of colonies were recovered in both conditions. For PCC7002 ΔccmK2K1LMN, $5*10^8$ CFU mL^{-1} were recovered in 5% CO_2, but no colonies were observed in ambient air where 4 mL of culture ($2*10^9$ cells) were plated. The survival rate of PCC7002 ΔccmK2K1LMN in ambient air is therefore less than $5*10^{-10}$ CFU^{-1} (**Table 5-1**), two orders of magnitude lower than the NIH recommended limit of 10^{-8} CFU^{-1} (Moe-Behrens et al. 2013).

CCM functions can be complemented by genes from other cyanobacteria

While the HCR containment mechanism is sufficiently effective, escape could occur through horizontal gene transfer in which CCM genes are integrated from wild type cyanobacteria encountered in the industrial cultivation or the surrounding environment. The CCM genes are highly conserved in cyanobacteria (Scanlan et al. 2009), and the natural competence of PCC7002 could allow DNA fragments containing complementary CCM genes to be readily integrated into the chromosome and restore CCM function, permitting growth in ambient air. *Synechococcus elongatus* sp. PCC7942 and *Synechocystis sp.* PCC6803 are model cyanobacteria whose carboxysome genes could potentially complement PCC7002 ΔccmK2K1LMN to restore growth in ambient air. To test this hypothesis, we integrated the ccmK operons from each organism or the native ccmK2K1LMN operon into PCC7002 ΔccmK2K1LMN in the glpK locus and tested the ability to grow in ambient air. PCC7002 ΔccmK2K1LMN +ccmK2K1LMN[Native] (7002_RLC16) and PCC7002 ΔccmK2K1LMN +ccmK2K1LMN[6803] (7002_RLC23) were able to grow in ambient air, but PCC7002 ΔccmK2K1LMN +ccmKLMNO[7942] (7002_RLC22) was unable to grow in ambient air.

To verify that the restoration in ambient air growth was due to CCM restoration, we expressed a fusion of the RuBisCO large subunit to a green fluorescent protein (rbcL-sfGFP) to observe cellular localization of RuBisCO (**Figure 5-2**). In PCC7002 +rbcL-sfGFP (7002_RLC18), the rbcL-sfGFP aggregates into distinct puncta (carboxysomes) distributed throughout the cell as well as a large aggregate at one pole, known as the pro-carboxysome (Cameron et al. 2013). In PCC7002 ΔccmK2K1LMN +rbcL-sfGFP (7002_RLC24), all aggregation is abolished and green fluorescence is diffuse throughout the cytoplasm. In the native complement PCC7002 ΔccmK2K1LMN + ccmK2K1LMN[Native] +rbcL-sfGFP (7002_RLC19), the carboxysome and pro-carboxysome formation phenotype is restored. In the *Synechocystis* sp. PCC6803 ccmK operon complement PCC7002 ΔccmK2K1LMN + ccmK2K1LMN[6803] +rbcL-sfGFP (7002_RLC26), one aggregate occurs in each cell with an intermediate diameter (larger than carboxysomes from

PCC7002 +rbcL-sfGFP, smaller than pro-carboxysomes from PCC7002 +rbcL-sfGFP). As this strain grows in ambient air, this difference in apparent aggregation in the microscope images is either due to differences in carboxysomes when shell proteins from *Synechocystis* sp. PCC6803 interact with RuBisCO from PCC7002 or incompatibilities between the *Synechocystis* sp. PCC6803 carboxysome shell proteins and the rbcL-sfGFP fusion.

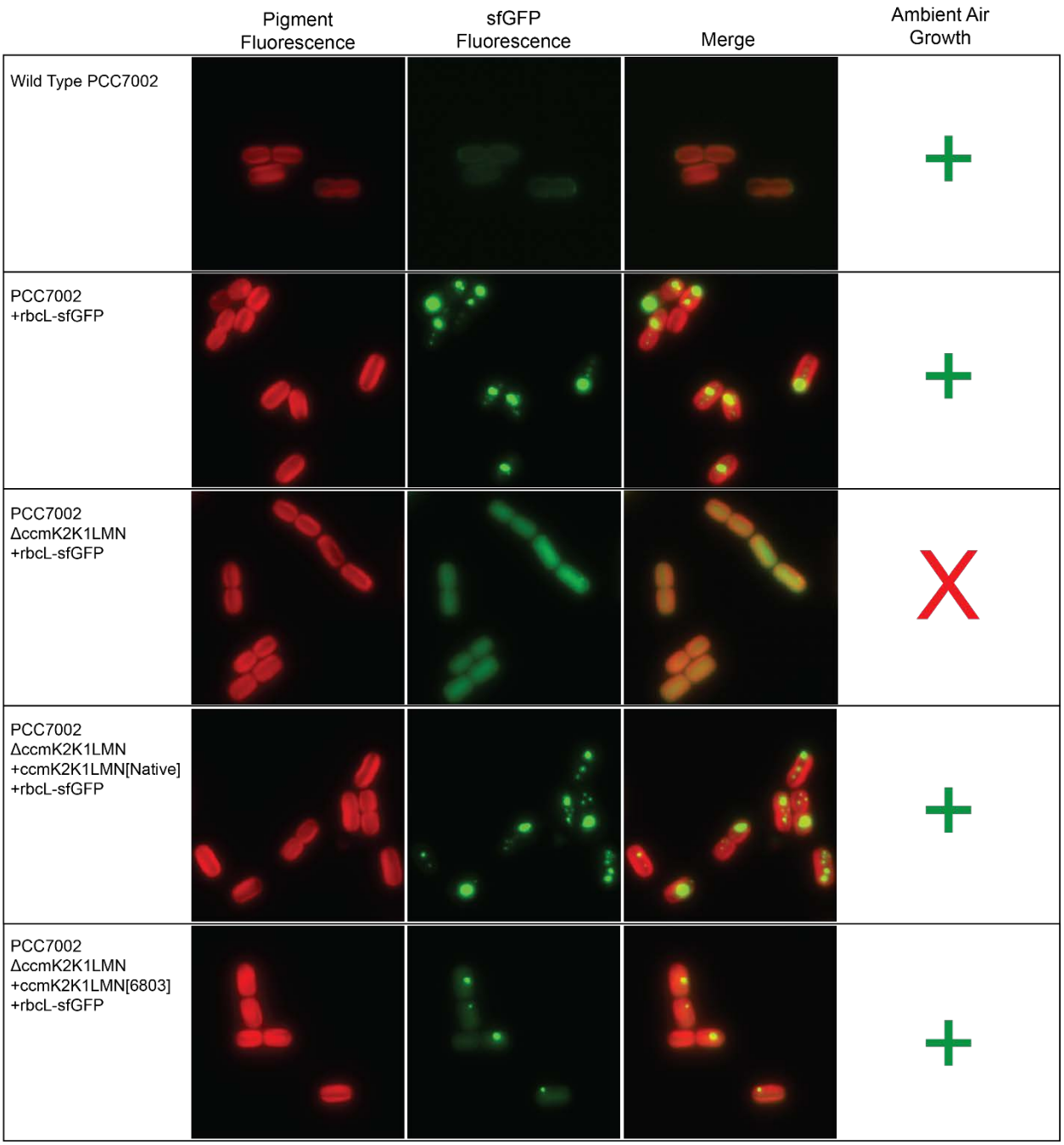

Figure 5-2. RuBisCO Localization in CCM Mutants of PCC7002. Pigment fluorescence represents the shape of the cell. sfGFP fluorescence shows the distribution of rbcL-sfGFP in the cell. Wild Type PCC7002 is included to show background fluorescence. The final column reports growth on Media A plates in ambient air. Detailed strain descriptions are given in Table 5-2.

Eliminating Natural Competence through Gene Knockouts

To reduce the risk of CCM restoration through horizontal gene transfer, we deleted genes involved in natural competence. It has been observed that elimination of the PCC7002 gene A1643, a homolog of

E. coli Hfq, eliminated its natural competence (Zess, Begemann, and Pfleger 2015). The Hfq homologue in the cyanobacterium *Synechocystis* sp. PCC6803 has been shown to be essential for generation of Type IV pili and thus for the natural competency of those cells (Dienst et al. 2008; Schuergers et al. 2014). To test the extent of this reduction in competency, we transformed PCC7002 ΔHfq (7002_RLC09) with a plasmid containing a gentamicin resistance gene and yellow fluorescent protein flanked by two 500 base pair regions of homology to the glpK neutral site (pALM232). We then plated dilutions of these transformed cells on Media A or with or without gentamicin to quantify the transformation efficiency (**Figure 5-3**). PCC7002 ΔHfq exhibited a four order of magnitude decrease in transformation efficiency relative to Wild Type PCC7002.

The Com apparatus is a Type IV secretion system known to be essential for natural competence in *Heliobacter pylori* and *Bacillus subtilis* (Dorer, Sessler, and Salama 2011). PCC7002 contains a homolog of comEC, an inner membrane protein thought to be involved in DNA uptake. We tested the natural competence of PCC7002 ΔcomEC (7002_GG90) using the previously described assay (**Figure 5-3**). PCC7002 ΔcomEC exhibited a decrease in transformation efficiency of at least four orders of magnitude relative to Wild Type PCC7002. From these experiments, we conclude that PCC7002's Hfq and comEC are both valid targets for reducing natural competence and could reduce the risk of CCM restoration in the HCR containment mechanism.

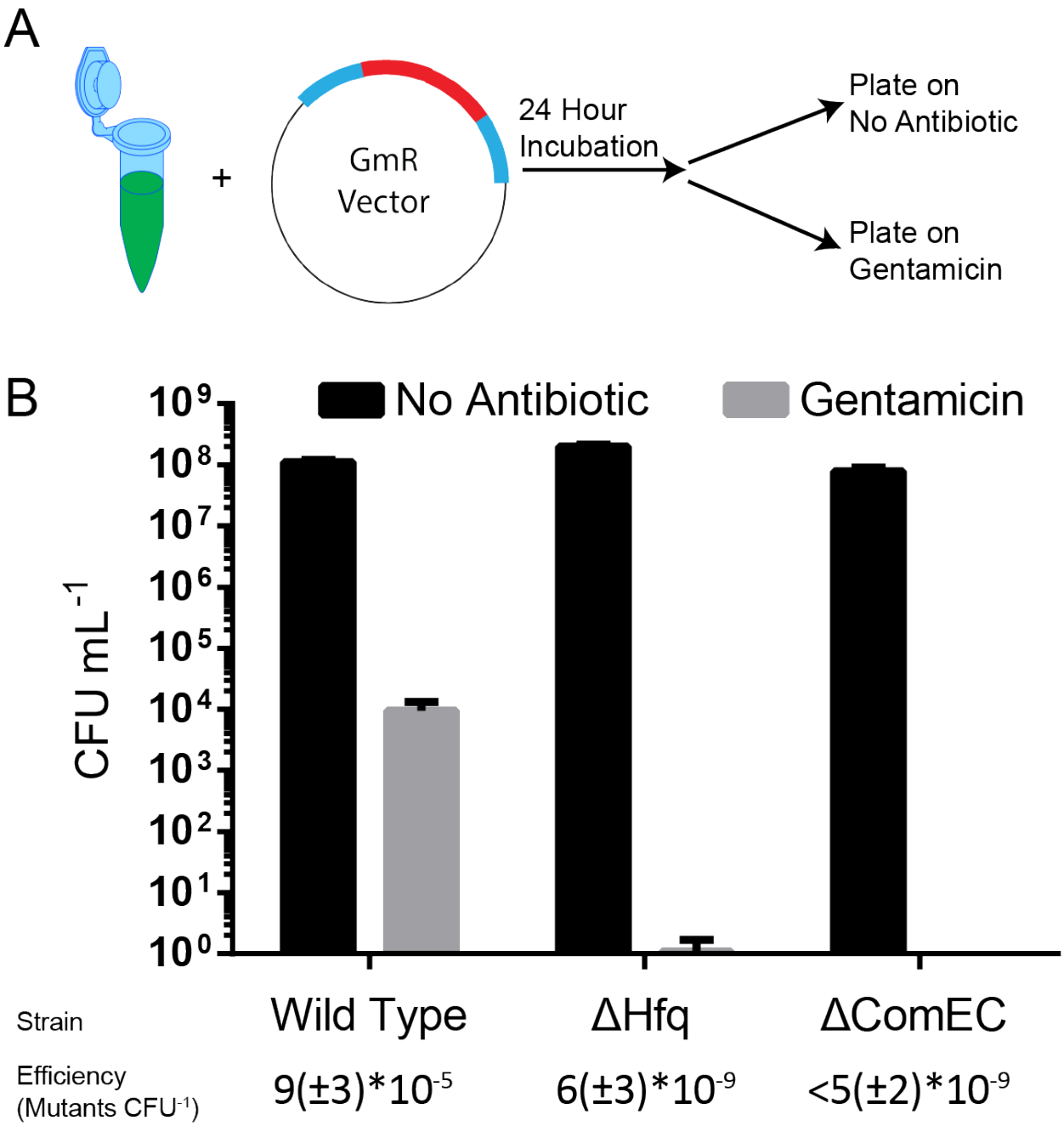

Figure 5-3. Transformation Efficiency Reduction in Competence Gene Deletion Mutants. A) To determine transformation efficiency, samples of culture were incubated for 24 hours in the light with 500 ng of plasmid DNA containing a gentamicin resistance gene (GmR) with regions of homology to PCC7002 glpK. Dilutions of these samples were then plated on Media A with or without gentamicin and grown for 4 days before colonies were counted to determine transformation efficiency. B) Colony Forming Units (CFU) mL^{-1} recovered for transformation samples plated on Media A with (Grey) or without (black) gentamicin. Error bars represent the standard error of at least three biological replicates. Transformation efficiencies are listed with standard error of the mean in parentheses. For PCC7002 ΔComEC, no colonies were recovered, so the transformation efficiency is reported as less than the inverse of the number of CFU plated on gentamicin.

Implementation of Containment Mechanism in L-lactate Production Strain

For useful implementation, a genetic containment mechanism should have minimal negative impact on the function of the organism of interest, such as the production of secreted molecules. To test whether the HCR containment mechanism has a negative impact on product synthesis, the productivity of a previously characterized strain of PCC7002 engineered for L-lactate production by introduction of a lactate dehydrogenase capable of utilizing NADPH, PCC7002 clac143-ldh* (7002_CC133) (Gordon et al. 2016), was compared to the HCR containment strain PCC7002 clac143-ldh* ΔccmK2K1LMN ΔHfq. Similar linear growth rates and linear L-lactate production rates were measured for each strain (**Figure 5-4**). This suggests that the HCR containment mechanism does not negatively impact the productivity of secreted molecules.

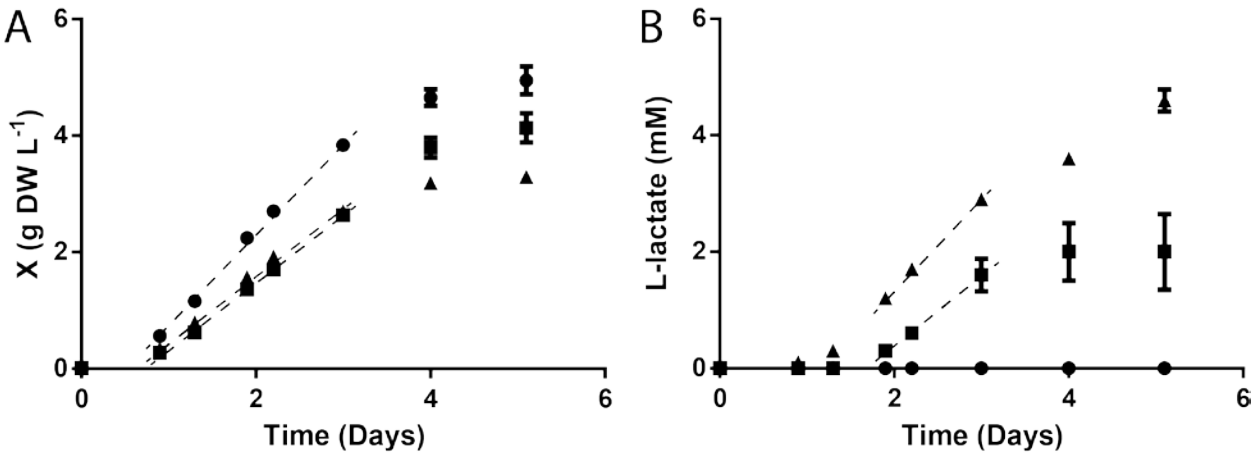

C

	Strain	LGR[A]	LPR[B]	ρ[C]
●	Wild Type PCC7002	66(±2)	0	0
■	PCC7002 clac143-ldh*	48(±1)	50(±5)	1.0(±0.1)
▲	PCC7002 clac143-ldh* ΔccmK2K1LMN ΔHfq	48(±1)	62(±2)	1.3(±0.1)

Figure 5-4. HCR Containment Mechanism Has No Effect on L-lactate Productivity. Wild Type PCC7002, PCC7002 clac143-ldh*, and PCC7002 clac143-ldh* ΔccmK2K1LMN ΔHfq were grown in bubble tubes with 5% CO_2 to determine the impact of the HCR containment mechanism on growth (A) and L-lactate productivity (B). The dashed lines represent the linear growth rate (LGR) and linear production rate of L-lactate (LPR) reported in (C). Error bars and values in parentheses represent the standard error of the mean of three biological replicates. ρ is the growth associated productivity calculated from the ratio of LPR to LGR as described in Chapter 3. [A][mg DW L^{-1} hr^{-1}] [B][μM L-lactate hr^{-1}] [C][mmol L-lactate (g DW)$^{-1}$]

5.3. Conclusions

In this work, we have presented a proof of concept for high CO_2 requirement as a containment mechanism for cyanobacteria. We have shown that the survival rate in ambient air of PCC7002 lacking the carboxysome shell proteins is less than $5*10^{-10}$ CFU^{-1}. We have identified horizontal gene transfer as a likely escape mechanism from high CO_2 requirement and have identified two candidate genes involved in natural competence whose deletions dramatically reduce the natural competence of PCC7002. We implemented this containment mechanism in a previously characterized strain of PCC7002 engineered for L-lactate production and observed no negative impact on growth or productivity.

5.4. Methods

Culturing Cyanobacteria

All strains were maintained on plates of Media A adapted from Stevens et al (Stevens, Patterson, and Myers 1973) (308 mM NaCl, 20 mM $MgSO_4$, 0.08 mM Na_2EDTA, 8 mM KCl, 3 mM $CaCl_2$, 12 mM $NaNO_3$, 0.37 mM KH_2PO_4, 8 mM Tris Base, 30 µM Ferric Ammonium Citrate, 554 µM H_3BO_3, 22 µM $MnCl_2$, 2.3 µM $ZnCl_2$, 208 nM MoO_3, 12 nM $CuSO_4$, 51 nM $CoCl_2$, 3 nM cobalamin) with 1.5% (w/v) Bacto-Agar (Fisher) supplemented with the appropriate antibiotics (kanamycin, 100 µg mL^{-1}; gentamicin, 30 µg mL^{-1}; zeocin, 100 µg mL^{-1}; streptomycin, 100 µg mL^{-1}). A 2x Media A solution and a 2x Bacto-Agar solution were prepared and autoclaved separately and allowed to cool to 55°C before mixing and addition of cobalamin and antibiotics. For plates to be used in 5% CO_2, the 2x Media A solution was adjusted to a pH of 11 by addition of NaOH before being autoclaved. Inoculum for experiments was prepared by transferring biomass from solid media to bubble tubes containing 20 mL of the appropriate medium with a sterile loop and bubbling the resulting culture with the specified CO_2 concentration in a custom temperature-controlled water bath outfitted with a white LED panel (Up to 275 µmol PAR m^{-2} s^{-1} from 4000 K White LED). Optical density at 730 nm was measured in a Genesys 20 spectrophotometer (Thermo Scientific) in 1 cm cuvettes. All samples were diluted into the linear range of OD730 between 0.01-0.30.

Strains

All strains used in this work are shown in **Table 5-2**. Genetic modifications were made through natural competence mechanisms as previously described (Begemann et al. 2013). Genetic modification vectors were made on plasmids cloned in *E. coli* DH5a and are shown in **Table 5-3**. Constructs were made using Gibson assembly (Gibson et al. 2009) with regions of homology added in the 5' end of the primer.

Exponential Growth Rate Experiments

Exponential growth rate experiments were performed in bubble tubes with the specified CO_2 concentration as described in **Chapter 3**. The irradiance was 125 µmol PAR m^{-2} s^{-1} 4000K white LED light (50 µmol accessible photons m^{-2} s^{-1}) and the temperature was 38°C.

Microscopy

rbcL-sfGFP imaging was performed as described previously (Gordon et al. 2016). Briefly, cells were spotted onto 1% (w/v in Media A) agarose pads in a 16-well chamber slide, air-dried, and covered with a 0.17 mm coverslip. Images were acquired on a Zeiss Axioimager Z2 for GFP (excitation: BP 470/40 nm; beam splitter: FT 495 nm; emission: BP 525/50 nm), and pigments (excitation: BP 545/25 nm; beam splitter: FT 570 nm; emission: BP 610/70 nm) using a 100x oil-immersion objective (NA=1.3). Images were analyzed with ImageJ (Abràmofff, Magalhães, and Ram 2005).

Transformation Efficiency Assay

Cultures were grown to OD_{730} between 1-4 in 10% CO_2 and then diluted to OD_{730} of 1. Samples of these cultures (1 mL) were placed in 1.6 mL Eppendorf tubes and 500 ng of pALM232 was added to each sample. The samples were incubated for 24 hours in 150 µmol PAR m^{-2} s^{-1} cool white fluorescent light (45 µmol accessible photons m^{-2} s^{-1}) with a temperature of 38°C. Dilutions of the samples were then plated on Media A with or without 30 µg mL^{-1} gentamicin and grown in in 150 µmol PAR m^{-2} s^{-1} cool white fluorescent light (45 µmol accessible photons m^{-2} s^{-1}) with a temperature of 38°C for 4 days before counting colonies to quantify transformation efficiency.

L-lactate Production Assay

Pre-cultures of Wild Type PCC7002, PCC7002 clac143-ldh* (7002_CC133), and PCC7002 clac143-ldh* ΔccmK2K1LMN ΔHfq (7002_RLC29) were grown to OD_{730} between 1-4 in 10% CO_2 and then diluted to OD_{730} of 0.05 and induced with 1 mM isopropyl β-D-1-thiogalactopyranoside (IPTG) at time zero. Cultures were bubbled with 5% CO_2 at 38°C under an irradiance of 275 µmol PAR m^{-2} s^{-1} (110 µmol accessible photons m^{-2} s^{-1}) and 1 mL samples were taken at the specified time points for OD_{730} measurement. After OD_{730} measurements, these samples were pelleted and the supernatant was frozen until L-lactate concentration was measured. Cell dry weight was determined using a standard curve with a slope of 0.26 g DW L^{-1} OD_{730}^{-1} as described in **Chapter 3**.

L-lactate quantification

L-lactate was quantified via HPLC (Shimadzu CO., Columbia, MD,USA) equipped with a quaternary pump, autosampler, vacuum degasser, photodiode array, and refractive index detector as described previously (Gordon et al. 2016). Briefly, separations were performed using an Ultra Aqueous C18 column (Restek) with a mobile phase containing 50 mM KH_2PO_4 (pH 2.5, 1% acetonitrile), flow rate of 0.31 mL min^{-1}, and 30°C column temperature for a run time of 10 minutes with a 10 µL injection volume. L-lactate concentration was determined from the photodiode array 210 nm signal by comparison to solutions of known sodium L-lactate concentration in Media A with 1 mM IPTG.

Table 5-2. PCC7002 Strains Used in This Work.

Strain	Genotype	Description	Source
7002_RLC01	A1799-1803::KanR	Carboxysome shell protein operon knockout	Gordon et al 2016
7002_RLC09	A1643::aadA	Hfq homolog knockout	Zess et al 2016
7002_RLC16	A1799-1803::KanR, A1838::rbcL-sfGFP(ZeoR)	Carboxysome shell protein operon knockout, RuBisCO large subunit fused to sfGFP in acsA	This work
7002_RLC18	A1838::rbcL-sfGFP(ZeoR)	RuBisCO large subunit fused to sfGFP in acsA	This work
7002_RLC19	A1799-1803::KanR, A1838::rbcL-sfGFP(ZeoR), A2842::ccmK2K1LMN[7002](GmR)	Carboxysome shell protein operon knockout, RuBisCO large subunit fused to sfGFP in acsA, Native ccmK2K1LMN Operon in glpK	This work
7002_RLC22	A1799-1803::KanR, A2842::ccmK2K1LMN[7942](GmR)	Carboxysome shell protein operon knockout, *Synechococcus elongatus* sp. PCC7942 ccmK2K1LMN Operon in glpK	This work
7002_RLC23	A1799-1803::KanR, A2842::ccmK2K1LMN[6803](GmR)	Carboxysome shell protein operon knockout, *Synechocystis* sp. PCC6803	This work
7002_RLC24	A1799-1803::KanR, A1838::rbcL-sfGFP(ZeoR)	Carboxysome shell protein operon knockout, RuBisCO large subunit fused to sfGFP in acsA	This work
7002_RLC26	A1799-1803::KanR, A1838::rbcL-sfGFP(ZeoR), A2842::ccmK2K1LMN[6803](GmR)	Carboxysome shell protein operon knockout, RuBisCO large subunit fused to sfGFP in acsA, *Synechocystis* sp. PCC6803 ccmK2K1LMN Operon in glpK	This work
7002_RLC28	A2842::clac143-ldh*(GmR), A1799-1803::KanR	Mutant lactate dehydrogenase on IPTG inducible promoter in glpK, Carboxysome shell protein operon knockout	This work
7002_RLC29	A2842::clac143-ldh*(GmR), A1799-1803::KanR, A1643::aadA	Mutant lactate dehydrogenase on IPTG inducible promoter in glpK, Carboxysome shell protein operon knockout, Hfq homolog knockout	This work
7002_GG90	A0827::KanR	comEC knockout	This work
7002_CC133	A2842::clac143-ldh*(GmR)	Mutant lactate dehydrogenase on IPTG inducible promoter in glpK	Gordon et al 2016

Table 5-3. Plasmids Used for Cloning in This Work.

Plasmid	Genotype	Source
pRLC10	A1799-1803::KanR	Gordon et al 2016
pEZ22	A1643::aadA	Zess et al 2016
pRLC20	A1838::rbcL-sfGFP(ZeoR)	This work
pRLC13	A2842::ccmK2K1LMN[7002](GmR)	This work
pRLC22	A2842::ccmK2K1LMN[6803](GmR)	This work
pGCG65	A0827::KanR	This work

5.5. References

Abràmofff, M. D., Paulo J. Magalhães, and Sunanda J. Ram. 2005. "Image Processing with ImageJ Part II." *Biophotonics International* 11(7):36–43.

Angermayr, S. Andreas, Aleix Gorchs Rovira, and Klaas J. Hellingwerf. 2015. "Metabolic Engineering of Cyanobacteria for the Synthesis of Commodity Products." *Trends in Biotechnology* 33(6):352–61.

Badger, Murray R. et al. 1998. "The Diversity and Coevolution of Rubisco, Plastids, Pyrenoids, and Chloroplast-Based CO_2-Concentrating Mechanisms in Algae 1." *Canadian Journal of Botany* 1071:1052–71.

Begemann, Matthew B. et al. 2013. "An Organic Acid Based Counter Selection System for Cyanobacteria." *PLoS ONE* 8(10):e76594.

Cai, Yizhi et al. 2015. "Intrinsic Biocontainment: Multiplex Genome Safeguards Combine Transcriptional and Recombinational Control of Essential Yeast Genes." *Proceedings of the National Academy of Sciences of the United States of America* 112(6):1803–8.

Cameron, Jeffrey C., Steven C. Wilson, Susan L. Bernstein, and Cheryl a Kerfeld. 2013. "Biogenesis of a Bacterial Organelle: The Carboxysome Assembly Pathway." *Cell* 155(5):1131–40.

Chan, Clement T. Y., Jeong Wook Lee, D.Ewen Cameron, Caleb J. Bashor, and James J. Collins. 2015. "'Deadman' and 'Passcode' Microbial Kill Switches for Bacterial Containment." *Nature Chemical Biology* 12(2):82–86.

Clark, Ryan L., Jeffrey C. Cameron, Thatcher W. Root, and Brian F. Pfleger. 2014. "Insights into the Industrial Growth of Cyanobacteria from a Model of the Carbon-Concentrating Mechanism." *AIChE Journal* 60(4):1269–77.

Curtiss, Roy. 1978. "Biological Containment and Cloning Vector Transmissibility." *Journal of Infectious Diseases* 137(5):668–75.

Dienst, Dennis et al. 2008. "The Cyanobacterial Homologue of the RNA Chaperone Hfq Is Essential for Motility of *Synechocystis* Sp. PCC 6803." *Microbiology* 154(10):3134–43.

Dorer, Marion S., Tate H. Sessler, and Nina R. Salama. 2011. "Recombination and DNA Repair in *Helicobacter Pylori*." *Annual Review of Microbiology* 65:329–48.

Gee, Christopher W. and Krishna K. Niyogi. 2017. “The Carbonic Anhydrase CAH1 Is an Essential Component of the Carbon-Concentrating Mechanism in *Nannochloropsis Oceanica*.” *Proceedings of the National Academy of Sciences of the Unites States of America* 114(17):4537–42.

Gibson, Daniel G. et al. 2009. “Enzymatic Assembly of DNA Molecules up to Several Hundred Kilobases.” *Nature Methods* 6(5):12–16.

Gordon, Gina C. et al. 2016. “CRISPR Interference as a Titratable, Trans-Acting Regulatory Tool for Metabolic Engineering in the Cyanobacterium *Synechococcus* Sp. Strain PCC 7002.” *Metabolic Engineering* 38:170–79.

Li, Qin and Yi Jun Wu. 2009. “A Fluorescent, Genetically Engineered Microorganism That Degrades Organophosphates and Commits Suicide When Required.” *Applied Microbiology and Biotechnology* 82(4):749–56.

Liao, James C., Luo Mi, Sammy Pontrelli, and Shanshan Luo. 2016. “Fuelling the Future: Microbial Engineering for the Production of Sustainable Biofuels.” *Nature Reviews Microbiology* 14:288–304.

Malyshev, Denis A. et al. 2014. “A Semi-Synthetic Organism with an Expanded Genetic Alphabet.” *Nature* 509(7500):385–88.

Mandell, Daniel J. et al. 2015. “Biocontainment of Genetically Modified Organisms by Synthetic Protein Design.” *Nature* 518:55–60.

Moe-Behrens, Gerd H. G., Rene Davis, and Karmella A. Haynes. 2013. “Preparing Synthetic Biology for the World.” *Frontiers in Microbiology* 4:5.

Molin, S. et al. 1987. “Conditional Suicide System for Containment of Bacteria and Plasmids.” *Nature Biotechnology* 5(12):1315–18.

Oliver, Neal J. et al. 2016. “Cyanobacterial Metabolic Engineering for Biofuel and Chemical Production.” *Current Opinion in Chemical Biology* 35:43–50.

Orf, Isabel et al. 2015. “Integrated Analysis of Engineered Carbon Limitation in a Quadruple CO_2/HCO_3^--Uptake Mutant of *Synechocystis* Sp. PCC 6803.” *Plant Physiology* 169:1787–1806.

Price, G. D. and M. R. Badger. 1989. “Isolation and Characterization of High CO_2-Requiring Mutants of the Cyanobacterium *Synechococcus* PCC7942.” *Plant Physiology* 91:514–25.

Raven, John A., John Beardall, and Patricia Sánchez-Baracaldo. 2017. “The Possible Evolution, and Future, of CO_2-Concentrating Mechanisms.” *Journal of Experimental Botany*.

Rovner, Alexis J. et al. 2015. “Recoded Organisms Engineered to Depend on Synthetic Amino Acids.” *Nature* 518:89–93.

Scanlan, D. J. et al. 2009. “Ecological Genomics of Marine Picocyanobacteria.” *Microbiology and Molecular Biology Reviews* 73(2):249–99.

Schmidt, Markus and Victor de Lorenzo. 2016. “Synthetic Bugs on the Loose: Containment Options for Deeply Engineered (Micro)organisms.” *Current Opinion in Biotechnology* 38:90–96.

Schuergers, Nils et al. 2014. “Binding of the RNA Chaperone Hfq to the Type IV Pilus Base Is Crucial for Its Function in *Synechocystis* Sp. PCC 6803.” *Molecular Microbiology* 92(4):840–52.

Stevens, S. E., C. O. P. Patterson, and J. Myers. 1973. “The Production of Hydrogen Peroxide by Blue-Green Algae: A Survey.” *Journal of Phycology* 9:427–30.

Yenkie, Kirti M. et al. 2016. “A Roadmap for the Synthesis of Separation Networks for the Recovery of Bio-Based Chemicals: Matching Biological and Process Feasibility.” *Biotechnology Advances* 34(8):1362–83.

Zess, Erin K., Matthew B. Begemann, and Brian F. Pfleger. 2015. “Construction of New Synthetic Biology Tools for the Control of Gene Expression in the Cyanobacterium *Synechococcus* Sp. Strain PCC 7002.” *Biotechnology and Bioengineering*. 113(2):424-32.

Chapter 6: Summary and Future Directions

6.1. Research Summary

The work described in this document addressed two key challenges for the industrial cultivation of cyanobacteria. First, theoretical and experimental investigations into light-limited growth of cyanobacteria provided a standard for comparison of cyanobacterial productivity which will enable more intuitive comparisons of metabolic engineering efforts (**Chapter 3**). Second, a theoretical understanding of cyanobacterial CO_2-fixation (**Chapter 4**) provided a guide for the development of a containment mechanism for cyanobacteria which utilizes a genetically imposed requirement for high CO_2 concentration (**Chapter 5**).

Because CO_2 and soluble nutrients such as bio-available nitrogen, iron, and phosphorous can be provided from waste sources, an optimal cyanobacterial cultivation should seek to maximize photon utilization by ensuring light is the sole limiting substrate. This is not typically the case in laboratory experiments, so nutrient sufficient conditions were developed such that growth to stationary phase was achieved with light as the sole limiting substrate. Then, a theoretical description of light-limited growth was used to define two key parameters (photon utilization efficiency, η, and growth-associated productivity, ρ) easily determined from experimental measurements which can be used for comparison of metabolically engineered cyanobacteria (**Chapter 3**).

To understand situations under which CO_2 is a limiting substrate, a model of the CO_2-concentrating mechanism was developed and compared to a theoretical cyanobacterium lacking the CO_2-concentrating mechanism (CCM). This model showed that diffusion is not a limiting factor in cyanobacterial CO_2-fixation and allowed prediction of CO_2-fixation rate as a function of CO_2 concentration with a trend matching data from the literature. The resulting model predicted that cyanobacteria lacking the CCM fix a negligible amount of CO_2 in ambient air, but fix CO_2 at approximately the same rate as wild type in 10% CO_2 (**Chapter 4**).

Using the results of the CO_2-fixation model, a mechanism for containment within a high CO_2 environment was devised in which the CCM was disrupted through carboxysome gene deletion. CCM-lacking cyanobacteria were shown to be unable to propagate in ambient air, but grew at the same rate as wild type in 5% CO_2. Since horizontal gene transfer can provide a potential method of escape, the deletion of natural competence genes was performed resulting in a reduction of transformation efficiency of a standard antibiotic resistance vector by at least six orders of magnitude. Carboxysome deletion and competence gene deletion were implemented in a cyanobacterial strain engineered for L-lactate production resulting in no negative impact of L-lactate productivity (**Chapter 5**).

6.2. Future Directions

The work described above suggests several interesting ideas for future research. First, we will consider areas for improvement in understanding light-limited growth and chemical production. Second, we will discuss how the current understanding of light-limited growth suggests ways to improve cyanobacterial productivity. Finally, we will consider ways in which the high CO_2 requirement (HCR) based containment mechanism could be improved.

Improving Light-Limited Growth Theory

The work described in **Chapter 3** focused on experimental conditions that commonly vary between laboratory experiments performed by different researchers. The results allowed comparison between laboratory vessels of varying geometry and volume (*i. e.* 20 mL tube scaled to 900 mL bottle). To improve upon this understanding, experiments should be performed in pilot-scale raceway ponds with light as the sole limiting nutrient to verify that the scaling rules hold for much larger vessels (*i. e.* 1 L bottle scaled to 100 L pond). It would also be interesting to determine if growth under day-night cycles can be sufficiently described by the theoretical framework while varying I_{IN} with time.

Peak solar irradiance is an order of magnitude higher than the highest irradiance used in the experiments in **Chapter 3** (Bird et al. 1986; Ooms et al. 2016) and photoinhibition has been shown to have

a significant negative impact on growth with varying magnitude between cyanobacterial strains (Bernstein et al. 2016; Xiong et al. 2015). Thus, it would be interesting to quantify the effects of irradiances approaching peak solar irradiance on cyanobacteria tolerant to high irradiance (*i. e. Synechococcus* sp. PCC7002) and use adaptive evolution methods to improve their tolerance to high irradiance.

As observed in **Chapter 3**, a simple growth-associated productivity model is insufficient to describe the productivity of some secreted products in later time points over the course of light-limited batch growth. This suggests that metabolic changes with increasing cell density affect cell-specific productivity. For future metabolic engineering efforts, it would be useful to perform transcriptomic and metabolomic analyses on cultures where productivity of secreted molecules is significantly lower than predicted by the growth-associated productivity model to determine what changes in enzyme or metabolite content of the cells are limiting product synthesis.

Improving Cyanobacterial Productivity and Titer

The photon utilization efficiencies determined in **Chapter 3** average to a value of 0.63. This means that if all accessible photons are efficiently utilized, linear productivity of biomass and secreted molecules can be increased by no more than 1.6-fold (inverse of the efficiency). However, if the number of accessible photons were increased by engineering cyanobacteria to access photons of wavelengths that are currently unusable, further increases in productivity could be achieved. Pigments found in red algae could be used to access photons in the range of 500-600 nm (Ooms et al. 2016). Chlorophyll *f*, a chlorophyll *a* derivative found in *Chlorogloepsis fritschii* PCC9212 which absorbs higher wavelength photons, was recently synthesized in *Synechococcus* sp. PCC7002 and could allow access to far-red photons (Ho et al. 2016). Chlorophyll *b*, is even further far-red shifted and could further increase the number of accessible photons (Canniffe and Neil Hunter 2014). The key challenge moving forward in this area is coupling the

excitation of these pigments to the light reactions to allow conversion of currently inaccessible photons into chemical energy in cyanobacteria.

As observed in **Chapter 3**, cyanobacteria grown with light as the sole limiting substrate transition to stationary phase at cell densities ~30% lower than predicted by the theoretical framework. As final cell and product titers are major factors in technoeconomic analyses of cyanobacterial production processes (Yenkie et al. 2016; Yenkie, Wu, and Maravelias 2017), this is a key limitation that could potentially be solved through a systems biology understanding. The abrupt nature of the stationary phase transition suggests it is induced by cellular regulatory mechanisms. We hypothesize that the regulatory mechanism is triggered through the stringent response as the rate of energy generation per cell drops below a certain threshold. This mechanism has been shown to be responsible for triggering transcriptional responses for cyanobacteria transitioning from light to dark conditions (Hood et al. 2016), a condition that could be mimicked by sufficient cell shading. This hypothesis could be tested by quantifying the ppGpp content and transcript abundance of genes regulated by the stringent response in cyanobacteria before and after the light-limited stationary phase transition. If this hypothesis is confirmed, a key engineering challenge will be overcoming this regulatory growth limitation without disrupting viability under day-night cycling.

Improving the High CO_2 Requirement Containment Mechanism

The high CO_2 requirement-based containment mechanism described in **Chapter 5** has been indirectly shown to have a reduced risk of escape through horizontal gene transfer by measuring the transformation efficiency reduction in natural competence gene-deletion mutants. A more direct experiment would involve co-culture of wild type cyanobacteria with a CCM-lacking mutant to determine the frequency of escape through horizontal gene transfer. The experiment could then be repeated with CCM-lacking strains with natural competence gene deletions to measure the decrease in escape frequency.

Two strategies could be implemented to further reduce the likelihood of escape through horizontal gene transfer. First, multiple CCM functions could be deleted to decrease the likelihood of restoring CCM

function in a single horizontal gene transfer event. Second, multiple natural competence genes could be deleted to further reduce the frequency of horizontal gene transfer events. Both of these strategies require methods for making multiple gene knockouts in one strain which could be enabled by Cas9 (Wendt et al. 2016) or Cpf1 (Ungerer and Pakrasi 2016) mediated gene deletion technologies which have been developed in other model cyanobacteria. Many natural competence and CCM-related gene deletion targets could be identified through random barcode transposon insertion sequencing, a method that has been developed in the model cyanobacterium *Synechococcus elongatus* sp. PCC7942 (Rubin et al. 2015) and is further discussed in **Appendix B**.

Horizontal gene transfer is only one potential method of escape. Another potential method for escape could be phage-mediated gene complementation. Cyanophage have been found to encode many genes involved in photosynthesis and central carbon metabolism and to inhibit CO_2-fixation during infection (Puxty et al. 2016). Thus, an undiscovered cyanophage could conceivably carry genes that could restore the CCM. If such a cyanophage were discovered, a CRISPR/Cas-mediated mechanism could be engineered to prevent infection by degrading problematic DNA molecules inside the cell, capitalizing on the natural immunity function of the CRISPR/Cas system (Horvath and Barrangou 2010).

6.3. References

Bernstein, Hans C. et al. 2016. “Unlocking the Constraints of Cyanobacterial Productivity: Acclimations Enabling Ultrafast Growth.” *mBio* 7(4)

Bird, Richard E., Carol Riordan, Richard E. Bird, and Carol Riordan. 1986. “Simple Solar Spectral Model for Direct and Diffuse Irradiance on Horizontal and Tilted Planes at the Earth’s Surface for Cloudless Atmospheres.” *Journal of Climate and Applied Meteorology* 25(1):87–97.

Canniffe, Daniel P. and C. Neil Hunter. 2014. “Engineered Biosynthesis of Bacteriochlorophyll B in *Rhodobacter Sphaeroides*.” *Biochimica et Biophysica Acta* 1837(10):1611–16.

Ho, Ming-Yang, Gaozhong Shen, Daniel P. Canniffe, Chi Zhao, and Donald A. Bryant. 2016. “Light-Dependent Chlorophyll *f* Synthase Is a Highly Divergent Paralog of PsbA of Photosystem II.” *Science* 353(630):886.

Hood, Rachel D., Sean A. Higgins, Avi Flamholz, Robert J. Nichols, and David F. Savage. 2016. “The Stringent Response Regulates Adaptation to Darkness in the Cyanobacterium *Synechococcus*

Elongatus." *Proceedings of the National Academy of Sciences of the United States of America* 113(33):E4867–76.

Horvath, P. and R. Barrangou. 2010. "CRISPR/Cas, the Immune System of Bacteria and Archaea." *Science* 327(5962):167–70.

Ooms, Matthew D., Cao Thang Dinh, Edward H. Sargent, and David Sinton. 2016. "Photon Management for Augmented Photosynthesis." *Nature Communications* 7:12699.

Puxty, Richard J., Andrew D. Millard, David J. Evans, and David J. Scanlan. 2016. "Viruses Inhibit CO 2 Fixation in the Most Abundant Phototrophs on Earth." *Current Biology* 26:1585–89.

Rubin, Benjamin E. et al. 2015. "The Essential Gene Set of a Photosynthetic Organism." P*roceedings of the National Academy of Sciences of the United States of America* 112(48):E6634–43.

Ungerer, Justin and Himadri B. Pakrasi. 2016. "Cpf1 Is A Versatile Tool for CRISPR Genome Editing Across Diverse Species of Cyanobacteria." *Scientific Reports* 6:39681.

Wendt, Kristen E., Justin Ungerer, Ryan E. Cobb, Huimin Zhao, and Himadri B. Pakrasi. 2016. "CRISPR/Cas9 Mediated Targeted Mutagenesis of the Fast Growing Cyanobacterium *Synechococcus Elongatus* UTEX 2973." *Microbial Cell Factories* 15:115.

Xiong, Qian et al. 2015. "Integrated Transcriptomic and Proteomic Analysis of the Global Response of *Synechococcus* Sp . PCC 7002 to High Light Stress." *Molecular and Cellular Proteomics* 14(4):1038–53.

Yenkie, Kirti M. et al. 2016. "A Roadmap for the Synthesis of Separation Networks for the Recovery of Bio-Based Chemicals: Matching Biological and Process Feasibility." *Biotechnology Advances* 34(8):1362–83.

Yenkie, Kirti M., Wenzhao Wu, and Christos T. Maravelias. 2017. "Synthesis and Analysis of Separation Networks for the Recovery of Intracellular Chemicals Generated from Microbial-Based Conversions." *Biotechnology for Biofuels* 10:119.

Appendix A: Photobioreactor Documentation

A.1. Background and Motivation

As described in the main chapters of this work, a large field of research has developed for the study of cyanobacteria for photosynthetic chemical production (Angermayr, Gorchs Rovira, and Hellingwerf 2015). Understanding the bioenergetics of growth and product secretion of cyanobacteria requires experiments, such as those described in previous chapters, in controlled environments with volumes large enough to allow sampling over time without removing most of the culture medium. The cost of commercial laboratory photobioreactors makes these experiments inaccessible to many researchers and limits experimental throughput. In this work, we designed and constructed a system of 12 independent, sterilizable cyanobacterial photobioreactors for cultures up to 1 L in volume for a cost less than a single commercial photobioreactor (**Figure A-1**, **Table A-1**). This system allows gas mixing to a desired CO_2 concentration for transfer to the culture medium, discrete modulation of light intensity through addition/removal of fluorescent tubes, temperature control in the range of ambient temperature to 45°C, and simple sterile sampling for monitoring throughout long-term growth experiments. In the following sections, we will describe the assembly and operation of this photobioreactor system.

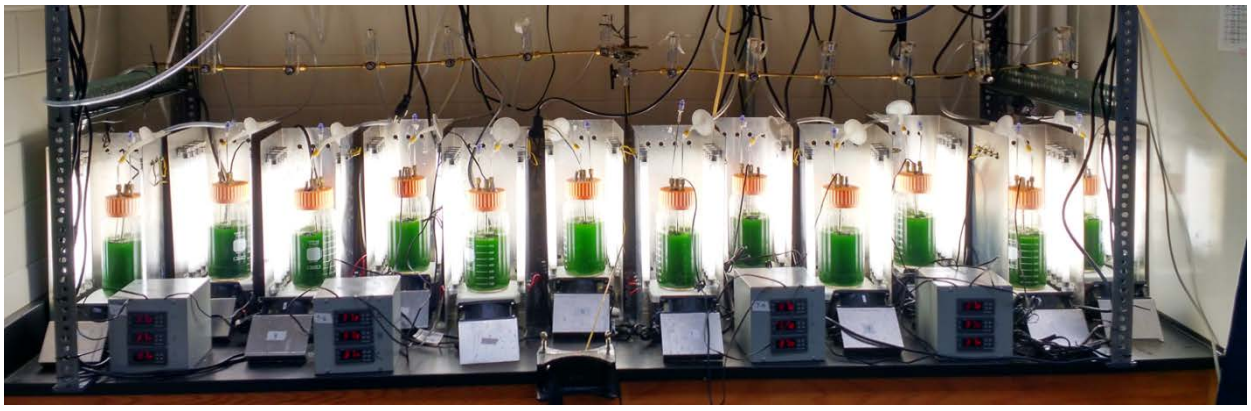

Figure A-1. Photobioreactor System in Operation. This 12-reactor system was used to simultaneously grow cyanobacteria under varying conditions. Gas delivery could have the same composition for all 12 reactors or one composition for the first six (from the left) and a different composition for the second six. Temperature control systems were combined in sets of three, but temperature set points were independent for each reactor.

Table A-1. Photobioreactor Parts List

Function	Reference Code	Item Description	Source	Item Number	Cost Per Item*	Number	Total Cost for 12 Reactors
Gas Mixing	G1	Air Mass Flow Controller	Alicat Scientific	MC-20SLPM-D / 5M, LIN, 5IN, GAS: Air	$1,344.25	2	$2,688.50
	G2	CO2 Mass Flow Controller	Alicat Scientific	MC-2SLPM-D / 5M, LIN, 5IN, GAS: CO2	$1,154.25	2	$2,308.50
	G3	Select - Brass Round Tubes Material: Yellow Brass Outside Diameter (Inch): 1/8	MSC Industrial Supply	32008674	$10.67	3	$32.01
	G4	Brass Swagelok Tube Fitting, Male Connector, 1/8 in. Tube OD x 1/8 in. Male NPT	Swagelok	B-200-1-2	$2.91	4	$11.64
	G5	Brass Swagelok Tube Fitting, Union Tee, 1/8 in. Tube OD	Swagelok	B-200-3	$9.22	1	$9.22
	G6	Rotameter	Omega	FL-2011	$57.00	1	$684.00
	G7	Brass Swagelok Tube Fitting, Male Run Tee, 1/4 in. Tube OD x 1/4 in. Male NPT x 1/4 in. Tube OD	Swagelok	B-400-3-4TMT	$9.32	1	$111.84
	G8	Brass Hose Connector, 1/8 in. Male NPT, 1/4 in. Hose ID	Swagelok	B-4-HC-1-2	$3.50	1	$42.00
	G9	2 L Wide Mouth Corning Bottle	Fisher	13-700-405	$42.31	1	$507.72
	G10	Tubing, Seamless, 1/4 In, 3 Ft, PK 5	Grainger	4EEL9	$37.75	5x3ft.	$37.75
	G11	Brass Hose Connector, 1/4 in. Female NPT, 1/4 in. Hose ID	Swagelok	B-4-HC-7-4	$8.20	0.08	$8.20
	G12	Brass Swagelok Tube Fitting, Male Connector, 1/4 in. Tube OD x 1/4 in. Male NPT	Swagelok	B-400-1-4	$2.90	0.08	$2.90
	G13	Stainless Steel 1-Piece 40GGG Series 3-Way Ball Valve, 0.90 Cv, 1/4 in. Swagelok Tube Fitting	Swagelok	SS-43GXS4	$112.30	0.08	$112.30
	G14	Brass Cap for 1/4 in. OD Tubing	Swagelok	B-400-C	$2.00	0.08	$2.00
Reactor Vessel	V1	1 L Wide Mouth Corning Bottle	Elemental Scientific, LLC	13-700-404	$21.11	1	$253.32
	V2	Brass Swagelok Tube Fitting, Bulkhead Union, 5/16 in. Tube OD	Swagelok	B-500-61	$18.24	1	$218.88
	V3	Brass Swagelok Tube Fitting, Bulkhead Union, 1/8 in. Tube OD	Swagelok	B-200-61	$21.93	3	$789.48
	V4	5/16"x10" Stainless Steel Thermocouple Protection	Omega	SS-516-10CLOSED	$12.16	1	$145.92
	V5	Tubing, Welded, 1/8 In, 6 ft, 316 SS	Grainger	3ADK4	$15.94	0.08	$15.94
	V6	Millipore* Aervent-50 Disposable Filters	Fisher	MTGR 85010	$11.92	1	$143.04
	V7	DASGIP BIOTOOLS LLC 78200077 SAMPLING VALVE	Fisher	NC9725776	$2.44	1	$29.28
Temperature	T1	Elitech 110V All-Purpose Temperature Controller+ Sensor 2 Relay Output Thermostat Stc-100C	Amazon	http://goo.gl/m4NXt7	$16.99	1	$203.88
	T2	Fan	Grainger	4WT49	$28.90	1	$346.80
	T3	Fan Guard	Grainger	4YD85	$1.34	1	$16.08
	T4	BUD Box	Newark	95F2597	$17.93	0.33	$71.72
	T5	Inlet Male Power Socket with Fuse Switch 10A 250V 3Pin	Amazon	http://goo.gl/NZjuSk	$4.28	0.33	$16.95
	T6	Universal Power Cord	Amazon	http://goo.gl/HYVRLF	$5.97	0.33	$23.64
	T7	AC Adapter 2-Prong Power Cord	Amazon	http://goo.gl/scOfLl	$3.20	1	$38.40
	T8	Leviton 1374-1 15Amp 125 Volt Snap in Receptacle	Amazon	http://goo.gl/hAzx5Q	$6.31	1	$75.72
Lighting	L1	Aluminum Sheet (0.05"x24"x24")	MSC Industrial Supply	32004780	$31.89	1	$382.68
	L2	Electrical Ballast	1000bulbs.com	BF-WH5120LC	$27.56	2	$661.44
	L3	Inlet Male Power Socket with Fuse Switch 10A 250V 3Pin	Amazon	http://goo.gl/NZjuSk	$4.28	1	$51.36
	L4	Universal Power Cord	Amazon	http://goo.gl/HYVRLF	$5.97	1	$71.64
	L5	Mini Bi-Pin Socket	1000bulbs.com	SOCK-EG897S	$1.04	16	$199.68
	L6	8 Watt/T5 Bulbs	1000bulbs.com	F-08T5CW	$0.74	8	$71.04
Misc. Supplies	M1	Heat Shrink Tubing Kit	Amazon	http://goo.gl/jNIzhd	$9.45	1	$9.45
	M2	#5-40 x 3/8" Phillips Machine Screws	MSC Industrial Supply	9173329	$6.00	100 per box	$6.00
	M3	#5-40 Hex Nuts	MSC Industrial Supply	87921268	$1.00	100 per box	$1.00
	M4	#5 Flat Washers	MSC Industrial Supply	67491043	$1.00	100 per box	$1.00
	M5	Fuses	Digi-Key	F4708-ND	$0.65	25	$0.65
	M6	Masterflex Tygon E-Lab ext tubing, nonphthlate/non-DEHP, 0.51mm, 100ft	Cole Parmer	GH-06460-18	$71.93	100 ft.	$71.93
	M7	Female Luer Lug Style to Classic Series Barb, 1/16" (1.6 mm) ID Tubing	Nordson Medical	FTL10-6005	$26.20	100	$26.20
	M8	10 mL syringe with BD luer-lok	Fisher Scientific	14-823-2A	$45.54	Case	$45.54
	M9	Male Luer Connector 3/16" 500 series	Value Plastics	MLRL035-1	$13.50	100	$13.50
	M10	3/16" ID Polypropylene Tubing	Amazon	https://goo.gl/3DLbRo	$48.26	100 ft.	$48.26
Total Cost for 12 Reactor System							$10,609.00

*Prices as of 4/1/2017.

A.2. Photobioreactor System Assembly

Reactor Vessel

1 L Wide Mouth Corning Bottles (V1) were used for the reactor vessel as they are a standardly available and cost-effective item that provided the desired working volume and substantial space for instrument installation in the cap. As shown in **Figure A-2**, holes were drilled in the plastic cap of the vessel to allow installation of bulkhead fittings for (1) a sample port, (2) gas delivery, (3) off-gas exit, and (4) thermocouple protection.

The sample port used a Brass Swagelok Bulkhead Union for 1/8 inch Tube OD (V3). A short piece of 1/8 inch stainless steel tubing (V5) was attached to the Swagelok fitting of the bulkhead union (V3) on the outside of the cap which was connected to a short length of 0.51mm Masterflex Tygon E-Lab tubing (M6). To this tubing a female Luer lock to 1/16 inch barb connector (M7) was attached which was connected to a DASGIP Sampling Valve (V7). A 7.25 inch piece of 1/8 inch stainless steel tubing (V5) was attached to the Swagelok fitting of the bulkhead union (V3) on the inside of the cap. The resulting sample port allowed for online sampling of culture from near the bottom of the reactor using a Luer lock syringe.

The gas delivery port also used a Brass Swagelok Bulkhead Union for 1/8 inch Tube OD (V3). A short piece of 1/8-inch stainless steel tubing (V5) was attached to the Swagelok fitting of the bulkhead union (V3) on the outside of the cap which was then connected to a short length of 0.51mm Masterflex Tygon E-Lab tubing (M6). To this tubing a female Luer lock to 1/16 inch barb connector (M7) was attached which was connected to a male Luer lock to 3/16 inch barb (M9). A short piece of 3/16 inch ID polypropylene tubing (M10) was attached to this 3/16 inch barb (M9) and subsequently to a Millipore Aervent-50 Disposable Filter (V6). This filter would eventually be attached to the gas delivery manifold discussed later. A 7.25 inch piece of 1/8 inch stainless steel tubing (V5) was attached to the Swagelok fitting of the bulkhead union (V3) on the inside of the cap. The resulting gas delivery port allowed delivery of sterile filtered gas to the bottom of the reactor vessel for CO_2 delivery.

The off-gas exit port also used a Brass Swagelok Bulkhead Union for 1/8 inch Tube OD (V3). No experiments performed with this system have taken advantage of the off-gas exit port, but Swagelok fittings could be used to capture the off-gas for further analysis if desired.

The thermocouple protection port used a Brass Swagelok Bulkhead Union for 5/16 inch Tube OD (V2). A 5/16 inch stainless steel thermocouple protection piece (V4) was cut to a length of 7.25 inches and attached to the Swagelok fitting of the bulkhead union (V2) on the inside of the cap. The resulting thermocouple protection port allowed a thermocouple to sample the reactor temperature without contacting the culture medium.

The resulting reactor vessel was suitable for cultivation of photosynthetic microorganisms with culture volumes of 500-1000 mL in conjunction with the light delivery, gas delivery, and temperature control systems described hereafter.

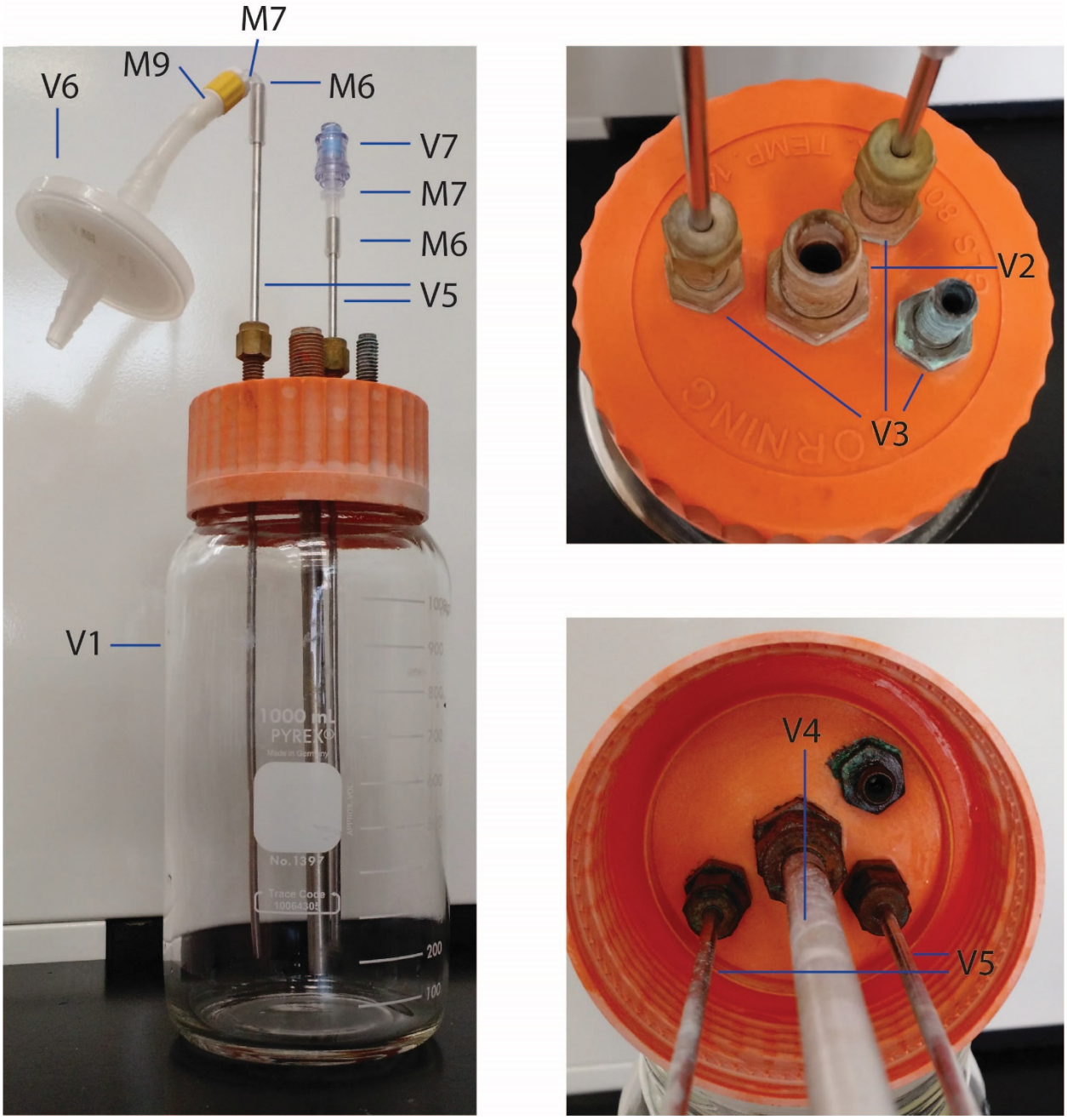

Figure A-2. Reactor Vessel. (Left) Image of fully assembled reactor vessel. (Right Top) Top down view of reactor cap shows how instrumentation was installed on the top of the cap. (Right Bottom) Bottom up view of reactor cap shows how instrumentation was installed on the bottom of the cap. All labels reference the parts shown in Table A-1.

Gas Delivery System

An overview of the gas delivery system used to deliver a gas phase with a desired CO_2 concentration is shown in **Figure A-3**. Two Alitech Mass Flow Controllers (G1, G2) were used to mix ambient air and industrial CO_2 to the desired partial pressure of CO_2. The ambient air was provided by a house compressed air line fitted with a regulator to achieve the appropriate pressure. Industrial grade CO_2 was provided by a gas cylinder fitted with a regulator to achieve the appropriate back pressure. All plumbing for the mixing system used brass tubing with 1/8 inch OD (G3) and brass Swagelok tube fittings. A piece of 0.51mm MasterFlex Tygon E-Lab tubing (M6) was attached to the end of the brass tubing extending from the point of mixing and attached to another piece of brass tubing entering the water bubbler to hydrate the gas phase before entering the reactor.

The water bubbler was made using a 2 L Wide Mouth Corning Bottle (G9) with a cap machined to hold two Brass Swagelok Bulkhead Unions for 1/8 inch tube OD (V3), one for the gas inlet and one for gas outlet. A small piece of 1/8 inch OD stainless steel tubing (V5) was attached to the outside Swagelok fitting of each bulkhead union (V3) and a 7.25 inch piece of 1/8 inch OD stainless steel tubing (V5) was attached to the inside Swagelok fitting of the bulkhead union for gas inlet (V3) to submerge the inlet opening. This bubbler was filled approximately ¾ full with distilled water. A piece of 0.51mm MasterFlex Tygon E-Lab tubing (M6) was attached to the outlet. To this tubing a female Luer lock to 1/16 inch barb connector (M7) was attached which was connected to a male Luer lock to 3/16 inch barb (M9). A piece of 3/16 inch ID polypropylene tubing (M10) was attached to this 3/16 inch barb and subsequently to the gas delivery manifold. Two of these gas delivery systems were built to allow for simultaneous experimentation with different gas phases.

The gas delivery system consisted of 12 rotameters (G6) connected in parallel with ¼ inch OD brass tubing (G10) and brass Swagelok tube fittings. A three-way valve (G13) was placed after the sixth rotameter to allow two operating modes: one in which all 12 rotameters are fed from one gas mixing

system and a second in which two different gas phases could feed the first six and the second six rotameters. In the first case, the 3/16 inch ID tubing (M10) from the first gas mixing system was attached to the manifold upstream of all 12 rotameters. In the second case, the 3/16 inch ID tubing (M10) from the second gas mixing system was attached to the manifold at the three-way valve (G13). Each rotameter had a brass hose connecter for ¼ inch hose ID (G8) which was used to deliver gas to the inlet of each reactor. Flow rates for individual reactors were adjusted using the rotameter valve.

The gas mixing apparatus was contained in a chemical safety hood to prevent CO_2 accumulation in the laboratory. During operation, CO_2 concentration was monitored in the laboratory using a TIM10 Desktop CO_2, Temperature, and Humidity Monitor (co2meter.com) to ensure CO_2 did not accumulate to unsafe levels in the laboratory.

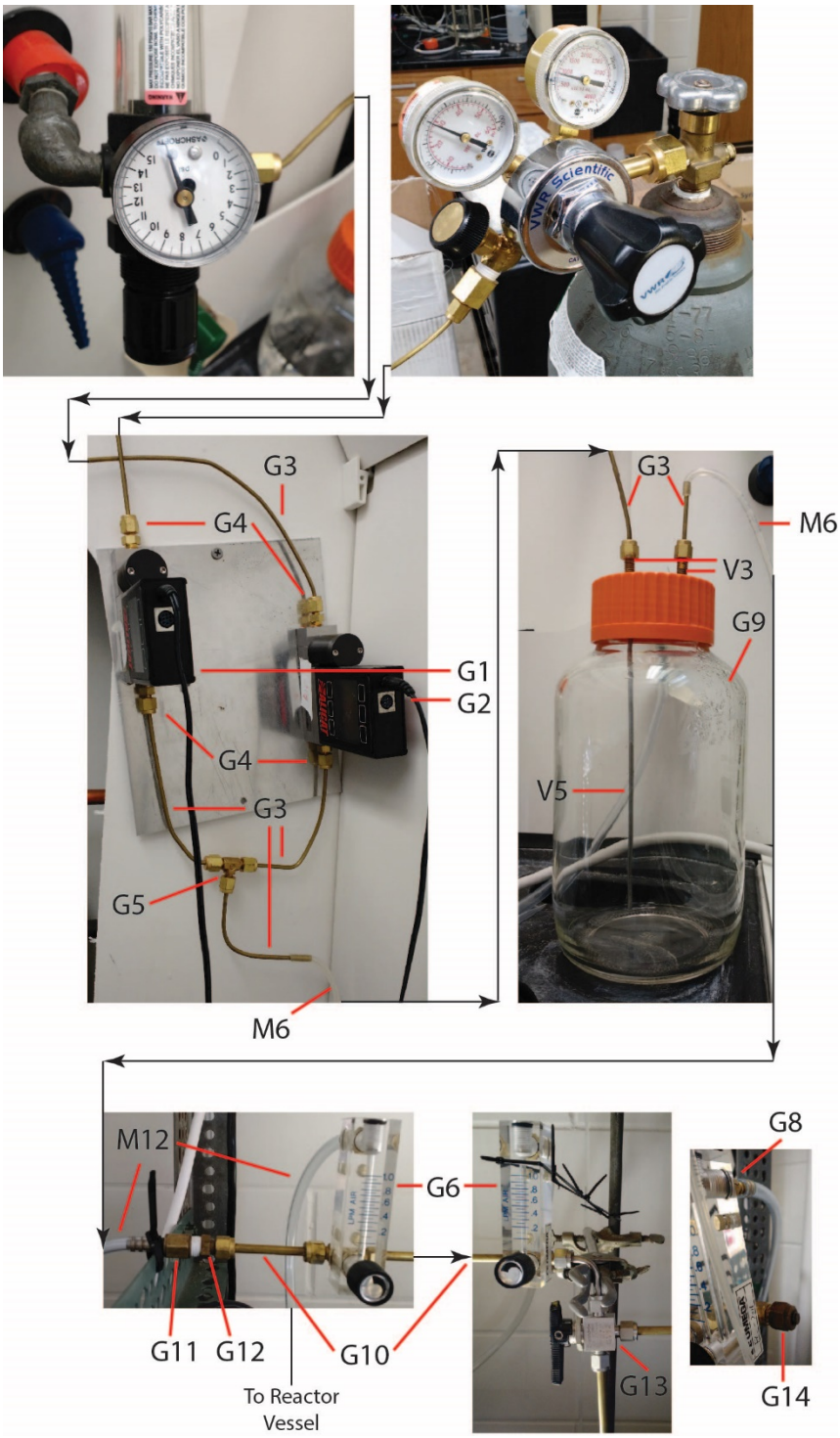

Figure A-3. Gas Mixing System. (Top Left) Ambient air was fed from house air fitted with a regulator to achieve desired pressure. (Top Right) Industrial grade CO_2 was fed from a gas cylinder fitted with a regulator to achieve desired pressure. (Middle Left) The flow rate of gases was controlled using mass flow controllers and mixed by combining the output flows. (Middle Right) The mixed gas stream was fed through a water bubbler to hydrate the air (shown without water). (Bottom Left) The hydrated gas phase was fed into a gas manifold for delivery to individual reactor vessels using rotameters to control gas flow rate. All labels reference the parts shown in Table A-1.

Lighting System

The lighting system for the photobioreactors fulfilled two roles: providing light to the culture and providing heat to the system. The temperature control system described in the subsequent section provided cooling to offset the heat provided by the fluorescent tubes and maintain the desired temperature set point. An image of the lighting system is shown in **Figure A-4**.

An overview of the assembly of the lighting system is shown in **Figure A-5**. A piece of sheet metal (L1) was sheared to the appropriate size and holes were cut using a sheet metal punch. The sheet was then bent at a 90° angle using a bender brake. Each mini bi-pin socket (L5) had a hole drilled in its base using a drill press. This hole was used to affix the sockets to the inside of the sheet metal fixture using a machine screw (M2), washer (M4), and nut (M3). Wires from the ballasts (L2) were then inserted into the corresponding sockets to provide power to the fluorescent bulbs per the manufacturer's instructions. Two ballasts were required for each lighting system, with each ballast powering 4 fluorescent tubes. Power was provided to the ballasts from a power socket with a fuse switch (L3) to allow the lights to be turned on and off. To simplify wiring, lighting systems were grouped into sets of three with one power socket with switch controlling all three lighting systems.

Experiments in this work were performed using 4100K cool white fluorescent tubes (L6). This lighting system will work with any F8T5/CW 8-watt fluorescent tubes if a different light quality is desired. Light intensity was modulated in a discrete manner by changing the number of fluorescent bulbs installed in the system as shown in **Figure A-6**. Luminous flux was determined with a Traceable Dual-Range Light Meter (Fisher Scientific).

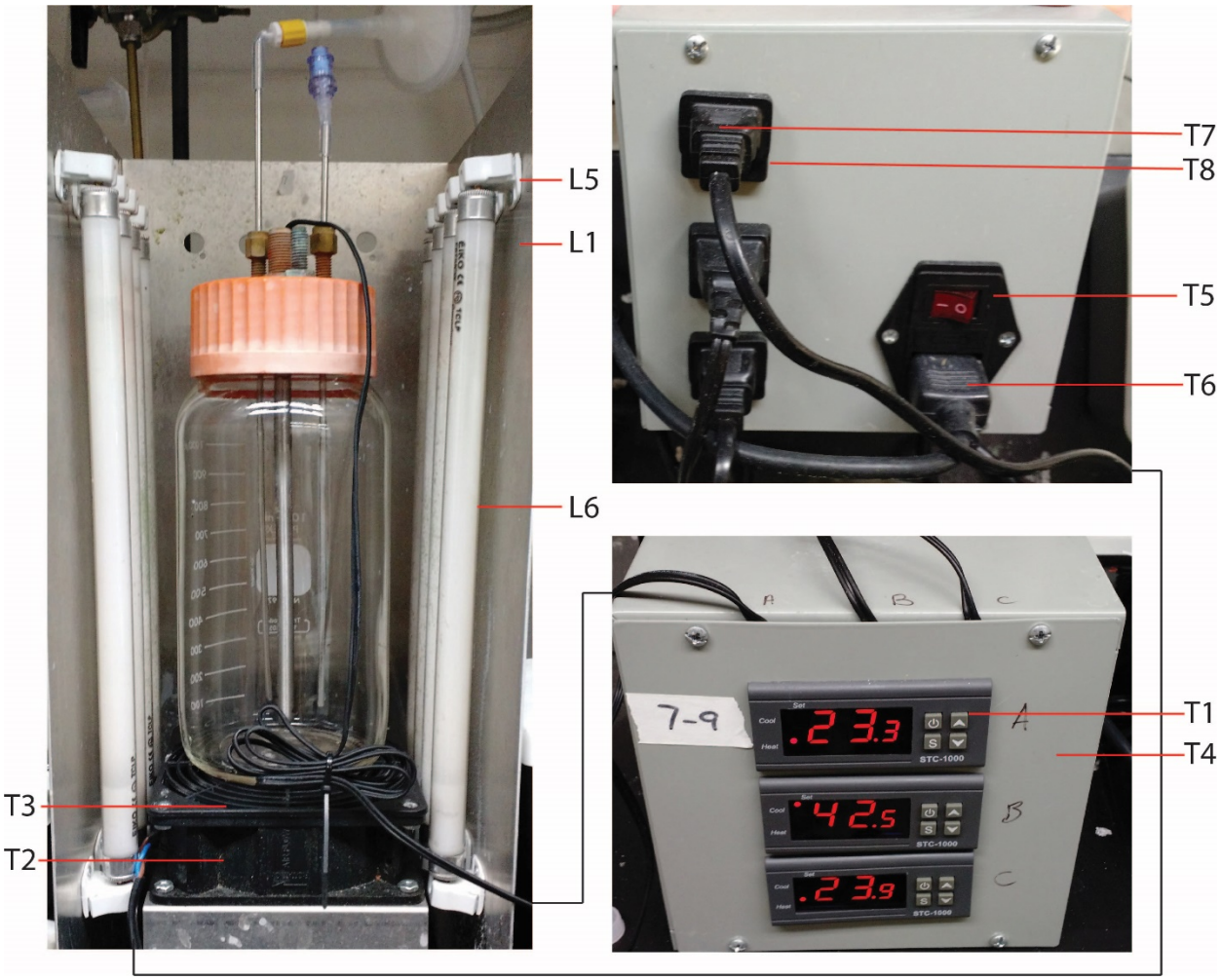

Figure A-4. Lighting and Temperature Control System. (Left) The reactor vessel rested on top of the fan assembly (Figure A-7) and light was provided from the sides of the reactor by the fluorescent light assembly (Figure A-5). (Bottom Right) Front view of the temperature control assembly which used the temperature probe as an input. (Top Right) Back view of the temperature control assembly which turned the fan on or off per the control parameters of the temperature controller. The power input on the back of temperature control assembly provided power for both the controllers and the fans. All labels reference the parts shown in Table A-1.

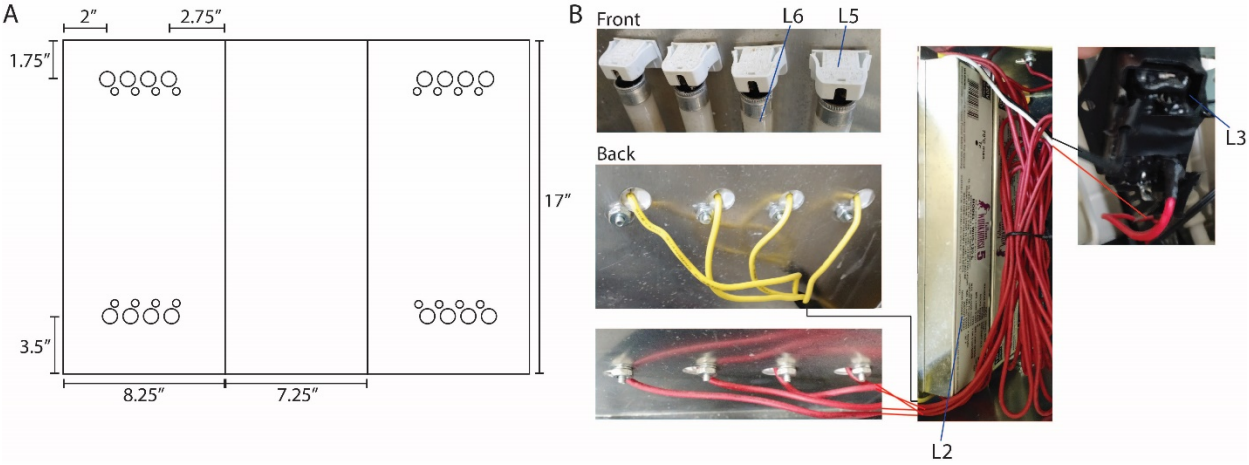

Figure A-5. Lighting System Assembly. (A) The sheet metal (L1) was cut to the size shown here and holes were punched for fastening and wire access to the mini bi-pin sockets for the fluorescent bulbs (L5). The sheet metal was folded at a ninety-degree angle on the two indicated lines to form the three-sided shape allowing the assembly to stand up. (B) (Top Left) L5 were installed on the inside of the sheet metal casing at all the locations indicated in (A) for a total of 16. These held the fluorescent tubes in place and provided power from the ballasts. (Middle Left) the sockets on the top of each side were wired to the yellow leads from the ballast (4 bulbs per ballast). (Middle Bottom) the sockets on the bottom of each side were wire to the red leads from the ballast (4 bulbs per ballast). (Center) The ballasts were fixed to the back of the sheet metal assembly. (Right) The black and white power supply leads from the ballasts were wired to a power socket for control of power supply. All labels reference the parts shown in Table A-1.

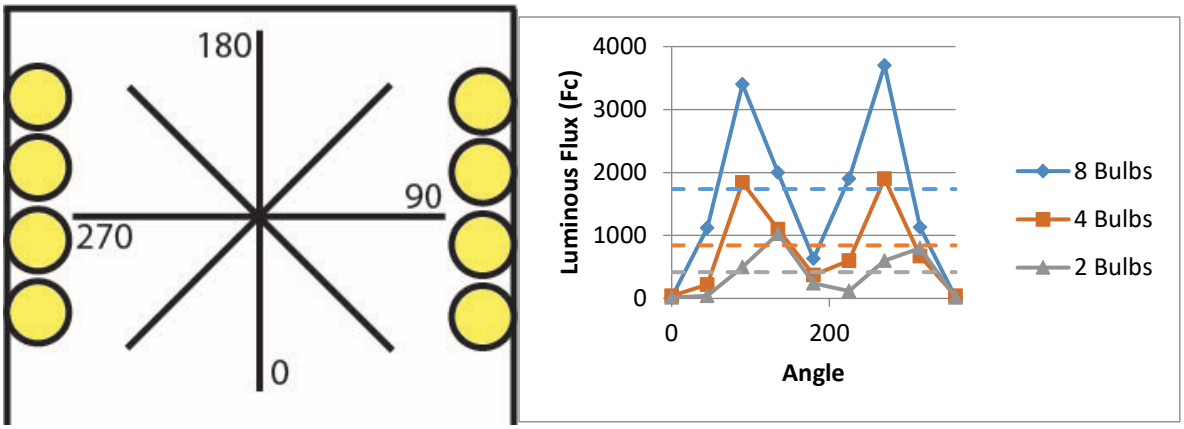

Figure A-6. Irradiance of Lighting System. (Left) Top down schematic of lighting system. 4 bulb set up had second and fourth bulb remove on the left and first and third bulb remove on the right. 2 bulb set up had only top bulb on the right and only the bottom bulb on the left. Numbers represent the angles at which luminous flux was measured. (Right) Luminous flux as a function of angle for each lighting setup. The dashed line represents the average luminous flux for a given number of bulbs.

Temperature Control

As mentioned above, heat was provided to the system by the fluorescent tubes. Without cooling and with all 8 bulbs installed in a lighting system, the temperature of liquid in the reactor vessel rose to over 40°C. To maintain cultures at a constant temperature, a temperature control system provided cooling

based on temperature measurements as shown in **Figure A-4**. The thermocouple inserted into the stainless-steel thermocouple protector on the reactor vessel detected the temperature and the temperature controller output power to the corresponding fan to cool the reactor to the desired set point. The temperature set point could be achieved for any temperature between ambient room temperature and 40°C. The temperature controller and fan were wired per the manufacturer's instructions as shown in **Figure A-7**.

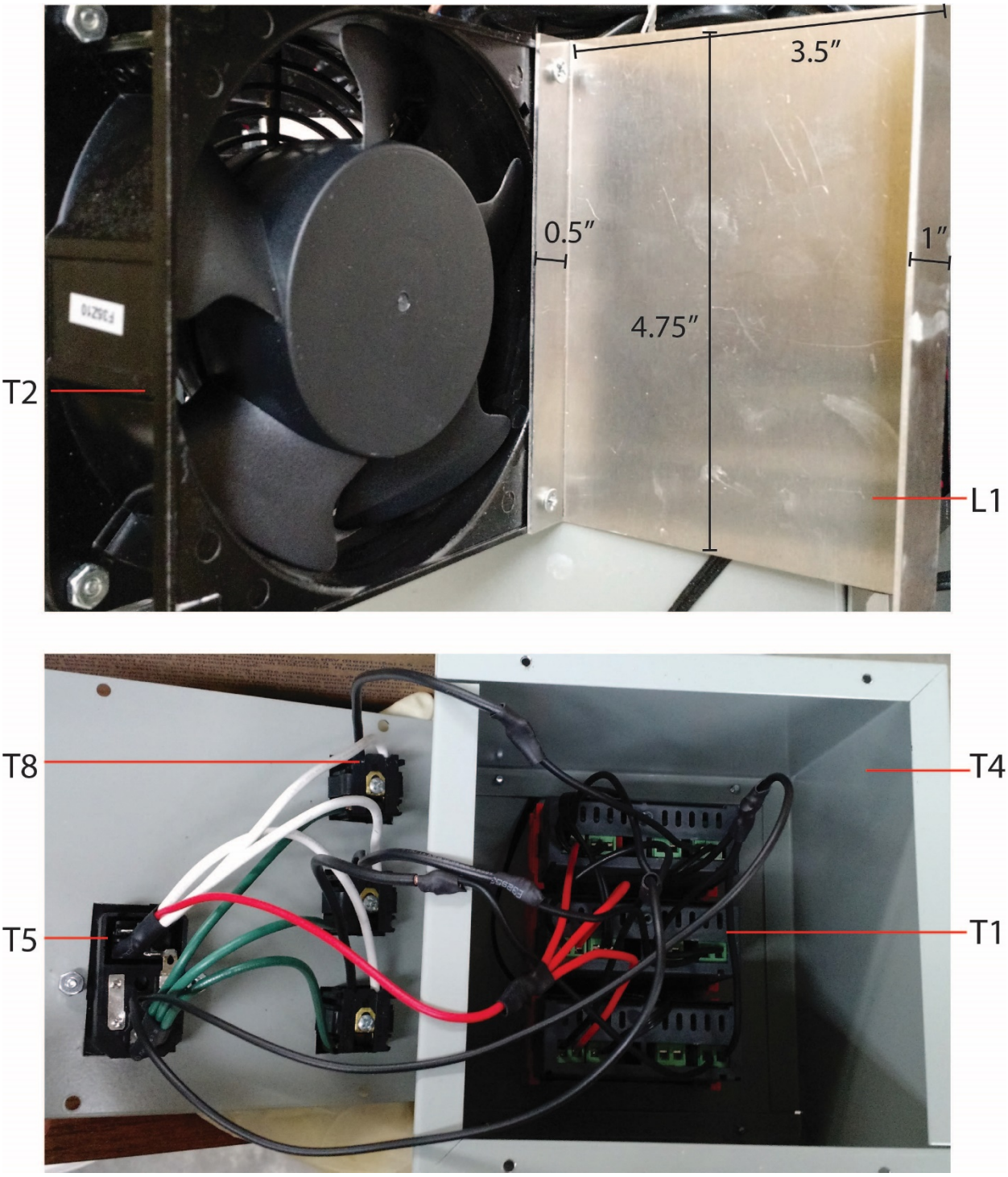

Figure A-7. Temperature Control System Assembly. (Top) Sheet metal supports for the fan were machined and fixed to the fan as shown allowing the fan to sit upright and act as a stand for the reactor vessel (one support removed for image). (Bottom) Temperature controllers were wired per the manufacturer's instructions with the power supply coming from the power socket (T5) and the output for cooling leading to the snap in receptacles (T8). All labels reference the parts shown in Table A-1.

A.3. Example Operating Procedure

Media Preparation

Media A was used in the photobioreactors for cultivation of *Synechococcus* sp. PCC7002 (components shown in **Table A-2**, adapted from Stevens, et al.(Stevens, Patterson, and Myers 1973)). All components were added in the order listed to a 50 L carboy, and the solution was mixed between additions by shaking. Media was made in one large batch to be distributed to the photobioreactors for autoclaving. Sodium chloride and magnesium sulfate were added as solids and each dissolved completely before the addition of the next component. All other components were added from 100x stock solutions, with the trace elements combined into a single 100x stock. To prepare this stock, ferric ammonium citrate, boric acid, and manganese chloride were added as solids, and the remaining components were added using stocks of the concentrations shown in **Table A-3**. The trace elements stock was filter sterilized immediately after preparation.

Reactor Assembly and Sterilization

900 ml of media was used in each reactor. Immediately before media was measured and added to the reactors, it was mixed by shaking to suspend any small amount of precipitate that may have settled out. After the reactors were filled, the caps were loosely attached and wrapped in foil. They were then autoclaved for 40 minutes to sterilize the media and internal components. Foil remained over the gas outlet until the reactors were attached to the air delivery system to block any convection of nonsterile air into the reactor. B_{12} (typically via a 1000x stock solution) was added to achieve a concentration of 3 nM, and any necessary antibiotics and inducers were also added. The reactors were then inoculated to a target OD_{730} of 0.05 from a pre-culture of the organism to be studied.

Table A-2. Concentration of Media Components.

Component	Concentration (mM)
NaCl	308
$MgSO_4 \cdot 7H_2O$	20
$Na_2EDTA \cdot 2H_2O$	0.08
KCl	8.1
$CaCl_2 \cdot 2H_2O$	2.5
$NaNO_3$	12
KH_2PO_4	0.37
Tris	8.3
Trace elements	(μM)
Ferric Ammonium Citrate	30
H_3BO_3	554
$MnCl_2\ 4H_2O$	22
	(nM)
$ZnCl_2$	2310
MoO_3	208
$CuSO_4 \cdot 5H_2O$	12
$CoCl_2 \cdot 6H_2O$	51

Table A-3. Concentration of Trace Element Stock Solution

Component	Concentration of Stock Solution
$ZnCl_2$	10,000x
MoO_3	100,000x
$CuSO_4 \cdot 5H_2O$	10,000x
$CoCl_2 \cdot 6H_2O$	10,000x

Concentrations are relative to the final concentration of the media.

Sampling Protocol

Prior to sampling, bioreactor volumes were adjusted to account for evaporation losses by adding sterile water through the DASGIP sampling valve. Evaporation losses were typically about 10-20 ml per day and slightly variable among reactors. Sterile water was stored in a bottle fitted with a DASGIP sampling valve of the same type used on the bioreactor assembly. Both valves were sterilized with a 70% aqueous ethanol solution immediately before a syringe was used to transfer the water.

The syringe was then used to sample the reactor. During sampling, the syringe was filled and emptied several times while attached to the reactor before collecting the final sample to flush out the sample port. Sample volumes were typically 1 mL or less to measure cell density and pigmentation, although larger volumes were taken for more complex sample analysis. Samples of 1 ml or less were regarded as negligible to the overall reactor volume, but larger samples were accounted for when adjusting for evaporation losses the following day. The OD_{730} was measured to observe cell density over time. **Figure A-8** shows a representative growth curve for Synechococcus sp. PCC7002 grown in Media A in the photobioreactors.

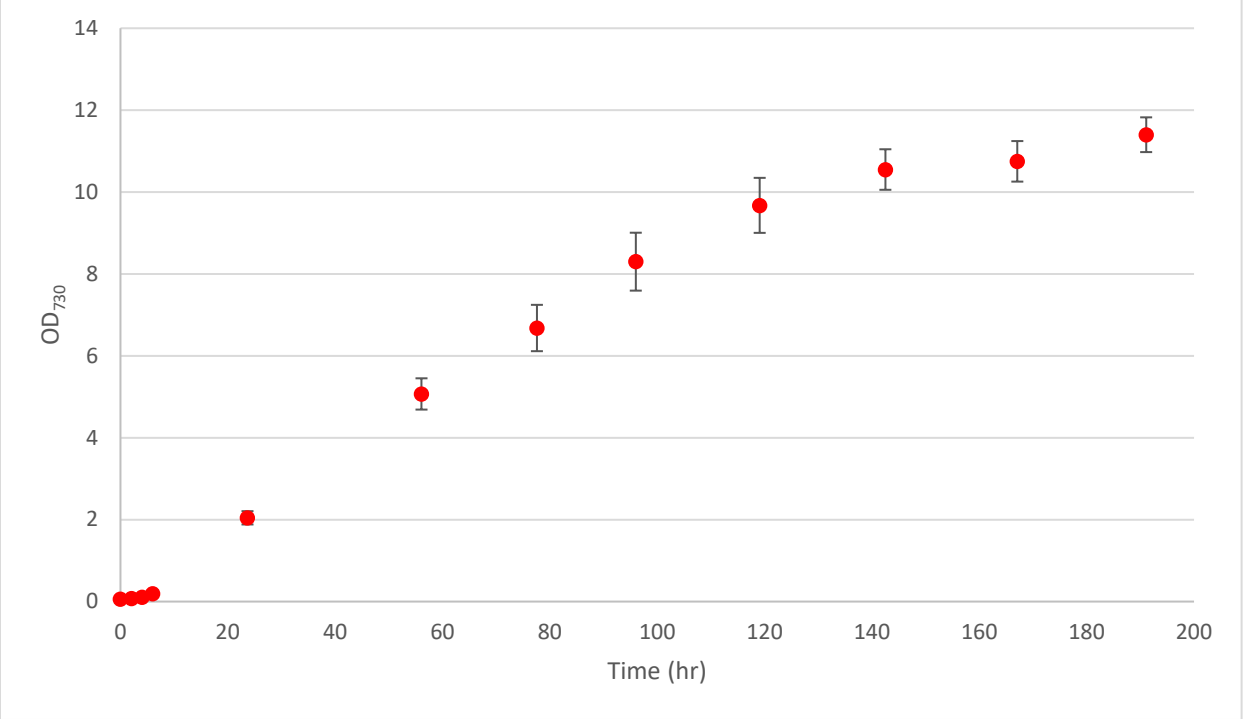

Figure A-8. Representative Growth Curve for *Synechococcus* sp. PCC7002 in Photobioreactors. 900 mL cultures of *Synechococcus* sp. PCC7002 were grown in the photobioreactors bubbled with 10% CO_2 and maintained at a temperature of 37°C by the temperature control system. Error bars are standard deviation of two biological replicates.

A.4. References

Angermayr, S. Andreas, Aleix Gorchs Rovira, and Klaas J. Hellingwerf. 2015. "Metabolic Engineering of Cyanobacteria for the Synthesis of Commodity Products." *Trends in Biotechnology* 33(6):352–61.

Stevens, S. E., C. O. P. Patterson, and J. Myers. 1973. "The Production of Hydrogen Peroxide by Blue-Green Algae: A Survey." *Journal of Phycology* 9:427–30.

Appendix B: RB-TnSeq in *Pseudomonas putida*

B.1. Background and Motivation

As described in **Chapter 6**, further work towards a robust containment mechanism for genetically modified cyanobacteria would be identification and elimination of many genes involved in the CO_2-concentrating mechanism (CCM) and natural competence. Towards this goal, we started a project with the goal of using transposon insertion sequencing to compile two lists of genes from the model cyanobacterium *Synechococcus* sp. PCC7002 (PCC7002): (1) those genes necessary for growth in ambient air but not for growth in elevated CO_2 concentration and (2) those non-essential genes necessary for the uptake and integration of foreign DNA into the chromosome of the cyanobacterium through natural competence.

Transposon insertion sequencing is a method for determining the necessity of genes for a given organism under one growth condition relative to a reference growth condition by measuring the transposon insertion frequency (TIF) in each locus under each condition (Chao et al. 2016). Random barcode transposon insertion sequencing (RB-TnSeq) builds upon transposon insertion sequencing by including a random DNA barcode in the transposable element. After mapping each barcode to its insertional location through transposon library sequencing, the TIF for a condition can be determined by sequencing of a PCR amplification of the barcode region from a library population exposed to the condition of interest (Wetmore et al. 2015).

This project is ongoing; here we will outline the proposed methods of the project and describe an implementation of (RB-TnSeq) to investigate Levulinic Acid (LA) metabolism in *Pseudomonas putida* as part of another project in the Pfleger Lab, which we completed in the process of learning the technique.

B.2. Ongoing Project: Identifying CCM and Natural Competence Genes in PCC7002

The first part of the proposed project is to create an RB-TnSeq library in PCC7002 using previously described methods (Rubin et al. 2015; Wetmore et al. 2015). This library will be prepared under a

reference condition of aqueous medium containing kanamycin in equilibrium with a gas phase containing 10% CO_2; this is a concentration typical of industrial CO_2 waste streams and is able to support the growth of a CCM-deficient strain of PCC7002, as described in **Chapter 4** (Clark et al. 2014). TIF determined through transposon sequencing of the resulting library will provide a list of essential, beneficial, and non-essential genes for growth of PCC7002 under excess CO_2 concentrations which will be interesting for comparison to a recent study on the essential gene set of another model cyanobacterium, *Synechococcus elongatus* PCC7942 (Rubin et al. 2015).

This population of transposon insertion mutants will subsequently be subjected to two other growth conditions for comparison. In the first condition, this population of cells will be grown for several generations in aqueous medium containing kanamycin in equilibrium with ambient air (~400 ppm CO_2). Quantifying the TIF across the genome of the resultant population relative to the reference population will yield a list of genes essential for growth in ambient air but non-essential for growth in excess CO_2.

In the second condition, the excess CO_2 population of transposon insertion mutants will be subjected to many parallel transformations of a gentamicin resistance cassette targeted to a known neutral site in the genome of PCC7002. These samples will then be plated in the presence of gentamicin to select for colonies growing from cells that could integrate the resistance cassette. Pooling millions of colonies and quantifying the TIF across the genome of the resultant population relative to the reference population will yield a list of genes essential for the natural competence of PCC7002.

The resultant information from these studies will yield a list of target genes that can be knocked out to reduce the risk of restoration of a functioning CCM in genetically modified cyanobacteria. Additionally, eliminating any other non-essential genes given from analysis of the TIF in the reference population could result in a reduction of cellular maintenance energy, improving the economics of large-scale cultivation.

B.3. Training Project: Investigating LA Metabolism Genes in *Pseudomonas putida*

LA is a byproduct from the conversion of lignocellulosic biomass to soluble sugars due to the degradation of glucose under harsh acidic conditions (Huber, Iborra, and Corma 2006). The yield of molecules produced by microbes from such feedstocks can thus be increased if the host organism can metabolize the LA byproduct. *Pseudomonas putida* is able to metabolize LA (Martin and Prather 2009), so the pathway and genes responsible were investigated in the Pfleger lab by Rand et al. (Rand et al. 2017) to better understand this process and to facilitate engineering common production organisms such as *Escherichia coli* for LA metabolism. The RB-TnSeq study described below expanded on the biochemical studies described in the main text of reference (Rand et al. 2017) to investigate LA metabolism on a systems level and was included in the supplemental note of the publication.

To investigate genes involved in LA metabolism on a systems level, random bar code transposon-site sequencing (RB-TnSeq) was performed for the growth of *Pseudomonas Putida* on LA and 4HV. A summary of genes identified as particularly interesting to the authors is shown in **Table B-1** including fitness scores for growth on minimal media with LA or 4HV relative to minimal media with glucose or the initial inoculum grown in LB. All data from these experiments is available through the fitness browser at http://fit.genomics.lbl.gov/cgi-bin/exps.cgi?orgId=Putida&expGroup=carbon%20source (Price et al. 2016).

Table B-1. Genes of Interest Identified from RB-TnSeq Experiments

Genes Mentioned in the Main Text of Rand et al. [7]				
Locus	Name	Annotation	LA/Gluc	4HV/Gluc
PP_0364	*bioH*	pimeloyl-ACP methyl ester esterase	0.3	0.02
PP_0988	*gcvP-1*	glycine dehydrogenase	-0.02	-0.003
PP_2332	-	ATP-dependent zinc protease family	-0.1	0.2
PP_2336	*acnA-II*	aconitate hydratase	-4.5	-3.5
PP_2337	*prpF*	aconitate isomerase	-4.4	-3.8
PP_2790	*lvaR*	Sigma-54 dependent sensory box protein	-3.9	-5.0
PP_2791	*lvaA*	Aminoglycoside phosphotransferase	-5.2	-4.2
PP_2792	*lvaB*	Hypothetical protein	NA	NA
PP_2793	*lvaC*	acyl-CoA dehydrogenase/reductase family	-5.2	-4.1
PP_2794	*lvaD*	Oxidoreductase, short chain dehydrogenase/reductase family	-6.5	-5.3
PP_2795	*lvaE*	Acyl-CoA synthetase	0.4	-4.6
PP_2796	*lvaF*	conserved protein of unknown function	0.2	0.7
PP_2797	*lvaG*	acetate permease	0.1	1.7
PP_3741	*mrdA-I*	transpeptidase	0.0	-0.06
PP_4217	*fpvA*	TonB-dependent outer membrane ferripyoverdine receptor	0.3	0.02
Important for Fitness in LA and 4HV				
PP_2217		enoyl-CoA hydratase	-2.0	-2.2
PP_2334		2-methylisocitrate lyase	-4.9	-3.3
PP_2335		methylcitrate synthase	-5.1	-4.7
PP_3286		DNA-binding transcriptional repressor PaaX(phenylacetyl-CoA)	-4.3	-4.1
PP_3753		Transcriptional regulator, AraC family	-4.8	-2.6
PP_3754		Beta-ketothiolase BktB	-5.8	-3.2
PP_3755		3-hydroxybutyryl-CoA dehydrogenase	-2.9	-3.1
Important for Fitness in LA but not 4HV				
PP_1291		PhoH family protein	-2.5	0.3
PP_2333		GntR family transcriptional regulator	-4.5	-0.7
PP_3121		transcriptional regulator, LysR family	-4.1	-0.3
PP_3122		acetoacetyl CoA-transferase (subunit A)	-2.3	-0.1
PP_3123		acetoacetyl CoA-transferase (subunit B)	-3.1	-0.02
PP_3925		conserved protein of unknown function	-2.1	-0.9
PP_4515		Transcriptional regulator, MarR family	-2.2	0.03
PP_4628		conserved protein of unknown function	-3.6	-1.3
Important for Fitness in 4HV but not LA				
PP_0951		Ribosome hibernation promoting factor	0.2	-2.4
PP_0995		Putative sigma factor regulator	-0.5	-2.6
PP_1328		Protein MraZ	-0.5	-4.2
PP_1764		Phosphoglycolate phosphatase 2	-1.3	-2.7
PP_1778		Lipopolysaccharide ABC export system, permease protein	0.2	-4.8
PP_1779		Lipopolysaccharide ABC export system, ATP-binding protein	0.003	-4.0
PP_1968		TetR family transcriptional regulator	-0.8	-2.1
PP_2082		phosphoenolpyruvate synthetase	-0.2	-2.7
PP_2436		Transcriptional regulator, LysR family	-0.3	-2.4
PP_4342		flagellar synthesis regulator, putative ATPase	-1.4	-2.0
PP_4571		cysteine synthase A	-0.1	-3.5
PP_4762		Acyl-CoA thioesterase II	0.3	-4.3
PP_4824		Sensor histidine kinase/response regulator	-0.7	-2.2
PP_4895		tRNA dimethylallyltransferase	-1.7	-2.0
PP_5203		5-formyltetrahydrofolate cyclo-ligase	-0.01	-3.0
PP_5210		Alcohol dehydrogenase, zinc containing	0.2	-2.5
PP_5502		ribosome modulation factor	-0.2	-3.5
Enhanced Fitness in 4HV				
PP_0191		Transcriptional regulatory protein AlgQ	0.6	2.7
PP_0395		putative type IV piliation protein	-0.3	3.2
PP_0396		conserved protein of unknown function	-0.5	3.1
PP_0397		protein kinase	-0.2	3.0
PP_0674		ADP/ATP ratio sensor and inhibitor of translation	-0.2	2.1
PP_1236		putative Glycine cleavage system transcriptional repressor	1.1	2.3
PP_2144		Transcriptional regulator, TetR family	1.3	5.6
PP_3603		Transcriptional regulator, GntR family	-0.5	2.3
PP_4734		Transcriptional regulator, GntR family	0.3	3.2
PP_4874		50S ribosomal protein L9	-0.5	2.6
PP_5145		phosphoenolpyruvate-dependent regulator	-1.2	4.6
PP_5146		RNA pyrophosphohydrolase	-1.0	2.9
PP_5232		conserved protein of unknown function	-1.4	3.4

Methods

Pseudomonas Putida Library Preparation

Our collaborators in the groups of Adam Arkin (University of California – Berkeley) and Adam Deutschbauer (Lawrence Berkeley National Labs) generated a DNA-barcoded transposon mutant library of *P. putida* KT2440 using previously described methods and resources (Wetmore et al. 2015). Briefly, they conjugated Wild Type *P. putida* KT2440 with an *E. coli* strain (WM3064) carrying the transposon vector library pKMW3 (Wetmore et al. 2015). pKMW3 is a mariner class transposon vector library containing a kanamycin resistance marker and millions of random 20mer DNA barcodes. Conjugations were performed at 1:1 donor:recipient ratio on LB + diaminopimelic acid (DAP) plates for 6 hours and finally plated on LB plates supplemented with 100 µg/mL kanamycin. The *E. coli* conjugation strain WM3064 is auxotrophic for DAP and does not grow on media that is not supplemented with this compound. They combined thousands of kanamycin-resistant *P. putida* colonies into a single tube, made multiple aliquots, and stored these samples at -80 °C for future use. They also extracted genomic DNA and mapped the transposon insertion locations and their associated DNA barcodes via a TnSeq-like Illumina sequencing protocol, as previously described (Wetmore et al. 2015). They named the final, sequenced mapped transposon mutant library Putida_ML5.

LA and 4HV Growth Experiments

An aliquot of the *P. Putida* RB-TnSeq library (Putida_ML5) was grown for 5 hours in a shake flask containing 25mL of LB media with 50 µg/mL Kanamycin Sulfate to late log phase (30°C, 250 RPM). 1 OD_{600}*mL of cells were pelleted, decanted, and frozen at -20°C for barcode sequencing as the time zero inoculum control. 1 OD_{600}*mL of cells per treatment were washed with three volumes of minimal media with no carbon source and then resuspended in 2x minimal media with no carbon source for a new OD_{600} measurement. These cells were diluted into 2x minimal media to an OD_{600} of 0.04. This culture was then diluted in half with 2x solutions of each carbon source of interest to a final volume of 10mL in a culture

tube for 4HV and 1.2mL total volume in the well of a 24-well microplate for LA. The carbon sources tested were 40mM 4HV (pH adjusted to 7 with NaOH), 40mM LA (pH adjusted to 7 with NaOH), 20mM potassium acetate, and 40mM glucose, each with two replicates. The 4HV and acetate experiments were performed one day and the LA experiments were performed on a different day, each day with its own 40 mM Glucose control. The culture tubes were placed in a shaker incubator (30°C, 250 RPM) until they achieved and OD_{600} of ~3 for 40 mM Glucose (~20 hours), ~0.25 for 20 mM potassium acetate (~44 hours), or ~0.3-0.5 for 40mM 4HV (~68 hours). For LA, the samples were grown in a 24-well microplate in a Multitron shaker set to 30°C and 700 rpm. We monitored the OD of the microplate in a Tecan M1000 microplate reader. A 1 mL sample from each culture tube was pelleted and frozen at -20°C for barcode sequencing.

BarSeq

Our collaborators performed DNA barcode sequencing (BarSeq) as previously described (Wetmore et al. 2015), with a slight variation in the common P1 oligo design. In this study, they used a mixture of P1 oligos with variable length N space regions (2-5 nt) to "phase" the BarSeq PCR products for sequencing on the Illumina HiSeq4000.

Data Analysis

Both the TnSeq data and the BarSeq data were processed using analysis scripts as described previously (Wetmore et al. 2015). Briefly, the fitness of a strain in the normalized $\log_2$ ratio of barcode reads in the experimental sample to barcode reads in the time zero sample. The fitness of a gene is the weighted average of the strain fitness for insertions in the central 10-90% of the gene. The gene fitness values are normalized so that the typical gene has a fitness of zero. The primary statistic t-value is of the form of fitness divided by the estimated variance across different mutants of the same gene. All experiments described herein pass the quality metrics described previously unless noted otherwise (Wetmore et al. 2015).

Identifying Genes of Interest

The fitness values reported in **Table B-1** are the average of 2 replicates. Fitness scores for LA and 4HV relative to glucose were calculated using the following equation:

$$Fitness\left(\frac{LA}{Glucose}\right) = Fitness(LA) - Fitness(Glucose)$$

Annotations in **Table B-1** and discussed in the text below were adapted from www.MicrobesOnline.org (Dehal et al. 2009).

Results and Discussion

RB-TnSeq Results are Consistent with Evidence Provided in Rand, et al. (Rand et al. 2017)

All genes mentioned in the main text of Rand, et al. (Rand et al. 2017) are shown with their fitness scores for growth on LA and 4HV in **Table B-1**. Genes that were identified as transposon library hits have their gene loci highlighted in red italics.

RB-TnSeq analysis suggests the genes identified as constituting the LA metabolism operon *lvaABCDEFG* as well as the proposed regulator *lvaR* were important for growth on both LA and 4HV with a few exceptions described as follows. *lvaB* was excluded from the data summary for growth on LA and 4HV due to insufficient barcode insertions in this small gene and *lvaE* (shown to not be essential for growth on LA in the main text) shows no phenotype on LA.

RB-TnSeq analysis suggests *lvaF* and *lvaG* are not important for growth on LA or 4HV, suggesting they are not required for transport of these metabolites at the concentrations used in the experiments. The positive fitness scores of these genes for growth on 4HV suggest that the 4HV concentrations used in this experiment had negative effects on fitness, an effect that would be alleviated by elimination of import system (See section below: *Potential Induction of Quorum-Sensing Systems by γ-Valerolactone*). None of the remaining transposon library hits from the main text exhibited interesting phenotypes in the RB-TnSeq experiment, suggesting they may have been dependent upon the transposon library experiment.

In addition to genes identified in the main text, genes of interest shown in **Table B-1** were identified using the following criteria:

Important for Fitness in LA and 4HV: Fitness scores lower than -2 for both LA and 4HV.

Important for Fitness in LA but not 4HV: Fitness score for LA lower than -2 and fitness score for 4HV greater than -2.

Important for Fitness in 4HV but not LA: Fitness score for 4HV lower than -2 and fitness score for LA greater than -2.

Enhanced Fitness in 4HV: Fitness score greater than 2 for 4HV.

This list of genes of interest was further refined by eliminating genes that shared a phenotype with growth on acetate as these results were considered not relevant to the scope of this work.

β-Oxidation of 3-Hydroxyvaleryl-CoA to Propionyl-CoA and Acetyl-CoA by Genes Important for Growth on LA and 4HV

As proposed in the main text of Rand et al. (Rand et al. 2017), the 3-hydroxyvaleryl-CoA metabolite produced in LA metabolism could be utilized through β-Oxidation to form Propionyl-CoA and Acetyl-CoA. RB-TnSeq analysis helped to identify potential candidate genes for this pathway:

PP_3755 is annotated as a 3-hydroxybutyryl-CoA dehydrogenase, suggesting that this enzyme catalyzes the conversion of 3-hydroxyvaleryl-CoA to 3-ketovaleryl-CoA.

PP_3754 is annotated as a β-ketothiolase, suggesting that this enzyme catalyzes the conversion of 3-ketovaleryl-CoA to propionyl-CoA and Acetyl-CoA.

PP_3753 is annotated as a transcriptional regulator and its location directly upstream of the two previous genes suggests a role in the regulation of these two β-oxidation genes.

Propionyl-CoA Metabolism by Genes Important for Growth on LA and 4HV

After propionyl-CoA is formed through the mechanism proposed in the previous section, it could be further metabolized to form succinate and pyruvate through the 2-methylcitrate cycle. PP_2337 is annotated as a methylaconitate isomerase (prpF), suggesting that the pathway utilized is the 2-

methylcitrate cycle II that passes through a *trans*-2-methyl-aconitate intermediate. RB-TnSeq analysis helped to identify potential candidate genes for this pathway:

PP_2335 is annotated as a methylcitrate synthase, suggesting that this enzyme catalyzes the reaction of propionyl-CoA with oxaloacetate to form 2-methylcitrate.

PP_2336 is annotated as an aconitate hydratase. PP_2339, an additional gene in close chromosomal proximity but with insufficient BarSeq data for analysis is also annotated as an aconitate hydratase. These results suggest that some combination of these two enzymes catalyze both the conversion of 2-methylcitrate to *trans*-2-methylaconitate and the downstream conversion of *cis*-2-methylaconitate to 2-methylisocitrate.

PP_2337 is annotated as a methylaconitate isomerase, suggesting that this enzyme catalyzes the conversion of *trans*-2-methylaconitate to *cis*-2-methylaconitate.

PP_2334 is annotated as a 2-methylisocitrate lyase, suggesting that this enzyme catalyzes the conversion of 2-methylisocitrate to succinate and pyruvate.

PP_2333 is annotated as a transcriptional regulator and its location directly upstream of the PP_2334-2339 genes suggests a role in the regulation of these propionyl-CoA metabolism genes.

Potential Levulinyl-CoA Transferase

In the main text of Rand, et al. (Rand et al. 2017), *lvaE* was shown to catalyze the conversion of LA to levulinyl-CoA as well as the conversion of 4HV to 4-hydroxyvalerly-CoA. *lvaE* is essential for growth on 4HV but not essential for growth on LA, suggesting that there is another enzyme capable of catalyzing the conversion of LA to levulinyl-CoA. PP_3122 and PP_3123 are annotated as acetoacetyl CoA-transferase subunits A and B respectively and are both important for growth on LA but not 4HV, suggesting they could fill the role of the additional catalyst for levulinyl-CoA formation. PP_3121 is also important for growth on LA but not 4HV and is annotated as a transcriptional regulator. Its genomic context suggests it regulates the expression of PP_3122 and PP_3123. This set of genes is analogous to the *dhcAB* operon involved in

catabolism of carnitine in *Pseudomonas aeruginosa*. PP_3121 shares 72% sequence identity across 95% of its sequence with *dhcR* (PA1998) and PP_3122 and PP_3123 share 86% and 90% identity across their entire sequences with *dhcA* (PA1999) and *dhcB* (PA2000), respectively. *dhcR* regulates expression of the *dhcAB* operon encoding a predicted 3-ketoacid CoA-transferase with evidence of activity on 3-dehydrocarnitine (Wargo and Hogan 2009). PP_3121-PP_3123 could serve a similar role in catabolism of LA.

Transcriptional Regulators Control Both Beneficial and Detrimental Systems for Fitness Under LA and 4HV Metabolism

PP_3286 and PP_3753 are annotated as transcriptional regulators and RB-TnSeq analysis suggests they are important for growth on LA and 4HV. The annotation for PP_3286 suggests involvement in the regulation of phenylacetic acid metabolism. As previously stated, genomic context suggests the involvement of PP_3753 in the regulation of the probable β-oxidation genes PP_3754-3755.

PP_3121 and PP_4515 are annotated as transcriptional regulators and RB-TnSeq analysis suggests they are important for growth on LA but not important for growth on 4HV. As previously stated, genomic context suggests PP_3121 regulates expression of the potential acetoacetyl-CoA transferase subunits PP_3122-3123. The regulatory role of PP_4515 is unclear.

Conversely, PP_0995, PP_1328, PP_1968, PP_2333, and PP_2436 are annotated as transcriptional regulators and RB-TnSeq analysis suggests they are important for growth on 4HV, but not important for growth on LA. PP_0995 shares 41% homology across its entire sequence with a gene in *Caulobacter crescentus* (CC3252) thought to be involved in sigma factor regulation for heavy metal stress, although its regulatory role in *Pseudomonas putida* is unclear (Kohler et al. 2012). As previously stated, genomic context suggests the involvement of PP_2333 in the regulation of the probable propionyl-CoA metabolism genes PP_2333-2339. The regulatory functions of PP_1328, PP_1968, and PP_2436 are unclear.

PP_0191, PP_1236, PP_2144, PP_3603, and PP_4734 are annotated as transcriptional regulators and RB-TnSeq analysis suggests their deletions are beneficial for growth on 4HV. PP_0191 is annotated as a

regulator of alginate bioaccumulation, suggesting a role in biofilm formation. PP_1236 is annotated as a regulator of a glycine cleavage system and a close homolog in *Pseudomonas aeruginosa* (PA1009) is involved in the regulation of host colonization (Koh et al. 2010). PP_2144 has a close homolog in *Pseudomonas syringae* (*psrA*) that is involved in the regulation of epiphytic fitness, quorum-sensing, and plant host interactions (Chatterjee et al. 2007).

PP_3603 and PP_4734 are annotated as fatty acid responsive transcriptional regulators with unknown regulatory roles.

Potential Induction of Quorum-Sensing Systems by γ-Valerolactone

4HV used in the RB-TnSeq experiments was synthesized from γ-valerolactone as described in the methods section of the main text of Rand, et al. (Rand et al. 2017). As a result, residual γ-valerolactone was likely present in the experiments for growth on 4HV. Several molecules in the lactone family are known to be used as quorum sensing signals in *Pseudomonads* (Pearson et al. 1995). Quorum sensing responses would likely cause physiological responses towards the formation of a biofilm in the culture vessel. Cells with disruptions in these regulatory systems would replicate themselves to a higher degree resulting in a perceived increase in fitness as is the case with the transcriptional regulators PP_0191, PP_1236, and PP_2144 discussed above. As γ-Valerolactone is being investigated as a promising solvent for nonenzymatic sugar production from biomass (Luterbacher et al. 2014), its effect on the quorum sensing systems of potential platform host organisms for bioprocessing should be further investigated.

B.4. References

Chao, Michael C., Sören Abel, Brigid M. Davis, and Matthew K. Waldor. 2016. “The Design and Analysis of Transposon Insertion Sequencing Experiments.” *Nature Reviews Microbiology* 14(2):119–28.

Chatterjee, Asita, Yaya Cui, Hiroaki Hasegawa, and Arun K. Chatterjee. 2007. “PsrA, the *Pseudomonas* Sigma Regulator, Controls Regulators of Epiphytic Fitness, Quorum-Sensing Signals, and Plant Interactions in *Pseudomonas Syringae* Pv. Tomato Strain DC3000.” *Applied and Environmental Microbiology* 73(11):3684–94.

Clark, Ryan L., Jeffrey C. Cameron, Thatcher W. Root, and Brian F. Pfleger. 2014. “Insights into the Industrial Growth of Cyanobacteria from a Model of the Carbon-Concentrating Mechanism.” *AIChE Journal* 60(4):1269–77.

Dehal, Paramvir S. et al. 2009. “MicrobesOnline: An Integrated Portal for Comparative and Functional Genomics.” *Nucleic Acids Research* 38:D396–400.

Huber, George W., Sara Iborra, and Avelino Corma. 2006. “Synthesis of Transportation Fuels from Biomass: Chemistry, Catalysts, and Engineering.” *Chemical Reviews* 106(9):4044–98.

Koh, Andrew Y. et al. 2010. “Utility of in Vivo Transcription Profiling for Identifying *Pseudomonas Aeruginosa* Genes Needed for Gastrointestinal Colonization and Dissemination.” *PLoS ONE* 5(12):1-14.

Kohler, Christian, Rogério F. Lourenço, Gabriela M. Avelar, and Suely L. Gomes. 2012. “Extracytoplasmic Function (ECF) Sigma Factor σF Is Involved in *Caulobacter Crescentus* Response to Heavy Metal Stress.” *BMC Microbiology* 12(210).

Luterbacher, Jeremy S. et al. 2014. “Nonenzymatic Sugar Production from Biomass Using Biomass-Derived γ-Valerolactone.” *Science* 343:277–80.

Martin, Collin H. and Kristala L. Jones Prather. 2009. “High-Titer Production of Monomeric Hydroxyvalerates from Levulinic Acid in *Pseudomonas Putida*.” *Journal of Biotechnology* 139(1):61-67.

Pearson, J. P., L. Passador, B. H. Iglewski, and E. P. Greenberg. 1995. “A Second N-Acylhomoserine Lactone Signal Produced by *Pseudomonas Aeruginosa*.” *Proceedings of the National Academy of Sciences of the United States of America* 92(5):1490–94.

Price, Morgan N. et al. 2016. “Deep Annotation of Protein Function across Diverse Bacteria from Mutant Phenotypes.” *bioRxiv*.

Rand, Jacqueline M. et al. 2017. “Elucidation of the Levulinic Acid Catabolic Pathway in *Pseudomonas Putida*.” *Nature Microbiology* Submitted.

Rubin, Benjamin E. et al. 2015. “The Essential Gene Set of a Photosynthetic Organism.” *Proceedings of the National Academy of Sciences of the United States of America* 112(48):E6634–43.

Wargo, Matthew J. and Deborah A. Hogan. 2009. “Identification of Genes Required for *Pseudomonas Aeruginosa* Carnitine Catabolism.” *Microbiology* 155(7):2411–19.

Wetmore, Kelly M. et al. 2015. “Rapid Quantification of Mutant Fitness in Diverse Bacteria by Sequencing Randomly Bar-Coded Transposons.” *mBio* 6(3):1–15.